FLORIDA INTERNATIONAL UNIVERSITY

Miami, Florida

ZINC-OXIDE NANOSTRUCTURE-BASED WEARABLE BIOSENSOR PLATFORM FOR SWEAT ANALYSIS

A dissertation submitted in partial fulfillment of

the requirements for the degree of

DOCTOR OF PHILOSOPHY

in

ELECTRICAL AND COMPUTER ENGINEERING

by

Fahmida Alam

2021

To: Dean John L. Volakis
College of Engineering and Computing

This dissertation, written by Fahmida Alam, and entitled Zinc-oxide Nanostructure-based Wearable Biosensor Platform for Sweat Analysis, having been approved in respect to style and intellectual content, is referred to you for judgment.

We have read this dissertation and recommend that it be approved.

_____
Shekhar Bhansali

_____
Jean Andrian

_____
Chunlei Wang

_____
Nezih Pala, Major Professor

Date of Defense: November 5, 2021

The dissertation of Fahmida Alam is approved.

_____
Dean John L. Volakis
College of Engineering and Computing

_____
Andrés G. Gil
Vice President for Research and Economic Development
and Dean of the University Graduate School

Florida International University, 2021

© Copyright 2021 by Fahmida Alam

All rights reserved.

DEDICATION

I dedicate this dissertation to my parents, Shamsun Nahar and Badiul Alam, and my husband Ahmed Hasnain Jalal for their unconditional love and support.

ACKNOWLEDGMENT

First and foremost, I would like to express my reverential gratitude to my supervisor Dr. Nezih Pala, Associate Professor, Department of Electrical and Computer Engineering, Florida International University, for his extraordinary, invaluable suggestions, and continuous encouragement in the preparation of this dissertation. Without his guidance and persistent support, this research would have not been possible to complete. I would also like to thank all my committee members, Dr. Bhansali, Dr. Wang , and Dr. Andrian for their interest in my research. I sincerely appreciate their invaluable time for reading the dissertation and providing comments and suggestions to improve it. I consider myself fortunate enough to collaborate with Dr. Bhansali and Dr. Wang which allowed me to explore new domains of research.

I also thank all other friends and colleagues at FIU who helped me make this memorable journey. I passed a wonderful time with them all these years. I would like to acknowledge University Graduate School (UGS) of FIU for providing the "DYF Fellowship" during my tenure at FIU. I would also like to acknowledge the "Advanced Materials Engineering Research Institute (AMERI)" at FIU for the support of my research.

ABSTRACT OF THE DISSERTATION

ZINC-OXIDE NANOSTRUCTURE-BASED WEARABLE BIOSENSOR PLATFORM FOR SWEAT ANALYSIS

by

Fahmida Alam

Florida International University, 2021

Miami, Florida

Professor Nezih Pala, Major Professor

The aim of this research is to develop highly sensitive, flexible, wearable enzymatic and immuno-sensor arrays for continuous and selective sensing of ethanol, lactate, and glucose in human sweat. Human sweat has clinical importance and has been recommended as an early pointer for many health conditions and diseases. Thus, for many health applications, point-of-care non-invasive monitoring of different biomarkers in sweat is ultimately important. The major challenges of the sweat analysis biosensors include selectivity, sensitivity, flexibility, sweat collection, and storage for analysis. In this research, sonochemical synthesis of two-dimensional (2D) Zinc Oxide Nanoflakes (ZnO NFs) and wearable sweat analysis biosensors based on them have been studied. ZnO-NFs with a high surface-to-volume ratio help improve the sensitivity. In electrochemical biosensors, selectivity is attained typically by using antibodies or enzymes. However, binding such biomolecules require a linker layer which introduces an additional resistive path for the electrons and hence adversely affects the sensitivity. With their high isoelectric point, ZnO-NFs do not require a linker layer and can deliver better sensitivity while

providing selectivity. Moreover, the well-oriented growth of ZnO nanostructures (NSs) can be achieved through the sonochemical method on arbitrary substrates, including polyethylene terephthalate (PET). These ZnO NSs/Au/PET-based biosensors are biocompatible and flexible. We prepared the flexible sensors that form conformal contact with the skin and minimizes the sweat volume to perform proper sweat analysis for continuous monitoring of the targeted biomarkers.

The research demonstrated highly sensitive, selective lactate, alcohol, and glucose sensors based on sonochemically synthesized ZnO-NFs. Biosensing capabilities of the fabricated sensors were characterized by cyclic voltammetry and electrochemical impedance spectroscopy measurements. The measured sensitivities were found to be significantly higher compared to the conventional sensors based on other electrode materials that require a binding agent. The repeatability measurements showed low relative standard deviation while the shelf-life studies demonstrated that the performance of the proposed sensors was significantly stable over a one-month period.

This platform would allow for non-invasive, continuous monitoring to ensure health and quality of life of patients; early detection of anomalies, developing and monitoring customized treatments, among many other potential health applications, thus saving countless lives.

TABLE OF CONTENTS

CHAPTER PAGE

CHAPTER I 1
INTRODUCTION 1
1.1 Background 1
1.2 Problem Hypothesis 4
1.3 Research Goal and Objectives 6
1.4 Dissertation Organization 6
1.5 References 8

CHAPTER II 11
LITERATURE REVIEW 11
2.1 Sonochemical Synthesis Technique of ZnO Nanoflakes 11
2.2 Current State-of-art in Wearable Biosensing 12
2.3 Sweat Analysis 14
2.3.1 Lactate Sensing Through Sweat 15
2.3.2 Alcohol Sensing Through Sweat 18
2.3.3 Glucose Sensing Through Sweat 20
2.4 Sensing Technique 22
2.4.1 Electrochemical Techniques 23
2.4.2 Optical Techniques 25
2.5 Conclusion 28
2.6 References 29

CHAPTER III 32
ZnO NANOFLAKES BASED IMMUNOSENSOR FOR ALCOHOL SENSING 32
3.1 Background 33
3.2 Materials and Method 37
3.2.1 Reagents and Chemicals 37
3.2.2. Fabrication of ZnO-NFs Based Immunosenso 38
3.2.3 Material Characterization 39
3.2.4 Electrochemical Characterization 41
3.3 Results and Discussion 42

3.3.1 CV Measurement 42
3.3.2 EIS Measurements 45
3.3.3 Repeatibility and Reproducibility Measurements 49
3.3.4 Shelf life-Studies 51
3.4 Conclusion 52
3.5 References 53

CHAPTER IV 58
ZnO NANOFLAKES BASED ENZYMATIC LACTATE BIOSENSORS 58
4.1 Background of Wearable Lactate Biosensor Measurement Systems 58
4.2 Experimental 61
4.2.1 Chemical and Apparatus 61
4.2.2 Fabrication and Surface Functionalization of ZnO-NFs Electrodes 62
4.2.3 Material Characterization of ZnO-NFs Based Electrodes 63
4.2.4 Working Principle of ZnO-NFs Based Lactat Sensor 66
4.3 Results and Discussions 67
4.3.1 Calibration of the Enzymatic Lactate Sensor Based on ZnO-NFs 67
4.3.2 Electrochemical Impedence Spectroscopy (EIS) Measurement 69
4.3.3 Measurement of Repeatibility and Reproducibility 71
4.3.4 Measurement of Lactic Acid in Biological Samples 72
4.4 Conclusion 73
4.5 References 74

CHAPTER V 78
THIN-FILM NANOSTRUCTURE-BASED ENZYMATIC ALCOHOL SENSOR 78
5.1 Background 79
5.2 Materials 81
5.2.1 Chemicals and Components 81
5.2.2 Fabrication Mechanism 82
5.2.3 Synthesis Technique 82
5.3 Results and Discussion 84
5.3.1 Characterizaion of the Electrodes 84
5.3.2 Calibration of AOX/ZnO-NFs/Au/PET Alcohol Sensor 85

5.4 Conclusion....86
5.5 References....87

CHAPTER VI....89
THIN-FILM NANOSTRUCTURE-BASED ENZYMATIC GLUCOSE SENSOR....89
6.1 Materials....90
6.1.1 Chemicals and Components....90
6.1.2 Fabrication Mechanism....90
6.1.3 Synthesis Technique....91
6.2 Results and Discussion....92
6.2.1 Characterizaion of the Electrodes....92
6.2.2 Calibration of GOX/ZnO-NFs/Au/PET Glucose Sensor....94
6.3 Conclusion....95
6.4 References....95

CHAPTER VII....97
MINIATURIZED, WEARBLE MULTI-CHANNEL POTENTIOSTAT....97
7.1 Experimental....97
7.1.1 Components and Apparatus....97
7.1.2 Interfacing Between Sensing Units and Integrated Potentiostat....98
7.1.3 Working Principle of the Potentiostat....99
7.1.4 Digital to Analog Convertor (DAC) Unit....100
7.1.5 Summing Amplifier Unit....100
7.1.6 Multiplexing/Demultiplexing Unit....102
7.1.7 Controlling Amplifier Unit....102
7.1.8 Electrochemical Signal Generation....102
7.1.9 Current to Voltage Converter (CVC) Unit....103
7.1.10 Selection of Arduino NANO 33 BLE....104
7.2 Results and Discussion....104
7.3 Conclusion....105
7.4 References....106

CHAPTER VIII....107
CONCLUSIONS....107

8.1 Summary and conclusions.....107
8.2 Recommendations for future research.....108
VITA.....109

LIST OF TABLES

TABLE PAGE

Table 3-1. Comparison of fabrication of ZnO-NSs based immunosensor with the state-of-the-art technologies 45

Table 3-2. Theoretical fit of experimental results obtained in stepwise fabrication process of BSA/EtG-AB/ZnO-NFs/Au/PET sensor from EIS measurements 49

Table 4-1. Determination of lactate in human sweat using the ZnO-NFs/Au/PET/Lox electrode 73

Table 7-1. Input/output voltage of the summing amplifier with PWM levels. 100

LIST OF FIGURES

FIGURE PAGE

Figure 1-1: Dissertation Organization 7

Figure 2-1: (a)Exercise intensity mode followed during continuous on-body lactate monitoring study wearing a lactate tattoo biosensor [183] (b) mouth-guard biosensor [189] (c) Response of the OECT vs. lactate concentration [182]] (d) contact lens based L-lactate sensor and its performance for monitoring of l-lactate levels in tear fluid [122] (e) eyeglasses biosensor system, which integrates a wireless circuit board along the arms of the spectacles and two electrochemical sensors for lactate and potassium on to the nose-bridge pads [193]. 16

Figure 2-2: Wearable non-invasive sweat alcohol sensor a)-i) alcohol detection cell for monitoring sweat alcohol concentration after iontophoretic stimulation with depiction of alcohol recognition reactions (ii) sweat alcohol levels in 40 human subjects with concurrent BAC b)-i) Schematic representation of screen-printed, wearable ionotophoretic delivery and alcohol detection platform (ii) depiction of wireless transmission of alcohol sensing data using flexible printed circuit board (iii) collection on-body alcohol detection data with human subjects, with or without drinking, correlated to concurrent BAC [26]. 19

Figure 2-3: Epidermal sweat glucose monitoring using a flexible sensor array. (a) photograph detection of wearable, flexible, sensor array applied to a sensor array (b) schematic representation of multiplexed, flexible sensor array (c) photograph detection of on-body sweat analysis using flexible sensor array with sweat generated through exercise (d) glucose signal of on body glucose monitoring using flexible sensor array compared to ex-situ calibration using collected sweat (e) photograph detection coupled autonomous sweat extraction and flexible sensing array (f) schematic representation of iontophoresis and sensing mode operation for autonomous sweat extraction and multiplexed, flexible sensing array (g) comparison of on body sweat glucose and blood glucose analysis in human subjects before and after a meal [28] 21

Figure 3-1: (a)Illustration of ZnO-NFs, prepared using sonochemical method along with immobilization anti-EtG antibody onto ZnO-NFs to fabricate electrochemical EtG immunosensor (b) Electrochemical response at the fabricatd electrode (c) Fabricated sensing electrode and its size and (d) its flexible nature. 38

Figure 3-2: (a) HRTEM at the edge of a flake with fringes almost parallel to the edge with a spacing of 2.74 Å (b) SAED image of ZnO-NFs (c) SEM characterization images of ZnO-NFs/Au/PET Substrate (before immobilization of EtG-AB) (d) SEM characterization images for ZnO-NFs/Au/PET substrate (After

immobilization of EtG-AB) (e) Raman spectra on ZnO-NFs/Au/PET electrode (f) Raman spectra of EtG-AB/ZnO-NFs immunoelectrodes 40

Figure 3-3: Reduction in the magnitude of oxidation current at different stages of the fabrication form bare Au electrode to BSA/EtG-AB/ZnO-NFs/Au/PET immuno-electrode. 43

Figure 3-4: (a) CV studies of immunosesnors as function of EtG concentration varying from 1ng/ml to 100ug/ml for BSA/EtG-AB/ZnO-NFs/Au/PET electrode (b) Calibration curve of the fabricated BSA/EtG-AB/ZnO-NFs/Au/PET biosensor for EtG concentration of 1ng/ml, 10ng/ml,100ng/ml and 100ug/ml 44

Figure 3-5: (a) Rise of Rct from bare Au electrode to BSA/ EtG-AB /ZnO-NFs/Au/PET immunoelectrodes, (b) Randles equivalent circuit, (c) Charge in EIS of BSA/ EtG-AB/ZnO-NFs/Au/PET immunoelectrode with respect to EtG concentrations with the frequency range of 1 Hz-13000 Hz (d) Dose responses of total impedance output in histogram for calibrating sensor for EtG (inset: the linear regression curve for real impedance, imaginary impedance and total impedance for the EtG sensor) and (e) Bode plot impedence spectra and (f) phase spectra for understanding the behavior of the sensor with the change of concentrations.....47

Figure 3-6: (a) Repeatability study for three different concentrations (b) Reproducibility study in between of two identical sensors for the concentration of 100 ng/ml 50

Figure 3-7: Shelf life of the ZnO-NFs based immunosensor, where the measurements were carried out for 100ug/ml of EtG (a) Short-time stability test during five consecutive days and (b) The performance of stability of one in a week during the period of 35 days after two months of short-time stability test. 52

Figure 4-1: (a) Enzymatic lactate sensor: Fabricating and immobilizing process (b) Working mechanism and redox reaction of enzymatic lactate sensor (c)PET/Au/ZnO-NFs based electrode and (c) flexibility of PET/Au/ZnO-NFs electrode 63

Figure 4-2: (a) SEM image of PET/Au/ZnO-NFs (b) FSEM image (3D) of PET/Au/ZnO-NFs (b) FSEM image (3D) of PET/Au/ZnO-NFs (c) SEM image of PET/Au/ZnO-NFs/LOx (d) SAED pattern of ZnO-NFs (e) AFM image of PET/Au/ZnO-NFs (f) HRTEM at the edge of a flake (g) Raman spectra on PET/Au/ZnO-NFs electrode and (h) Raman spectra of PET/Au/ZnO-NFs/LOx electrodes (i) EDS data ensures the grown of nano flakes are pure ZnO. 65

Figure 4-3: (a) CV studies of LOx immobilized ZnO NFs biosensor for LA concentration varying from 10 pM to 20 mM (b) Linear curve fitting (c) Responses

of PET/Au/ZnO-NFs/LOx electrode (solid blue circles) and PET/Au/DTSP/LOx electrode (solid red squares) for L-lactic acid detection.....69

Figure 4-4: Nyquist plots of EIS response of PET-Au-ZnO NFs-LOx when the immobilization of series concentrations of five samples: 1 nM to 20 mM concentrations. The inset shows the equivalent circuit model and (b) Dose responses of total impedance output for calibrating sensor for different concentration (1 nM-20 mM) of lactic acid.....70

Figure 4-5: Repeatability study of a single ZnO NFs based enzymatic lactate sensor for three different concentrations: 1 nM, 1 mM, and 20 mM identical sensors used for reproducibility study for the concentrations of 20 mM.....71

Figure 5-1: Cyclic Voltammetry studies with ethanol concentration varying from 1mg/dL to 400md/dL for ZnO NFs/Au/PET/AOX electrode.....84

Figure 5-2: Linear calibration fit (b) Calibration curve within the range from 1mgldL to 100mg/dL (segment 1) (c) Calibration curve within the range from 100mg/dL to 400mg/dL (segment 2).....85

Figure 6-1: (a) SAED and (b)HTEM of the center and edge of the flakes (c) SEM of PET/Au/ZnO-NFs and (d)PET/Au/ZnO-NFs/GOX electrode.....93

Figure 6-2: (a) Cyclic Voltammetry studies with glucose concentration varying from 1mM to 20mM for ZnO NFs/Au/PET/GOX electrode (b) Linear calibration curve within the range from 1mM to 20mM EtG.....94

Figure 7-1: Block diagram of the wireless sensing platform.....98

Figure 7-2: (a) Detailed block diagram of the circuit of the sensing platform, and (b) the circuit layout in Proteus chart representing steps involved in selective ethanol detection.....101

Figure 7-3: (a) DAC and summing amplifier output voltage Vs current; and (b) Counter electrode current Vs scanning voltage curve for different resistance values. 102

LIST OF ACRONYMS

IEP	Isoelectric point
1D	one dimensional
2D	Two dimensional
NWs	Nanowalls
NFs	Nanoflakes
NRs	Nanorods
AFM	Atomic force microscope
TEM	Transmission Electron Microscope
FESEM	Field Emission Scanning Electron Micros
BSA	Bovine saline albumin
CV	Cyclic Voltammetry
UV	UltraViolet
ZNH	Zinc Nitrate Hexahydrate
HRTEM	High Resolution Transmission Electron Microscope
EIS	Electrochemical Impedance Spectroscopy
XRD	X- ray diffraction
HMT	Hexamethylene tetramine
ZAD	Zinc Acetate dehydrate
PET	Polyethylene terephthalate
SEM	Scanning electron microscope
SAED	Selective area electron diffraction
EDX	Energy-dispersive X-ray
LoD	Limits of detection
POC	Point-of-care
DI	Deionized

EDS	Energy dispersive X- ray spectroscopy
BAC	Blood alcohol content
DUI	Drinking under the influence
BLE	Bluetooth low energy
ADC	Analog-to-digital converter
AOX	Alcohol oxidase
LOX	Lactate oxidase
EtG	Ethyl-glucuronide
AB	Antibody
PBS	Phosphate buffered Saline
NSs	Nano-structures
SD	Standard deviation
R_{ct}	Charge transfer resistance
Z_{tot}	Total impedance
LoA	Limits of Agreement
LDH	Lactate dehydrogenase
CPE	Constant Phase Element
LDH	Lactate dehydrogenase
Ti	Titanium
CVC	Current to Voltage Converter
PWM	Pulse Width Modulator
DAC	Digital to Analog Converter
CE	Counter Electrodes
PCB	Printed Circuit Board

CHAPTER I
INTRODUCTION

1.1 Background

Biosensing is the process of sensing bio-compounds through monitoring the physical, biological, or chemical changes that they cause with their presence [1,2]. Two significant types of biosensing techniques are commercially available: optical and electrochemical. In electrochemical bio-sensing, enzyme or antibody coupling (as biocatalyst) is a vital archetype to amplify signals. Immunosensors and enzymatic biosensors are simple, direct, and fast responses with biocompatibility, high selectivity, and sensitivity. Electrochemical metal-oxide-based biosensors [3,4] have demonstrated improved performance over other sensing methods, such as optical [5], colorimetric [6], or fuel cell-based [7-9] sensors. Their wide detection range, rapid and selective detection approach, and higher sensitivity make them the preferred sensing method for many biomolecules in point of care and wearable health quality monitoring applications. To achieve low detection limits and high sensitivity, the immobilizing matrix used in biosensors should have high surface functionality, high biomolecule loading, and a small resistance to electron transport with a high electron transfer rate [10]. This encourages researchers to explore the utilization of inorganic semiconductor nanostructures (NSs) as the potential immobilizing matrix for immunosensor and enzymatic sensor development to detect desired target analytes [11].

Human sweat is a vital body fluid that contains rich information about our health and fitness conditions. Sweat analysis is entirely non-invasive and reliable and thus opens a new door to diagnose and monitor health, optimize performance and save billions on

healthcare costs. As sweat is easily accessible from the skin surface of the human body, it has been fascinating for researchers for many years. Sweat is secreted by the eccrine glands and is rich physiological data containing electrolytes and metabolites. This upfront access extracts a particularly useful biofluid as it can be retrieved using non-invasive methods instead of other biofluids such as blood [12]. Therefore, for next-generation digital biomarkers, sweat analysis has the potential to provide non-invasive metabolic feedback.

Metal oxide-based nanostructures with a high isoelectric point (IEP) have recently become extremely significant as nanomaterials, which provide an effective and required surface for the immobilization of biomolecules with desired polarized plane orientation, better conformation, and high biological activity contributing to the development of enhanced biosensing platforms [13]. Among various semiconducting metal oxide-based nanomaterials, Zinc oxide (ZnO) has been found as an excellent candidate for wearable biosensing applications. Its piezoelectric nature, high catalytic efficacy, biocompatibility, chemical stability in physiological environments, low toxicity, and a high isoelectric point (IEP) of about 9.5 make it potential in many biosensing applications [14]. ZnO nanostructures (NSs) with different morphologies such as nanorods, nanowalls, nanobelts, and quantum dots have been used as immobilizing matrices in the fabrication of biosensors for the detection of physiologically relevant biomarkers such as cholesterol, galactose, glucose [15]. Considering their promising properties and potential applications, many techniques have been developed to synthesize various ZnO-NSs.

Compared to bulk materials, the two-dimensional 2D ZnO nanoflakes (ZnO-NFs) provide unique sensing advantages with polarized (0001) plane [16] orientation and high surface charge density, which could enhance antibody loading and thus improve sensing

performance. The high isoelectric point allows immobilization of most biomolecules without any additional binding layer [17,18]. This provides a direct, stable pathway for rapid electron transport when an analyte is immobilized on NFs and improves electron transfer rate. Moreover, the performance of a ZnO-based biosensor can be improved by tailoring the properties of the ZnO–biomolecule interface via engineering of morphology, plane orientation, particle size, effective surface area, functionality, adsorption capability, and electron-transfer properties [19]. Flexible platform technologies garner interest owing to their lightweight, low modulus, low cost, and high stretchability [20]. Such conformal factors are paramount to the convenient provision of vital physiological insights on a flexible, biocompatible platform. A need exists for robust, portable, and flexible biosensing platforms in clinical applications for disease diagnosis and treatment monitoring [21]. Such platform technologies can provide alternative solutions to point-of-care (POC) diagnostic assays for broad applications in personalized medicine. This necessitates an urge to mimic the physiological skin-to-skin contact entailing tactile stimuli and environmental variations, distinguishing between bodily movements and extracting the required physiological information. The ZnO-NFs have been fabricated on flexible polyethylene terephthalate (PET) substrate, which has gained popularity for wearables because of its intrinsic elasticity, thermal stability, hydrophobicity, excellent dielectric properties, low coefficient of thermal expansion, structural resiliency against repeated bending forces, and compatibility with roll-to-roll fabrication processes for low cost and scalable manufacturing. The biocompatibility and small form factor make this sensor a strong candidate for wearable biosensing and continuous monitoring device.

A single-step sonochemical approach was developed to synthesize a thin layer of ZnO-NFs virtually on any substrate [22]. This technique is fast, CMOS friendly, catalyst-free, less expensive, and ecologically benign. The rate of reaction of the sonochemical approach is 100 times faster than conventional hydrothermal procedures, which enables a well-oriented growth on PET over an extensive range. The temperature for the process is low enough to permit the application of different materials, for example, fabrics, paper, and polymers. The inherent properties of ZnO-NFs, such as its thermal stability, intrinsic elasticity, low thermal expansion coefficient, hydrophobicity, structural resiliency counter to frequent twisting forces, excellent dielectric properties, and its easy roll-to-roll manufacturing processes and low manufacturing cost, make it attractive for the applications in biosensing.

1.2 Research Hypotheses

This research addresses the challenge of developing a highly sensitive, selective, and reliable, low-cost, wearable sweat analysis sensor for monitoring critical biomarkers. We specifically investigated the following research hypotheses:

1. *Sonochemical synthesis allows the controllable growth of ZnO nanostructures on arbitrary substrates.*

A novel sonochemical synthesis method allows stable and well-oriented growth of ZnO-NSs on arbitrary substrates such as flexible polymers, fabrics, and paper with process temperature less than 50 °C. The growth of ZnO-NFs could be controlled by the energy and precursor concentrations. The thickness of a single nanoflakes remains constant around 15-20 nm irrespective of the time of synthesis. The dimension of the largest 2D ZnO nanoflakes is 10 μm at 15 min and remain the same as the time is increased. By controlling

the time and cycles of synthesis, the dimension, thickness and density of 2D ZnO nanoflakes can be efficiently controlled.

2. *ZnO nanostructures provide a mediator-free and significantly improved electrochemical sensing platform for sweat analysis.*

2D ZnO nanoflakes (ZnO-NFs) provide unique sensing advantages with high surface charge density, thermal stability, wide bandgap, and high exciting binding energy. These properties could offer a direct, stable pathway for rapid electron transport when an analyte is immobilized on NFs and improves the electron transfer rate. The high isoelectric point allows immobilization of most biomolecules without any additional binding layer. ZnO-NSs has a high isoelectric point which is suitable to enhance the long-term stability of the enzymes. 2D ZnO-NFs with high IEP (~9.5) have positive surface charge density, which provides an active and required surface for the immobilization of low-IEP (~4.2) biomolecules with high biological activity contributing to the development of enhanced biosensing platforms.

3. *ZnO nanostructure-based electrodes can be integrated with a miniaturized multi-channel potentiostat to develop wearable sweat analysis platforms.*

Potentiostats with integrated data acquisition units in small form factor and low power requirements are needed for wearable sweat analysis platforms. Modern microcomputers (e.g. Arduino) with integrated Bluetooth capabilities along with highly efficient circuit components can be used to build miniaturized multi-channel potentiostat integrated with a three-electrode system to monitor multiple analytes in sweat.

Detailed findings in response to these questions are presented in the subsequent chapters.

1.3 Research Goal and Objectives

The goal of this research is to develop a highly sensitive, wearable enzymatic and immune sensors array for continuous and selective sensing of ethanol, lactate, and glucose in human sweat. Considering the above-mentioned issues, the specific objectives are:

1. To study the synthesis of ZnO nanostructures using the sonochemical technique on flexible substrates and their material characteristics;
2. To investigate mediator-free electrochemical biosensing characteristics of the sonochemically synthesized ZnO nanostructures towards developing a wearable sweat analysis platform.
3. Fabricate multiplexed electrochemical sensor platform integrated with miniaturized potentiostat for wearable swear analysis.

1.4 Dissertation Organization

This dissertation includes eight chapters. Figure 1-1 summarizes the contents of the next seven chapters followed by this chapter (Chapter I: Introduction).

Figure 1-1: Dissertation Organization

1.5 References

1. Mehrotra, P., "Biosensors and their applications – A review," J Oral Biol Craniofac Res., vol. 6, pp. 153–159, 2016.

2. Bhalla, N., Jolly, P., N. Formisano and P. Estrela, "Introduction to biosensors" Essays in Biochem., vol. 60, pp. 1-8, 2016.

3. Santra, S., Sinha, A.K., A. De Luca, S. Z. Ali, F. Udrea, P. K. Guha, S. K. Ray, and J. W. Gardner, "Mask-Less Deposition of Au–SnO2 Nanocomposites on CMOS MEMS Platform for Ethanol Detection," Nanotechnology, vol. 27, no. 12, pp. 125502, 2016.

4. Jiang, G., Goledzinowski, M., Comeau, J. E., Zarrin, H., Lui, G. V., Lenos, J., Veileux, A., Liu, G., Zhang, J., and Hemmati, S.,"Free Standing Functionalized Graphene Oxide Solid Electrolytes in Electrochemical Gas Sensors," Adv. Funct. Mater, vol. 26, no. 11, pp. 1729–173, 2016

5. Semwal, V., Shrivastav, A. M., Verma, R., and Gupta, B.D., "Surface Plasmon Resonance Based Fiber Optic Ethanol Sensor Using Layers of Silver/silicon/hydrogel Entrapped with ADH/NAD," Sensors Actuators B Chem., vol. 230, pp. 485–492, 2016.

6. Williams, M. B., and Reese, H. D., "Colorimetric Determination of Ethyl Alcohol," Anal. Chem., vol. 22, no.12, 1556-1561,1950.

7. Jalal, A. H., Umasankar, Y., and Bhansali, S., "Development and Characterization of Fuel Cell Sensor for Potential Transdermal Ethanol Sensing," ECS Transactions, 2016, vol. 72, no. 31, pp. 25-31, 2016.

8. Swift, R. M., Martin, C. S., Swette, L., LaConti, A., and Kackley, N., "Studies on a Wearable, Electronic, Transdermal Alcohol Sensor," Alcohol. Clin. Exp. Res., vol. 16, no. 4, pp. 721–725, 1992.

9. Umasankar, Y., Jalal, A. H., Gonzalez, P. J., Chowdhury, M., Alfonso, A., and Bhansali, S., "Wearable alcohol monitoring device with auto-calibration ability for high chemical specificity," in 2016 IEEE 13th International Conference on Wearable and Implantable Body Sensor Networks (BSN), San Francisco, CA, 2016, pp. 353-358, 2017

10. Vabbina, P. K., Karabiyik, M., Al-Amin, C., Pala, N., Das, S., Choi, W., Saxena, T., and Shur, M., "Controlled Synthesis of Single-Crystalline ZnO Nanoflakes on Arbitrary Substrates at Ambient Conditions," Part. Part. Syst. Charact., vol. 31, no. 2, pp. 190–194,2014.

11. Vabbina, P. K., Nayyar, P., Nayak, A. P., Katzenmeyer, A. M., L. VJ, Pala, N., Islam, M. S., and Talin, A. A., "Synthesis of Crystalline ZnO Nanostructures on Arbitrary Substrates at Ambient Conditions," International Society for Optics and Photonics, vol. 8106, pp. 81060H, 2011.

11. Mena-Bravo, A., Luque de Castro MD., "Sweat: a Sample with Limited Present Applications and Promising Future in Metabolomics," J. Pharm. Biomed. Anal., Vol. 90, pp. 139–147, 2014.

12. Panneer Selvam, A., Muthukumar, S., Kamakoti, V. and Prasad, S. "A Wearable Biochemical Sensor for Monitoring Alcohol Consumption Lifestyle Through Ethyl glucuronide (EtG) Detection in Human Sweat," Sci. Rep., vol. 6, no. 1, pp. 23111, 2016.

13. Arya, S. K., Saha, S., Ramirez-Vick, J. E., Gupta, V., Bhansali, S., and Singh, S. P., "Recent Advances in ZnO Nanostructures and Thin Films for Biosensor Applications: Review," Anal. Chim. Acta, vol. 737, pp. 1–21,2012.

14. Psychoyios, V. N., Nikoleli, G.-P., Tzamtzis N., Nikolelis, D. P., Psaroudakis, N., Danielsson, B., Israr, M. Q., and Willander, M.,"Potentiometric Cholesterol Biosensor Based on ZnO Nanowalls and Stabilized Polymerized Lipid Film," Electroanalysis, vol. 25, no. 2, pp. 367–372,2013.

15. Vabbina, P. K., Karabiyik, M., Al-Amin, C., Pala, N., Das, S., Choi, W., Saxena, T., and Shur, M., "Controlled Synthesis of Single-Crystalline ZnO Nanoflakes on Arbitrary Substrates at Ambient Conditions," Part. Part. Syst. Charact., vol. 31, no. 2, pp. 190–194, 2014.

16. Zhou, J., Xu, N., and Wang, Z. L., "Dissolving Behavior and Stability of ZnO Wires in Biofluids: A Study on Biodegradability and Biocompatibility of ZnO Nanostructures," Adv. Mat., vol. 18, no.18, pp. 2432-2435,2006.

17. Li, Z., Yang, R., Yu, M., Bai, F., Li, C., and Wang, Z. L., "Cellular Level Biocompatibility and Biosafety of ZnO Nanowires," J. Phys. Chem. C, vol. 112, no. 51, pp. 20114–20117, 2008.

18. Vabbina, P. K., Sinha, R., Ahmadivand, A., Karabiyik, M., Gerislioglu, B., Awadallah, O., and Pala, N., "Sonochemical Synthesis of a Zinc Oxide Core–Shell Nanorod Radial P–n Homojunction Ultraviolet Photodetector," ACS Appl. Mater. Interfaces, vol. 9, no. 23, pp. 19791–19799, 2017.

19. Chen X., and Bao, Z., "Flexible and Stretchable Devices," Adv. Mater., vol. 28, pp. 4177–4179, 2016.

20. Shafiee, H., Asghar, W., Inci, F., Yuksekkaya, M., Jahangir, M., Zhang, M.H., Durmus, N.G, Gurkan, U.A., Kurtizkes, D.R., and Demirci, U., “Paper and flexible substrates as materials for biosensing platforms to detect multiple biotargets”, Sci. Rep., vol. 5, pp. 8719, 2015.

21. Pu, D., Liu, F., Dong, Y., Ni Q., and Fu, Y., “Interfacial adhesion and mechanical properties of PET fabric/PVC composites enhanced by SiO_2/Tributyl citrate hybrid sizing”, Nanomat., vol. 8, pp. 898, 2018.

CHAPTER II
LITERATURE REVIEW

This chapter provides a comprehensive literature review on the following topics: (a) sonochemical synthesis technique of ZnO nanostructures; (b) current state-of-art in wearable biosensing; (c) detection mechanisms explored in wearable biosensing, and (d) sweat analysis for ZnO nanostructure-based biosensors.

2.1 Sonochemical Synthesis Technique of ZnO Nanoflakes

In this dissertation, a single-step sonochemical approach was developed to synthesize a thin layer of ZnO-NFs virtually on any substrate [1]. This technique is fast, CMOS friendly, catalyst-free, less expensive, and ecologically benign. The rate of reaction of the sonochemical approach is 100 times faster than conventional hydrothermal procedures, which enables a well-oriented growth on PET over an extensive range. The temperature for the process is low enough to permit the application of different materials, for example, fabrics, paper, and polymers. The inherent properties of ZnO-NFs, such as its thermal stability, intrinsic elasticity, low thermal expansion coefficient, hydrophobicity, structural resiliency counter to frequent twisting forces, excellent dielectric properties, and its easy roll-to-roll manufacturing processes and low manufacturing cost, make it attractive for applications in biosensing.

For the NFs synthesis, a solution mixture with 20 mM ZNH and 20 mM HMT was prepared by stirring with a magnetic stir bar at the speed of 350 rpm at room temperature and pressure for the duration of 5 min to ensure the progress of 2D ZnO- NFs. By using a commercial high-intensity ultrasound set up, the submerged substrate in the solution was

then irradiated by using15 min. of four cycles at the intensity of 30 Wcm^{-2} and the frequency of 20 kHz. The temperature was maintained by ≤ 50° C of the aqueous mixture of ZNH and HMT. Lastly, DI water and N_2 were used for cleaning the substrate after each cycle in a similar manner.

ZnO nanoflakes (ZnO-NFs) offer several exclusive advantages compared to bulk materials. For example, polarized (0001) plane orientation enhances enzyme immobilization which improves sensing performance [2]. A high isoelectric point (9.5) of ZnO NFs [3,4] enhances the immobilization of any biomolecules, which eliminates the necessity of an additional binding layer. This elimination of additional layers and immobilization of the enzyme offers a steady and shorter pathway for quick electron transportation, increasing the electron transfer rate. Moreover, modification of the ZnO–biomolecules interface through the plane orientation enriches the sensing ability of a ZnO NFs-based enzymatic sensor. Engineering of the morphology and size of NFs, effective surface area and adsorption capability, functionality [5] also improve electron transport.

2.2 Current State-of-art in Wearable Biosensing

A cost-effective, user-friendly, minimally invasive, continuous, and real-time sensing technique to diagnose diseases can greatly improve healthcare and personal safety management. Wearable sensors or sensor arrays (e-noses), through precise calibration, play an alternate role in the easy-to-use, fast, precise, and continuous monitoring of specific diseases. According to the International Union of Pure and Applied Chemistry (IUPAC), “biosensors are considered as devices that transform biochemical information into an analytically useful signal.” [5] For timely evaluation of one’s concerning health condition,

the biosensors need [5]: i. accurate measurement, ii. rapid assessment, and iii. selective detection. These properties of the sensor enable a physician to accurately diagnose the specific disease and initiate required therapy to prevent further aggravation of the disease. The phenotypic characteristics of their excretion can be analyzed through the observation of their real-time sensor data [18].

Biosensing techniques have prominent prospects in biomarkers' detection on a wearable platform. There are different sensing techniques that have been employed for the detection of various biomarkers, such as electrochemical, chemical-resistive, optical, piezoelectric, and surface acoustic wave (SAW) sensors. These sensors have been miniaturized by advancements in micromachining and nanotechnology [29]. The incorporation of nanomaterials is known to influence their sensing performance and assists in a multi-sensing arrays platform [29]. The use and combination of different kinds of nanomaterial are therefore gaining interest in the design of clinical and diagnostic tools due to their advantages of higher surface-to-volume ratios. Their specific forms provide faster response and recovery times, in addition, to support specific detection through suitable alterations of their physical and chemical properties. Assisting in very-large-scale integration manufacturing and miniaturization to enable portability, they allow integration in point-of-care (POC) devices [31]. Current wearable biosensors in the market use mostly four measurement techniques [24]: optical, electrochemical, chemical-resistive sensors. Most of these sensors suffer from instability, non-linearity, cross-selectivity, inaccuracy at low concentrations, and some of them are not portable [5]. Electrochemical biosensors have typically been found to be most suitable for long-term sensing. These sensors offer

simplicity, relatively high accuracy, sensitivity, long working lifetime, scalability, and portability.

2.3 Sweat Analysis

The quality of sweat analysis depends on the efficiency of sample collection and the accuracy and sensitivity of analytical methods [2]. Various analytical approaches have been developed for the analysis of the unmetabolized drug in sweat. Most of the sweat analyzers work on the principle of potentiometry, colorimetry, conductivity, or osmolarity [43]. For the sweat analysis, GC-MS coupled with electron impact ionization is considered the most frequently used equipment [7]. Additionally, for the determination of drug concentration in sweat, LC-MS/MS coupled with electrospray ionization has also been successfully used. For sweat analysis, the selection of analytical instruments depends on the nature of the target analytes. For single moiety analysis, various analyzers are used, such as potentiometric Orion skin ion-selective electrode (ISE) for chloride (Orion Research, Cambridge, MA), or the colorimetric Scandipharm CF Indicator System chloride patch (Scandipharm, Birmingham, AL), the Wescor Sweat-Chek conductivity analyzer (Wescor, Logan, UT), and sweat osmolarity analyzer (Nikon Research, Cambridge, ML) [49]. As the volume of sweat samples varies, it is important to normalize sweat volume to get reliable results. Different studies suggested that it is suitable to use sodium ion concentration than potassium ion concentration for the normalization of the sampled volume of sweat. Sweat contains important biomarkers, electrolytes, and metabolites. Sweat has a significant influence on health care due to its noninvasive, laboratory-

independent, on-skin point-of-care facilities. These advantages allow the collection and sharing of personal health data, remote patient monitoring in real-time.

2.3.1 Lactate Sensing Through Sweat

Khodagholy *et al*. presented for the first time the detection of lactate in a relevant physiological range using an organic electrochemical transistor (OECT) sensor with an ion gel solid-state electrolyte on a flexible biosensor [6] as shown in Figure 4(c). They envision the use of this sensor as a wearable bandage-type sensor, which can be worn during exercise or health monitoring, allowing sweat to diffuse into the sensor with consequent detection of the lactate analyte. Jia *et al*. [7] demonstrated a noninvasive lactate sensor that was fabricated on a flexible substrate. This tattoo-based sensor was functionalized with LOx for the continuous monitoring of lactate levels from human sweat, as shown in Figure 2-1(a). The sensor was selective to lactate and was employed on human subjects for real-time monitoring of lactate throughout long-duration workouts. The resulting temporal lactate profiles reflect the changes in the production of sweat lactate upon varying the exercise intensity. This transdermal lactate biosensor shows linearity up to 20 mM of concentration. Cai *et al*. [8] demonstrated an ECL-based lactate biosensor with a detection limit of 8.9×10^{-12} mol/L was observed for real sweat samples. The biosensor was feasible for detecting the lactate in sweat samples of athletes during the exercise for evaluation of exercise degree.

Different authors have reported the possibility of determining the anaerobic threshold through saliva lactate concentration in incremental protocol and exercise using a cycle ergometer verifying high correlations between that in blood and in saliva.

Schabmueller *et al.* [9] demonstrated an amperometric lactate sensor from where lactate concentration levels were determined from the saliva during the workout in a real-time and

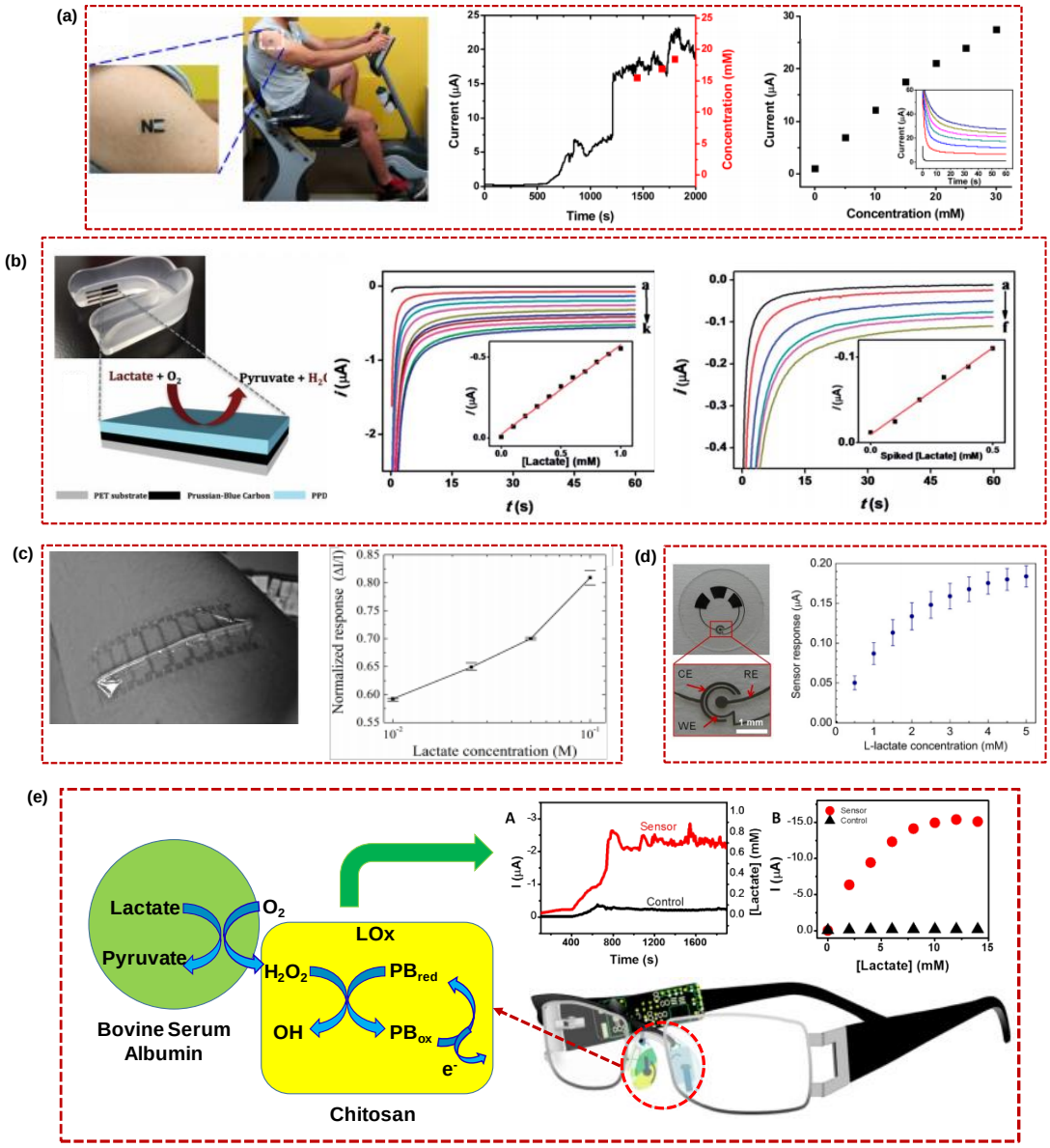

Figure 2-1: (a) exercise intensity mode followed during continuous on-body lactate monitoring study wearing a lactate tattoo biosensor (b) mouth-guard biosensor (c) Response of the OECT vs. lactate concentration (d) contact lens based L-lactate sensor and its performance for monitoring of l-lactate levels in tear fluid (e) eyeglasses biosensor system, which integrates a wireless circuit board along the arms of the spectacles and two electrochemical sensors for lactate and potassium on to the nose-bridge pads. [9]

non-invasive manner. Saliva was drawn due to the capillary effect to expedite the detection of lactate. This approach allowed for portability, with permanent real-time measurements and rapid response time. Kim *et al*. have also reported [10] a wearable metabolite sensor for detecting lactate in saliva, incorporating a printable enzymatic electrode on a flexible PET substrate on a mouth-guard as in Figure 2-1(b). This non-invasive mouth-guard sensor targets continuous monitoring of the said analyte enabling stability with high sensitivity and selectivity. Claver *et al.* demonstrated [11] an electro-chemiluminescent disposable biosensor for lactate in saliva through enzymatic recognition based on LOx. It provided a response from 10^{-5} to 5 $\times 10^{-4}$ M with a detection limit of 5×10^{-6} M and provided an RSD of 3.30%. This saliva-based lactate, prepared by hybrid materials of ZnO nanoparticles and multiwalled carbon nanotubes (MWCNT) in a glassy carbon electrode surface and then modified with LOx and Nafion, shows good repeatability, quick detection time (the 20s), and versatility [12].

Lately, wearable and flexible biosensors have attracted interest due to their lightweight and flexible nature. Contact lenses provide a safe, noninvasive platform for the collection of such associated biometric information, eliminating sampling procedures. A minimally invasive contact lens-based lactate sensor was fabricated for monitoring lactate levels in tear fluid for health care and assessment by Thomas et al. [13]. The platinum sensing structures were functionalized by cross-linkage of LOx with glutaraldehyde and bovine serum albumin and coated with medical-grade polyurethane for detecting lactate well within the physiological range, as shown in Figure 2-1(d). Their dual-sensor design also was reported to have had minimal interference with a Nafion membrane and functional at temperatures close to that of the eyes. Having been built on a polymer substrate, this also

provides good biocompatibility with the eyes to be worn like a contact lens [13]. Different isoenzyme forms of pyruvate, which is produced by glycolysis and converted to lactate by LDH, are present in a contact lens, and under normal aerobic conditions, it has been observed that around 70% of the glucose is converted to lactate. Wang *et al*. designed an amperometric lactate biosensor connected to nose-bridge pads, as shown in Figure 2-1(e). This can be interfaced with an electronic backbone on spectacle glass arms and can continually sense lactate for a few hours. Its positioning on separate nose pads minimized cross-talk and enabled isolated fabrication and replacement. These can reportedly transmit data wirelessly through Bluetooth to a remote mobile host device for data analysis and visualization. Here, the nose-bridge pads are interchangeable with multifunctional sensing applications.

2.3.2 Alcohol Sensing Through Sweat

Prolonged alcohol consumption can promote various fatal diseases, such as fatty liver disease, alcoholic hepatitis, liver cirrhosis, Wernicke-Korsakoff Syndrome, hepatic encephalopathy and fetal alcohol spectrum disorders, heart diseases, alcohol-induced pancreatitis, and cancers [1,2]. The excessive consumption of alcohol causes many health issues, such as colon, rectum, mouth, and throat cancers, liver cirrhosis, stroke, cardiovascular disease, and several psychiatric comorbidities. Alcohol addiction treatments also require close monitoring of consumption. The correlation of alcohol concentration levels in sweat with the blood alcohol content (BAC) encourages developing a wearable sensing platform for alcohol detection noninvasively, continuously, and in real-time. Moreover, sweat is considered one of the most useful body fluids for biosensing

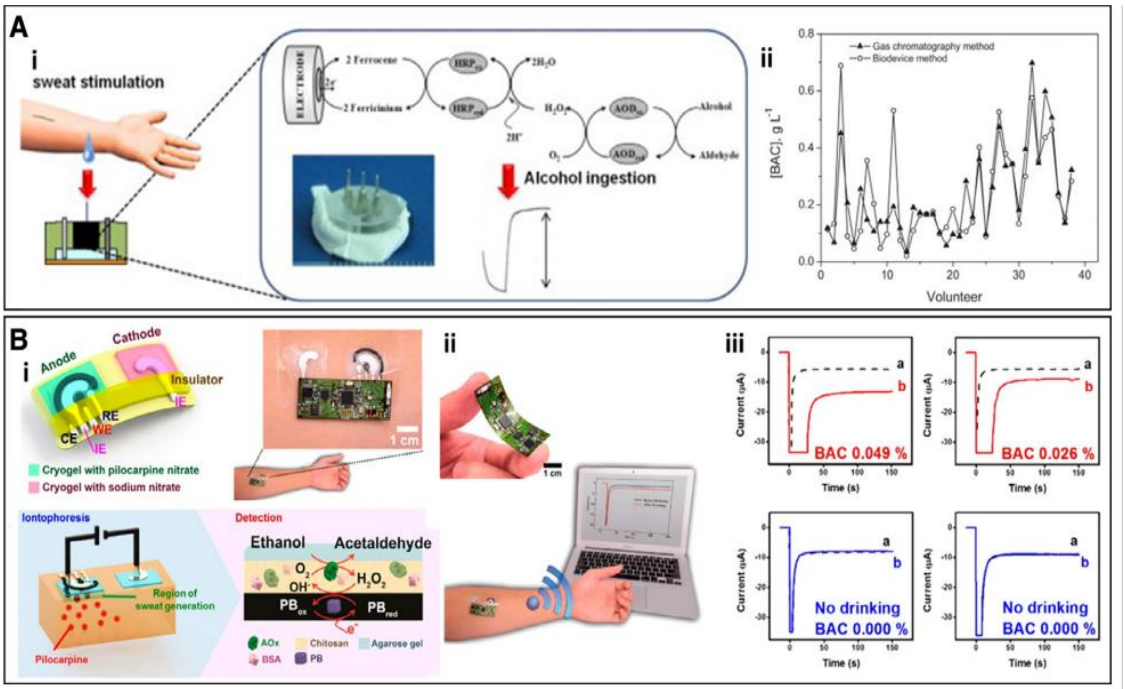

Figure 2-2: Wearable non-invasive sweat alcohol sensor a)-i) alcohol detection cell for monitoring sweat alcohol concentration after iontophoretic stimulation with depiction of alcohol recognition reactions (ii) sweat alcohol levels in 40 human subjects with concurrent BAC b)-i) Schematic representation of screen-printed, wearable ionotophoretic delivery and alcohol detection platform (ii) depiction of wireless transmission of alcohol sensing data using flexible printed circuit board (iii) collection on-body alcohol detection data with human subjects, with or without drinking, correlated to concurrent BAC [26].

applications since it contains several biomarkers with crucial medical information and is easy to collect. Enzyme-based electrochemical biosensors are promising for noninvasive alcohol detection from sweat. In the 1970s, Guilbault [6] and Christian [7] demonstrated that the enzyme – alcohol oxidase (AOX) could selectively detect alcohol in the presence of other interferants. AOX does not need any extrinsic cofactor, e.g., NAD+ along with ADH, and hereafter is not issuing to deteriorate these biosensors' stability and selectivity. Pingarrón et al. introduced a sweat-based alcohol monitoring device that detects alcohol in chemically induced sweat through a bio-enzymatic reaction.[27] Wang et al. developed a

tattoo-based alcohol detection system integrating pilocarpine-based iontophoretic sweat generation on a single platform (Figure 2-2b).[30] Prasad et al. designed an alternative wearable electrochemical immunosensor for the detection of alcohol through sweat. A noninvasive, continuous, and real-time monitoring system can ensure to fulfill such necessity and immediately diagnose the amount of alcohol consumption of AUD patients. Such information is more reliable than any self-reported data.

2.3.3 Glucose Sensing Through Sweat

According to the World Health Organization, 422 million people suffer from diabetes. Predicted to become the seventh leading cause of death, diabetes is dangerous because of its complications: cardiovascular diseases, blindness, risk of amputation, kidney failure, etc. The deficiency of insulin and hyperglycemia is caused by a metabolic disorder of diabetic patients [27]. This metabolic disorder promotes high risks of kidney failure, heart attack, chronic liver diseases, and blindness [28]. Thus, constricted day-to-day monitoring of glucose concentration is a demand for the diagnosis and treatment of diabetes. Also, fast, accurate, and continuous monitoring of glucose concentration is of great importance. As a successful consumer product of wearable biosensors, it is greatly important to demonstrate reliability, multiplexed functionality, and ease-to-use noninvasive monitoring of glucose from the body fluids [26].

As sweat glands disseminate through the body, hence it has advantages over other biofluids for use in noninvasive glucose monitoring. Sweat based glucose sensor is very attractive toward non-invasive, ease of access, ease of collection device placement, and sampling sites outside the body. As sweat sampling with small analytes at the shin surface

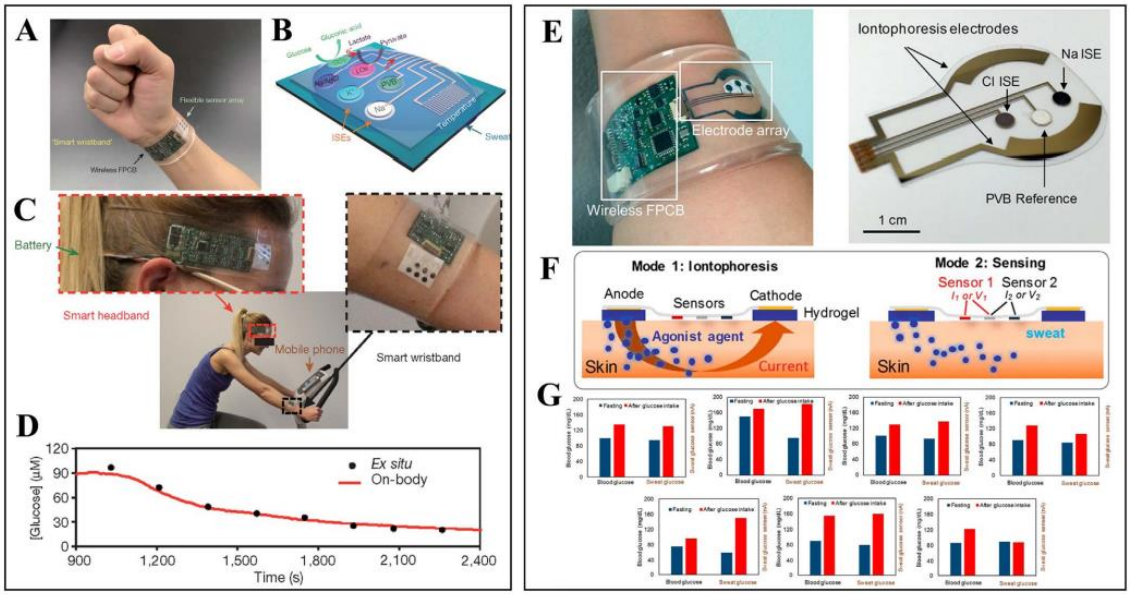

Figure 2-3: Epidermal sweat glucose monitoring using a flexible sensor array. (a) photograph detection of wearable, flexible, sensor array applied to a sensor array (b) schematic representation of multiplexed, flexible sensor array (c) photograph detection of on-body sweat analysis using flexible sensor array with sweat generated through exercise (d) glucose signal of on body glucose monitoring using flexible sensor array compared to ex-situ calibration using collected sweat (e) photograph detection coupled autonomous sweat extraction and flexible sensing array (f) schematic representation of iontophoresis and sensing mode operation for autonomous sweat extraction and multiplexed, flexible sensing array (g) comparison of on body sweat glucose and blood glucose analysis in human subjects before and after a meal. [28]

is rapid enough, so glucose rapidly diffusing into the sweat, fresh samples can be collected every several minutes with appropriate collection methods to give helpful information for continuous monitoring. Numerous types of sensors [Figure 2-3] have been industrialized to monitor sweat glucose during exercise conveniently. Wearable wristbands and patch-type sensors can continuously monitor the variations in sweat glucose by remaining attached to the skin for a long time[29]. Emaminejad et al. developed another glucose sensor that had an electronically controlled iontophoresis system [30]. Real-time glucose

sensing was employed using enzymatic sensors with microfluidic sweat sampling mechanisms. Lee et al. designed a gold-doped graphene-based sensor for sweat glucose monitoring and therapeutic drug delivery (Fig. 3A) [28]. Emaminejad et al. introduced an iontophoretic sweat stimulation system with an integrated glucose sensing system on a single, wearable platform [26]. Paper-based glucose-sensing systems were also explored to diagnose exercise-induced. Currently, a sweat-based glucose monitoring system was designed by employing an electrochemical, monolithic glucose sensor with pH and temperature corrections. The device was capable of sensing glucose levels in real-time from sweat and even included a drug dispensing microneedles for blood glucose adjustments. The potential of sweat-sampled glucose monitors will reduce the size of current devices and also allow trouble-free treatment of diabetes. A number of researches established the possible application of sweat as viable analytes for glucose monitoring, integration of painless monitoring devices, and patient-friendly protocols will strengthen the feasibility of noninvasive systems readily adopted in commercial and medical applications.

2.4 Sensing Technique

Electrochemical and optical sensors offer considerable promise owing to their miniaturized form factor and low cost. There exist some miniaturized LA bio-sensing devices in sports medicine for athletes and some which can optically detect the analyte with an electronic read out of the LA concentration in the body. Efforts, however, are still on for minimally invasive techniques in biomedicine for continuous monitoring and diagnosis.

2.4.1 Electrochemical Techniques

Electrochemical biosensors can be an attractive means for selective detection of analytes through the direct translation of enzymatic reactions into electrical signals in the presence of their specific enzyme. The fundamental operation of this technique depends on (i) electron transfer (ET) mechanism and (ii) enzyme immobilization technique. These two steps are integral to electrochemical sensing are described below.

In electrochemical biosensors, biocatalysts are immobilized onto a supporting substrate close to the electrode surface. Their response depends on the immobilization technique employed, the nature of the biocatalyst used, and the other adsorbed species through ET, mediators, and additives. Depending on the nature of the support and stability of the biomolecule, several techniques for immobilizing the enzyme can be used. These include (i) physical adsorption, (ii) entrapment behind a dialysis membrane or within a polymeric film, (iii) covalent coupling through a cross-linking agent, and (iv) incorporation within the bulk of a carbon composite matrix. The framework of ET can perform selective and specific reactions. In ET, electrons are transferred from the active site of the enzyme to the electrode. Since this mechanism between the bio-molecule and the electrodes is sluggish on planar electrodes, the immobilization medium should be engineered to provide enhanced electron transport. Different strategies have been used to construct enzymatic sensor electrodes to facilitate direct ET process or mediator-modified enzymes in analytes detection. Protein-mediated ET is a fundamental phenomenon in cellular processes. The redox enzyme acts as an electro-catalyst, facilitating ET between the electrode and the substrate. Such biosensors are known to offer improved selectivity since their operating potential is closer to the redox potential of the enzyme and hence less exposed to interfering

reactions. Several enzymes can undergo direct catalysis through direct (mediator-less) ET. This process is associated with: (i) ET from the electrode to the substrate molecule, or vice versa, via the active site of the enzymes such as alcohol oxidase, lactate oxidase, glucose oxidase; and (ii) catalytic nature of the whole process. ET between the active site of the enzyme and the transducer surface through the cross-linker. It can thus be concluded that in mediator-less bio-electro-catalysis, the electrode itself is a substrate for the reaction, and the enzymatic transformation on the electrode is not a separate reaction. On the other hand, diffusional electron mediators are employed as charge transporters between the active redox center of the enzyme and the transducer. Different catalysts and polymer-based mediators are integrated with the electrode to eliminate interference from the redox reaction. Examples include redox dye compounds, transition metal compound-based mediators polymeric, or perm selective membranes [14]. These have been found to enhance sensor performance with linearity, lower detection limit, enhanced stability, sensitivity, selectivity, and superior electron transport. Mediators and matrices in combination with a recognition layer of nanoparticles (NPs) have been found to repel interfering electro-active species, resulting in stable quantification of analytes. Cross-linkers have also been seen to exclude interference, providing greater stability, preventing fouling, and protecting the enzyme structure.

In electrochemical sensing mechanisms, two- or three-electrode sensing platforms are widely used for the detection of analytes in which the reference electrode (commonly made from Ag/AgCl) is kept at proximity to the working electrode to maintain a stable and known potential. The working electrode serves as a transducer, while the counter electrode establishes a path to pass the current due to the potential changes at the working electrode.

These sensors types are composed of a chemical (molecular) recognition system and a physicochemical transducer. Recognition systems react with the unknown analyte, whereas the transducer converts the chemical response into an electrical signal.

2.4.2 Optical Techniques

Optical detection relies on photon transfer, eliminating the need for transcutaneous connection. Optical enzymatic sensors reported in the literature are mostly into two major categories: (i) electro-chemiluminescence-based sensors and (ii) fluorescence-based enzymatic sensors. In electro-chemiluminescence (ECL) sensors, photons produced by the relaxation of excited molecules in an electrochemically initiated reaction are collected and analyzed. The photon intensity is directly proportional to the concentration of one or all the reactants involved in the electrochemical reaction. Light emission occurs in chemiluminescence transducers without any excitation, as the energy is released in the chemical reaction in the presence of O_2 or oxidation of H_2O_2. Such biosensors rely on the chemiluminescent reaction between H_2O_2 and luminol production in the enzymatic reactions. When the analyte is oxidized under catalysis and PA oxidase (PyOD) employing NAD^+ as co-enzyme, electroactive H_2O_2 is produced, which enhances the ECL of luminol to assist in detection. A simple, efficient and versatile biosensing platform has been reported that is capable of multiplexed detection of the enzymatic biosensor, along with glucose, alcohol, and lactate, developed from ECL, emitted on the same pole from luminol and in situ generated H_2O_2. The sensing bipolar electrode (BPE) arrays were successfully applied to determine glucose, lactate in the ranges of 0.01–1 mM, 0.01–1 mM, providing LO_x as 7.57 μM, Gox as 8.25 μM respectively from corresponding enzymes. Although

chemiluminescence lacks selectivity and depends on environmental conditions such as temperature and pH, it offers simple, low-cost instrumentation, lower detection limits, wide dynamic range, higher sensitivity and selectivity with good spatial control, and low signal to noise ratio.

Fluorescence-based biosensors rely on either the intensity of the emitted light or the lifetime of fluorescence after a period of excitation. Fluorescence spectroscopy is one of the most useful analytical tools in bioanalysis, and it causes little or no damage to the host system. Many fluorescent probes, such as europium coordination complexes, Amplex, quantum dots, gold nanoclusters, and cationic conjugated polymers, have been developed for the detection of H_2O_2. Their approach provided high selectivity and sensitivity using fluorescence resonance energy transfer mechanism by surface engineering the destabilized QDs sol with Nile Blue. Another hydrogel-based enzymatic sensor has been reported, which included an enzymatic microsensor embedded in a hydrogel matrix. The encapsulated oxidase acted as the bioactive component, while phosphorescent metalloporphyrin was used as the optical transducer. The permeability of analytics into the sensing system was controlled by coated polyelectrolyte multilayers on the sensor surface. The average sensitivity was determined to be 11 ± 0.90% dL mg^{-1}. The sensor is highly stable and was capable of performing without any loss till 20 cycles. Holographic enzymatic sensors were also explored with synthetic receptors for continuous monitoring of in-vivo biosensing. Changes in replay wavelength of these sensors characterize swelling behavior of the biofluid as a function of analytes concentration. Zheng et al. reported an enzymatic lactate sensor based on LDH and nanoscale optical fiber with a high spatial resolution to monitor LA in cancer cells [13]. It demonstrated the ability of the sensor to

distinguish from abnormal extracellular LA levels in cancer cells. Near-infrared light can pass through several centimeters of tissue, with the appropriate choice of fluorophore in detection. The molecules can be excited, investigating emissions from outside the body, providing potential for non-invasive sensing. Special fluorescence techniques can provide information about the structure and micro-environment of molecules, and their change in response to analyte variations can be monitored. Hexha et al. reported a study of a spectroscopy-based noninvasive glucose monitoring system to determine the glucose levels in the human body [14]. In vivo as well as in vitro experiments were conducted by using near-infrared transmission spectroscopy. Their study confirms a correlation between the sensor output voltage and glucose concentration levels.[22]. A novel, noninvasive technology was developed by Mindy et al. to evaluate an intoxication level of ethanol in perspiration on the skin surface [15].

Two different enzymes, such as horseradish peroxidase, and alcohol oxidase, were deployed to relate ethanol concentrations in perspiration. The outcomes of such controlled study during the drinking of the individuals reveal the capability of both the visualization system and the spectrophotometric approach to measuring the quantity of ethanol within actual sweat samples collected from individuals after the consumption of alcoholic beverages. Employing such a method, a smartphone was enabled to capture the data and can evaluate the intoxication levels of the human subject. This alcohol monitoring device is promising to influence both law enforcement and the general public, as well as the fields of forensic and biomedical engineering.

2.5 Conclusion

We provided an extensive overview of the technological progress in enzymatic sensor detection, particularly through wearable sensors. After briefly covering the clinical importance of the level of human glucose, alcohol, and lactate level, its interactions with two enzymes, were explained as they are commonly employed in sensing. Existing non-invasive techniques of detection from various bio-fluid matrices have been discussed, among which electrochemical methods have been reported to show more promise in simple, direct analysis, using enzymes partaking in its metabolic pathway. A comparison has been drawn on the detection mechanisms and sensing performances of the various existing enzymatic biosensors. Advancements in nano-scale materials and processing techniques greatly benefited the analytes sensing just like other sensors, electronic and photonic devices. These new materials and techniques increased the performance of the sensors and allowed the use of previously dismissed bio-fluid matrices such as sweat and the demonstration of novel non-invasive sensing methods such as tattoo and contact lens integrated sensors. However, there still are challenges yet to be overcome to achieve better selectivity, stability, reliability, and lifetime for wearable sensing platforms. The rapid expansion of mobile devices and services integrated into them is expected to attract increased investment in wearable health and wellness monitoring platforms which will most likely include integrated glucose, alcohol, and lactate level detectors as well. These integrated efforts will transform the future of personal healthcare in a way never imagined before.

2.6 References

1. Vabbina, P.K., Karabiyik, M., Al-Amin, C., Pala, N., "Controlled Synthesis of Single-Crystalline ZnO Nanofl akes on Arbitrary Substrates at Ambient Conditions," Part & Part. Syst. Charact., vol. 31, pp. 190-194, 2014.

2. Zhou, J., Xu, N., and Wang, Z. L., "Dissolving Behavior and Stability of ZnO Wires in Biofluids: A Study on Biodegradability and Biocompatibility of ZnO Nanostructures," Adv. Mat., vol. 18, no. 18, pp. 2432–2435, 2006

3. Li, Z., Yang, R., Yu, M., Bai, F., Li, C., and Wang, Z. L., "Cellular Level Biocompatibility and Biosafety of ZnO Nanowires," J. Phys. Chem. C., vol. 112, no. 51pp. 20114–20117, 2008.

4. Vabbina, P.K., Sinha, R., Ahmadivand, A., Karabiyik, M., Gerislioglu, B., Awadallah, O., and Pala, N., "Sonochemical Synthesis of a Zinc Oxide Core-Shell Nanorod Radial p-n Homojunction Ultraviolet Photodetector," ACS Appl. Mater. Interfaces., vol. 9, no. 23, 19791-19799, 2017.

5. Abrar, M.A., Dong, Y., Lee, P.K., Kim, W.S., "Bendable Electro-chemical Lactate Sensor Printed with Silver Nanoparticles,"Sci. Rep., vol. 6, pp. 30565, 2016.

6. Alam, F., Jalal, A.H., Sinha, R., Umasankar, Y., Bhansali, S., Pala, N., "Sonochemically Synthesized ZnO Nanostructured Piezoelectric Layers for Self-Powered Sensors Applications," MRS Adv., pp.1–6, 2018.

7. Baldari, C., Bonavolontà, V., Emerenziani, G. Pietro, Gallotta, M.C., Silva, A.J., Guidetti, L., "Accuracy, reliability, linearity of Accutrend and Lactate Pro versus EBIO plus Analyzer," Eur. J. Appl. Physiol., vol.107, pp. 105–111, 2009.

8. Ballesta Claver, J., Valencia Mirón, M.C., Capitán-Vallvey, L.F., "Disposable Electrochemiluminescent Biosensor for Lactate Determination in Saliva," Analyst, vol.134, pp. 1423, 2009.

9. Biswas, A., Bornhoeft, L.R., Banerjee, S., You, Y.-H., McShane, M.J., "Composite Hydrogels Containing Bioactive Microreactors for Optical Enzymatic Lactate Sensing,"ACS Sens., vol. 2, pp. 1584–1588, 2017.

10. Brahim, S., Narinesingh, D., Guiseppi-Elie, A., "Design and Characterization of a Galactose Biosensor Using a Novel Polypyrrole-hydroge Composite Membrane," Anal. Chim. Acta, vol. 448, pp. 27–36, 2001.

11. Cai, X., Yan, J., Chu, H., Wu, M., Tu, Y., "Gold Nanoparticles in Chemical and Biological Sensing," Sensors Actuators B Chem., vol. 143, pp. 655–659, 2010.

12. Chicharro, J.L., Lucía, A., Pérez, M., Vaquero, A.F., Ureña, R., "Saliva Composition and Exercise," Sports Med., vol. 26, pp. 17–27, 1998.

13. Choy, C.K., Cho, P., Chung, W.Y., Benzie, I.F., "Water-Soluble Antioxidants in Human Tears: Effect of the Collection Method," Ophthalmol. Vis. Sci., vol. 42, pp. 3130-4, 2001.

14. Dagar, K., Pundir, C.S., "A Biofuel Cell Based on Biocatalytic Reactions of Lactate on Both Anode and Cathode Electrodes - Extracting Electrical Power from Human Sweat," Enzyme Microb. Technol., vol. 96, pp. 177–186, 2017.

15. Dong, S., Wang, B., "Recent Nanoarchitectures in Metal Nanoparticle-modified Electrodes for Electroanalysis," Electroanalysis,vol. 14, pp. 7–16, 2002.

16. Driller, M., Plews, D., Borges, N., "Wearable near Infrared Sensor for Determining an Athlete's Lactate Threshold during Exercise," NIR news, vol. 27, pp. 8–10, 2016.

17. Felicity, K., Sartain, Xiaoping, Y., and, Lowe, C.R., "Holographic Lactate Sensor," 2006.

18. Ferrer, A.S., Santema, J.S., Hilhorst, R., Visser, A.J.W.G., "Differences in the Regulation of Iron Regulatory Protein-1 (IRP-1) by Extra- and Intracellular Oxidative Stress," Anal. Biochem., vol. 187, pp. 129–132, 1990.

19. Garcia-Alvarez, M., Marik, P., Bellomo, R., "Sepsis-associated hyperlactatemia," Crit. Care, vol. 18, pp. 503, 2014.

20. Ghindilis, A.L., Atanasov, P., Wilkins, E., "Electrochemical Biosensors Based on Nanostructured Carbon Black: A Review," Electroanalysis, vol. 9, pp. 661–674, 2014.

21. Girotti, S., Ghini, S., Carrea, G., Bovara, R., Roda, A., Budini, R., "Compact Miniaturized Bioluminescence Sensor Based on Continuous Air-Segmented Flow for Real-Time Monitoring: Application to Bile Salt Hydrolase (BSH) Activity and ATP Detection in Biological Fluids," Anal. Chim. Acta, vol. 255, pp. 259–268, 1991.

22. Goodman, J.C., Valadka, A.B., Gopinath, S.P., Uzura, M., Robertson, C.S., "Impact of Pyrexia on Neurochemistry and Cerebral Oxygenation After Acute Brain Injury," Crit. Care Med., vol. 27, pp. 1965–73, 1999.

23. Goodwin, M.L., Harris, J.E., Hernández, A., Gladden, L.B., "Blood Lactate Measurements and Analysis During Exercise: a Guide for Clinicians," J. Diabetes Sci. Technol., vol. 1, pp. 558–569, 2007.

24. Heinis, A.M.F., Dinnissen, J., Spaanderman, M.E.A., Lotgering, F.K., Gunnewiek, J.M.T.K., "Infant Outcome at Four Years of Age After Intrapartum Sampling of Scalp

Blood Lactate for Fetal Assessment. A Cohort Study," Clin. Chem. Lab. Med., vol. 50, pp. 89–93, 2011.

25. Hickey, D.P., Reid, R.C., Milton, R.D., Minteer, S.D., "Self-Powered Biosensors," Bioelectron., vol. 77, pp. 26–31, 2016.

26. Jalal, A.H., Umasankar, Y., Gonzalez, P.J., Alfonso, A., Bhansali, S., "Lactate Biosensing: The Emerging Point-of-Care and Personal Health Monitoring," Biosens. Bioelectron., vol. 87, pp. 522–53, 2017.

27. Jin, L., Shang, L., Guo, S., Fang, Y., Wen, D., Wang, L., Yin, J., Dong, S., "Biomolecule-Stabilized Au Nanoclusters as a Fluorescence Probe For Sensitive Detection of Glucose," Biosens. Bioelectron., vol 26, pp. 1965–1969, 2010.

28. Khodagholy, D., Curto, V.F., Fraser, K.J., Gurfinkel, M., Byrne, R., Diamond, D., Malliaras, G.G., Benito-Lopez, F., Owens, R.M., "Organic Electrochemical Transistor Incorporating an ionogel as a Solid State Electrolyte for Lactate Sensing," J. Mater. Chem., vol. 22, pp. 4440, 2012.

29. Kim, J., Valdés-Ramírez, G., Bandodkar, A.J., Jia, W., Martinez, A.G., Ramírez, J., Mercier, P., Wang, J., "Wearable Salivary uric Acid Mouthguard Biosensor With Integrated Wireless electronics," Analyst, vol. 139, pp. 1632–6, 2014.

30. Lewenstam, A., J. Solid State Electrochem.,"Non-equilibrium potentiometry—the very essence," vol. 15, pp. 15–22, 2011.

31. Lupu, A., Valsesia, A., Bretagnol, F., Colpo, P., Rossi, F., "Biosensors Based on Electrochemical Lactate Detection: A Comprehensive Review," Sensors Actuators B Chem., vol. 127, pp. 606–612, 2007.

CHAPTER III
ZnO NANOFLAKES BASED IMMUNOSENSOR FOR ALCOHOL SENSING

Among various semiconducting metal oxide-based nanomaterials, Zinc oxide (ZnO) has been found as an excellent candidate for wearable biosensing applications. Its piezoelectric nature, high catalytic efficacy, biocompatibility, chemical stability in physiological environments, low toxicity, and a high isoelectric point (IEP) of about 9.5 make it potential in many biosensing applications [30]. ZnO nanostructures (NSs) with different morphologies such as nanorods, nanowalls, nanobelts, and quantum dots have been used as immobilizing matrices in the fabrication of biosensors for the detection of physiologically relevant biomarkers such as cholesterol, galactose, glucose [31-33]. Considering their promising properties and potential applications, many techniques have been developed to synthesize various ZnO-NSs. Compared to bulk materials, the 2D ZnO nanoflakes (ZnO-NFs) provide unique sensing advantages with polarized (0001) plane [28] orientation and high surface charge density, which could enhance antibody loading and thus improve sensing performance. The high isoelectric point allows immobilization of most biomolecules without any additional binding layer [34-36]. This provides a direct, stable pathway for rapid electron transport when an analyte is immobilized on NFs and improves electron transfer rate. Moreover, the performance of a ZnO-based biosensor can be improved by tailoring the properties of the ZnO–biomolecule interface via engineering of morphology, plane orientation, particle size, effective surface area, functionality, adsorption capability, and electron-transfer properties [37,38]. Therefore, ZnO NFs has been fabricated on flexible polyethylene terephthalate (PET) substrate, which has gained

popularity for wearables because of its intrinsic elasticity, thermal stability, hydrophobicity, excellent dielectric properties, low coefficient of thermal expansion, structural resiliency against repeated bending forces, and compatibility with roll-to-roll fabrication processes for low cost and scalable manufacturing. In this work, we utilize ZnO-NFs, synthesized on Au-deposited flexible polyethylene terephthalate (PET) substrate, as electrode sensing elements in developing a flexible, label-free, highly sensitive biosensor suitable for sweat based detection of it. This ZnO-based biosensing platform is expected to find applications in a new generation of miniaturized, smart biosensing devices for point of care and wearable health monitoring applications.

3.1 Background

Prolonged alcohol consumption can promote various fatal diseases, such as fatty liver disease, alcoholic hepatitis, liver cirrhosis, Wernicke-Korsakoff Syndrome, hepatic encephalopathy and fetal alcohol spectrum disorders, heart diseases, alcohol-induced pancreatitis, and cancers [1,2]. Moreover, 18.5 million adults are abused by alcoholism and driving under the influence (DUI) related accidents cause the death of 11,000 individuals and cost $132 billion per year in the U.S. [3,4] Hence, an instantaneous and real-time monitoring of alcohol in a wearable platform would be highly useful in numerous fields ranging from clinical monitoring to safety systems [5-8]. This point of care alcohol monitoring device can play a significant role in preventing, deterring, and monitoring impaired driving, which is one of the most critical causes for numerous road accidents.

Breath alcohol devices (e.g., breathalyzers) are mostly employed for their (ethanol) detection from breath by law enforcement agencies for random monitoring of DUI to

determine if drivers consumed alcohol before driving [9-12]. However, this random checking cannot ensure monitoring at a large extent of the population. Moreover, ethanol itself is considered as a less-reliable biomarker for diagnosing and monitoring long-term diseases incurred from alcohol abuse due to its low specificity and short window of detection. Also, it has a high risk of false detection in the bacteria exposed to sugar-containing body fluids of diabetics, which makes ethanol an unsuitable marker for alcohol detection in any other fluids than blood. Sensitivity, specificity, and a long window of detection are the most sought-after properties in the selection of an ideal biomarker for alcohol detection. Further, measurements in the clinical application are required over extended periods, ideally starting from 30 minutes before consumption and extending to 8 hours after the last drink, to understand the consumption and metabolism of alcohol of any subject. The offender can use this time gap to get intoxicated and sober before the next breath sampling. Among different non-oxidative direct metabolites of ethanol biochemical markers, ethyl-glucuronide (EtG) has been found as a promising indicator for alcohol detection due to its prolonged existence in sweat (24 hours for one or two “drinks” or 2-4 days for binge drinking), which prevents relapsing[4]. It has been reported that about 0.1% of ethanol consumption is excreted in sweat through human perspiration, whereas 0.7% is excreted in breath, 0.3% in urine, and mostly over 98% is metabolized by the liver [13]. Ethanol exposure and its kinetics have been well characterized through detailed investigation of EtG, a minor metabolite of alcohol produced by conjugation pathways [14]. EtG is metabolized in the body by glucuronidation following exposure to ethanol. Ethanol reacts with glucuronic acid, a substance constantly working to detoxify drugs by turning them into water-soluble compounds, which are then easily removed from the body

and can be detected in body fluids such as sweat, urine, and hair [17,18]. In comparison to other body fluids, human sweat analysis is the most promising method due to the possibility of detection and quantification of EtG in real-time using wearable biosensors.

Electrochemical metal-oxide based immunosensors [19-20] demonstrate improved performance over other sensing methods, such as optical [21-23], colorimetric [24], or fuel cell-based [25-27] sensors. Their wide detection range, rapid and selective detection approach, and higher sensitivity make them the preferred sensing method for many biomolecules in point of care and wearable health quality monitoring applications. To achieve low detection limits and high sensitivity, the immobilizing matrix used in immunosensors should have high surface functionality, high biomolecule loading, and a small resistance to electron transport with a high electron transfer rate [28]. This encourages researchers to explore the utilization of inorganic semiconductor nanostructures (NSs) as the potential immobilizing matrix for immunosensor development to detect desired target analytes [29]. Metal oxide-based nanostructures with a high isoelectric point (IEP) have recently become extremely significant as nanomaterials, which provide an effective and required surface for the immobilization of biomolecules with desired polarized plane orientation, better conformation, and high biological activity contributing to the development of enhanced biosensing platforms [4]. Among various semiconducting metal oxide-based nanomaterials, Zinc oxide (ZnO) has been found as an excellent candidate for wearable biosensing applications. Its piezoelectric nature, high catalytic efficacy, biocompatibility, chemical stability in physiological environments, low toxicity, and a high isoelectric point (IEP) of about 9.5 make it potential in many biosensing applications [30]. ZnO nanostructures (NSs) with different morphologies such as nanorods,

nanowalls, nanobelts, and quantum dots have been used as immobilizing matrices in the fabrication of biosensors for the detection of physiologically relevant bi biomarkers such as cholesterol, galactose, glucose [31-33]. Considering their promising properties and potential applications, many techniques have been developed to synthesize various ZnO-NSs. Compared to bulk materials, the 2D ZnO nanoflakes (ZnO-NFs) provide unique sensing advantages with polarized (0001) plane [28] orientation and high surface charge density, which could enhance antibody loading and thus improve sensing performance. The high isoelectric point allows immobilization of most biomolecules without any additional binding layer [34-36]. This provides a direct, stable pathway for rapid electron transport when an analyte is immobilized on NFs and improves electron transfer rate. Moreover, the performance of a ZnO-based biosensor can be improved by tailoring the properties of the ZnO–biomolecule interface via engineering of morphology, plane orientation, particle size, effective surface area, functionality, adsorption capability, and electron-transfer properties [37-38]. Therefore, ZnO NFs has been fabricated on flexible polyethylene terephthalate (PET) substrate, which has gained popularity for wearables because of its intrinsic elasticity, thermal stability, hydrophobicity, excellent dielectric properties, low coefficient of thermal expansion, structural resiliency against repeated bending forces, and compatibility with roll-to-roll fabrication processes for low cost and scalable manufacturing. In this work, we utilize ZnO-NFs, synthesized on Au-deposited flexible polyethylene terephthalate (PET) substrate, as electrode sensing elements in developing a flexible, label-free, highly sensitive biosensor suitable for sweat based detection of it. This ZnO-based biosensing platform is expected to find applications in a new generation of

miniaturized, smart biosensing devices for point of care and wearable health monitoring applications.

3.2 Materials and Method

3.2.1. Reagents and Chemicals

Antibody for EtG was purchased from EastCoast Bio (North Berwick, ME, USA). The antibody was purified monoclonal and stored at 4 °C. EtG antigen was purchased from EastCoast Bio (North Berwick, ME, USA). Antibody stock solution was stored and diluted in 0.1 M PBS (Phosphate buffered Saline) solution. Antigen stock solution was stored in DI water (deionized water). Zinc Nitrate hexahydrate [ZNH; $Zn(NO_3)_2.6H_2O$] and Hexamethylenetetramine [HMT; $(CH_2)_6\ N_4$] were all purchased from Sigma-Aldrich (USA). All other chemicals were of analytical grade and were used without further purification.

An atomic force microscope (Nanonics AFM), scanning electron microscope (SEM, JOEL 7000FSEM), and Nomadic Raman Spectrometer by BaySpec (532 nm laser) were used for characterization of the material properties of the synthesized structures and fabricated devices. An electrochemical analyzer (CHI604D, CH Instruments, USA) was employed for the electrochemical impedance spectroscopy (EIS) and cyclic voltammetry (CV) measurements.

3.2.2 Fabrication of ZnO-NFs Based Immunosensor

2D ZnONFs were synthesized by one step sonochemical method on 60 nm thick Au deposited by e-beam evaporation over flexible PET substrate, as shown in Figure 3-1a. We selected this method since it is fast, inexpensive, catalyst-free, CMOS compatible, and environmentally benign. Sonochemical reaction rate is 100 times faster compared to other and similar hydrothermal methods, and it allows for a well-oriented growth over a wide range of substrates. In addition, the process temperature is less than 50 ^{0}C which allows the use of a wide variety of substrates. The fabrication of ZnO-NFs on gold-coated PET substrates was as follows: First, 60 nm thick gold layer was deposited on PET substrates by e-beam evaporation. Then, the gold-coated PET substrates were washed with deionized water and dried by N_2 gas. A solution of 20mM ZNH and 20 mM HMT, prepared at room

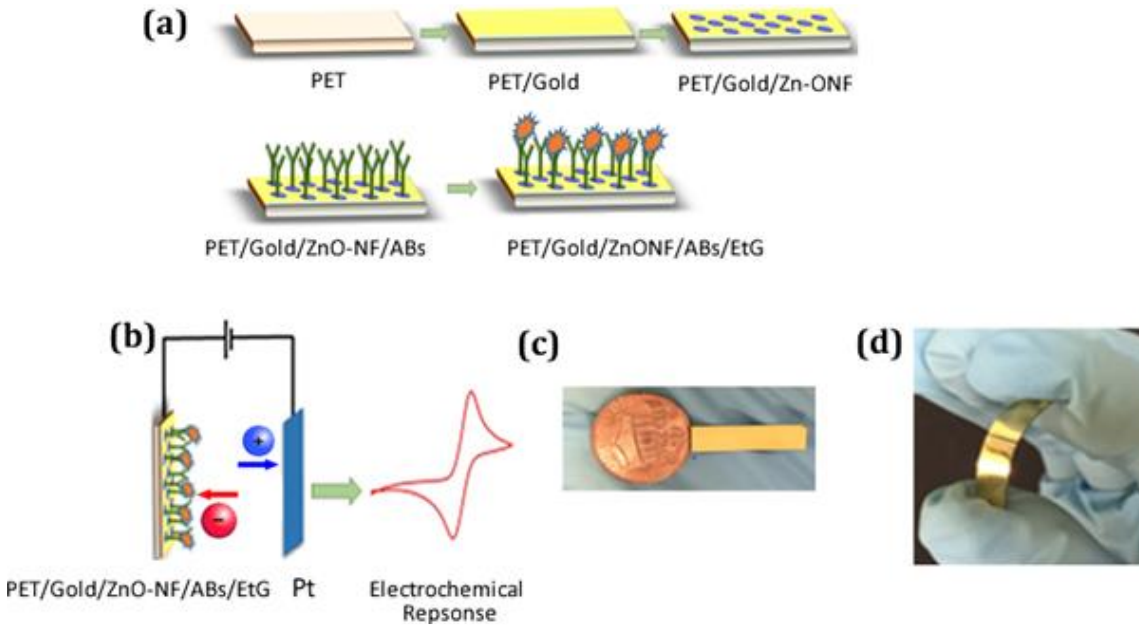

Figure 3-1: (a)Illustration of ZnO-NFs, prepared using sonochemical method along with immobilization anti-EtG antibody onto ZnO-NFs to fabricate electrochemical EtG immunosensor (b) Electrochemical response at the fabricatd electrode (c) Fabricated sensing electrode and its size and (d) its flexible nature

temperature by stirring with a magnetic stir bar at 350 rpm for 5 min to ensure a mixed solution was used as the only solution for the growth of 2D ZnO-NFs as shown in Figure 3-1a. The solution with the immersed substrate was then irradiated using a commercially available high-intensity ultrasound setup (750 W ultrasonic processor, Sonics and Systems) for 15min cycles at an amplitude of 70% of the maximum amplitude of the ultrasonic probe for 20 min providing the solution with an intensity of $30Wcm^{-2}$ and frequency of 20 kHz. The temperature of the aqueous solutions did not exceed 50°C. The substrate was rinsed with DI water and then dried with N_2 after each cycle. For the preparation of ZnO-NSs based immunosensor, 10µL of EtG antibody was covalently immobilized on the electrodes via electrostatic interaction due to the difference in IEPs of ZnO (9.5) and antibody (4.5). Monoclonal EtG antibody (ABs) at a concentration of 10mg/L was incubated on the sensor surface for 30 minutes at room temperature, followed by phosphate buffer saline (PBS, pH 7.4, 10 mM) washing to remove any unbound molecules. PBS solution was prepared by dissolving 1 PBS tablet in 200mL of de-ionized water. The non-binding sites of EtG-AB/ZnO-NSs/Au/PET bio electrode were blocked by immobilizing 10µL of bovine serum albumin (BSA) for 30 min, followed by PBS washing and drying at room temperature. The fabricated BSA/EtG-AB/ZnO-NFs/Au/PET immune-electrodes (shown in Figures 1c and 1d) were stored in a refrigerator at 4 °C when not in use.

3.2.3 Material Characterization

The morphological study of the surface of ZnO nanostructures was carried out during various stages of electrode fabrication by using scanning electron microscopy

(SEM, JOEL 7000FSEM), and we found well-aligned and uniform ZnO-NFs were grown on the gold-coated PET substrates. Figure 3-2a and 3-2b show high-resolution transmission electron microscopy (HRTEM) images of ZnO-NFs and selective area electron diffraction (SAED), respectively confirming that ZnO-NFs are single crystalline and oriented in [0001] direction with wurtzite structure with a = 3.25Å and c = 5.21Å. Figure 3-2c shows scanning electron microscopy (SEM) images of uniformly grown 2D ZnO-NFs over Au/PET substrate. ZnO-NFs are 20nm thick and have the average lateral dimensions of 5µm× 5µm. Figure 3-2d depicts that the electrode surface becomes more uniform and smoother after the antibody is introduced. This change in the morphology suggests that the antibody has been successfully immobilized over the ZnO nanoparticles matrix. Surface

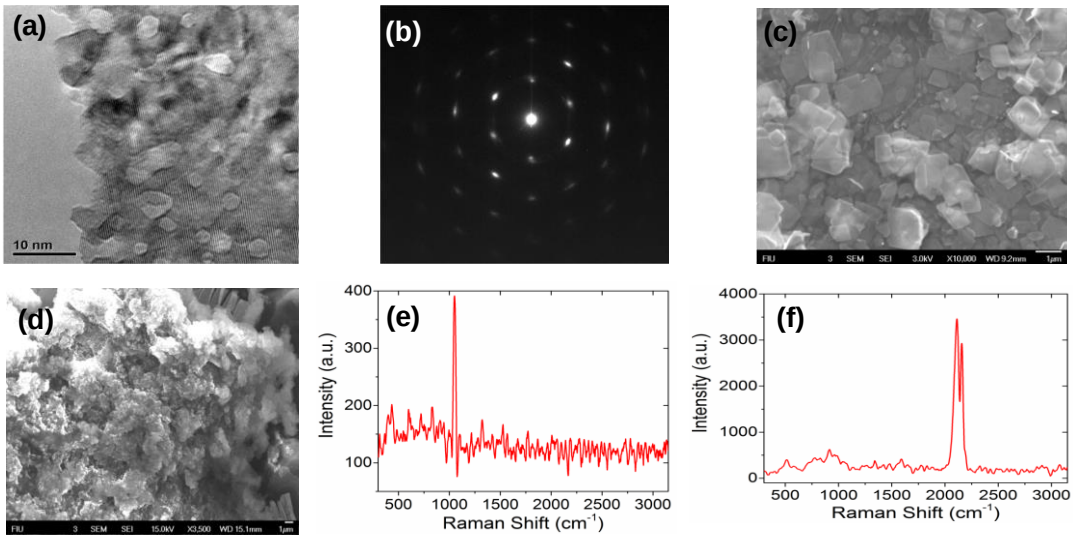

Figure 3-2: (a) HRTEM at the edge of a flake with fringes almost parallel to the edge with a spacing of 2.74 Å (b) SAED image of ZnO-NFs (c) SEM characterization images of ZnO-NFs/Au/PET Substrate (before immobilization of EtG-AB) (d) SEM characterization images for ZnO-NFs/Au/PET substrate (After immobilization of EtG-AB) (e) Raman spectra on ZnO-NFs/Au/PET electrode (f) Raman spectra of EtG-AB/ZnO-NFs/Au/PET immunoelectrodes.

roughness was measured by using an atomic force microscope operated in resonance frequency using Cr tip with a resonant frequency of 34.95 kHz and tip diameter 20 nm. After the introduction of the antibody, the measured average surface roughness of EtG-AB/ZnO-NFs/Au/PET was 0.319 μm while ZnO-NF/Au/PET electrode shows a higher average roughness of 0.676 μm. The drop-in roughness value is due to the immobilization of EtG Ab, which fills the porous surface of the electrode. The Raman spectroscopy study for ZnO-NFs is shown in Figure 3-2e. The peak at 1050 cm^{-1} corresponds to the second-order longitudinal optical phonon vibration [39]. Raman spectroscopy of EtG-AB/ZnO-NFs/Au/PET electrodes in Figure 2f shows smaller peaks other than that characteristic of wurtzite ZnO-NFs and a shift of the major peak to around 2100 cm^{-1} which suggests a successful binding of EtG-AB over ZnO-NFs surface.

3.2.4 Electrochemical Characterization

CV studies and EIS were performed to understand the electroactive behavior of the working electrode. Oxidation takes place at the biomolecule immobilized electrode-electrolyte interface, where these molecules are oxidized by losing electrons (Figure 3-2b). The released electrons are rapidly transferred through the electrode material. However, most biomolecules are insulating in nature which increases the charge transfer resistance impeding the charge carriers. This change in resistance causes variation of current and allows the external potentiostat to determine this variation for the detection of the targeted biomolecules. The distinct oxidation peaks are monitored for varying concentrations of the biomolecule, otherwise called an antigen, in CV measurements. Therefore, factors such as high antibody binding and electron transfer rate play a pivotal role in any electrochemical

biosensor. 2D ZnO-NFs with high IEP (~9.5) has a positive surface charge density at a pH value of below 9.5. The experimental protocol follows the pH value of 7.4 throughout this work which allows the binding sites of antibody (Anti-EtGab) having with the IEP 4.2. Therefore, the antibody is negatively charged under this experimental condition. Moreover, 2D ZnO-NFs also present higher binding sites due to the large surface area in the (0001) plane, allows higher catalytic activity and lower charge transfer resistance. The binding of the antibody to the nanomaterials is studied with the help of AFM, SEM, and Raman, as shown in Figure 3-2. The electro-activity of ZnO-NFs/Au/PET and EtG-AB/ZnO-NFs/Au/PET electrodes was studied using three electrodes system in 3ml PBS (p^H 7.4) containing 5mM $[Fe(CN)_6]^{3-/4,}$ which acts as an electrolyte. A conventional three-electrode system comprising of the fabricated BSA/EtG-AB/ZnO-NFs/Au/PET bioelectrode as working electrode, Pt as an auxiliary electrode, and Ag/AgCl, 0.1M KCl as a reference electrode were employed for all measurements. Here the dimension of the working electrode was 0.5 cm x 0.5 cm. All the experiments were performed at room temperature.

3.3 Results and Discussions

3.3.1. CV Measurement

The samples were characterized at different steps of the fabrication by CV measurements within the potential range of -0.1V to 0.8V, at a scan rate of 50 mVs^{-1}. The magnitude of oxidation current reduces from the bare gold electrode to BSA/EtG-AB/ZnO-NFs/Au/PET electrodes with every step due to the increase of the corresponding charge transfer resistances, as shown in Figure 3-3.

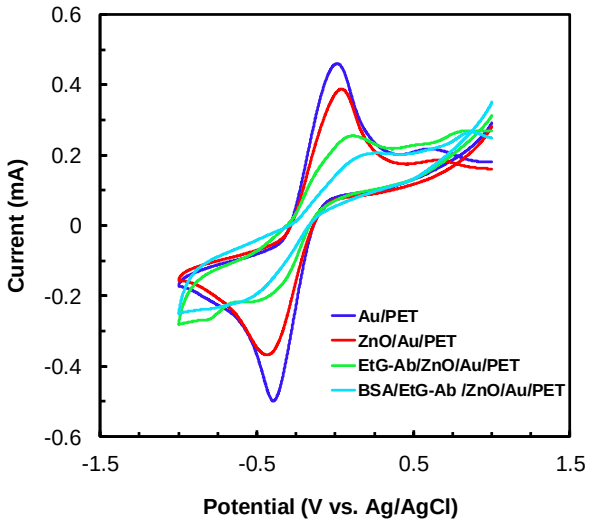

Figure 3-3: Reduction in the magnitude of oxidation current at different stages of the fabrication form bare Au electrode to BSA/EtG-AB/ZnO-NFs/Au/PET immuno-electrode.

The electroactive behavior of ZnO-NFs/Au/PET electrodes has been investigated through the CV measurements over a range of EtG concentrations from 1 ng/ml to 100 µg/ml. Five different concentrations within this range have been explored for the calibration of the sensor. In preparation, electrodes with BSA/EtG-AB/ZnO-NFs/Au/PET were incubated in a 10µL solution containing a specific concentration of EtG for 30 min. During this incubation process, antigen binds with the antibody (EtG-AB), creating an insulating immune complex in between EtG antibody and antigen. This insulating layer impedes the charge (electron) transport from an electrolyte to the electrode and further increases the charge transfer resistance (R_{ct}). Hence, the CV measurements presented downward trends for the maximum oxidation current with the addition of EtG to the electrode, confirming the increase in R_{ct}. This current reduction increases with the increasing concentration of EtG of the proposed ZnO-NFs based EtG biosensor, as shown in Figure 3-4a. The current responses for these five different concentrations were obtained

within the potential range of -0.1V to 0.8V, at a scan rate of 50 mVs^{-1}. The peak oxidation currents for different concentrations are shown in Figure 3-4b, which allowed us to determine the sensitivity of the sensor as 0.032 mA/log (μM)/cm^2. The coefficient of determination (R^2) was calculated as 96.13% that supports its significantly linear characteristics. The minimum detection limit was determined at ~1 ng/ml, and the sensor's response time was measured on an average of ~ 45s for each measurement. A comparison of the performance of the presented sensor with the recent alcohol/EtG sensors reported in the literature is presented in Table 3-1.

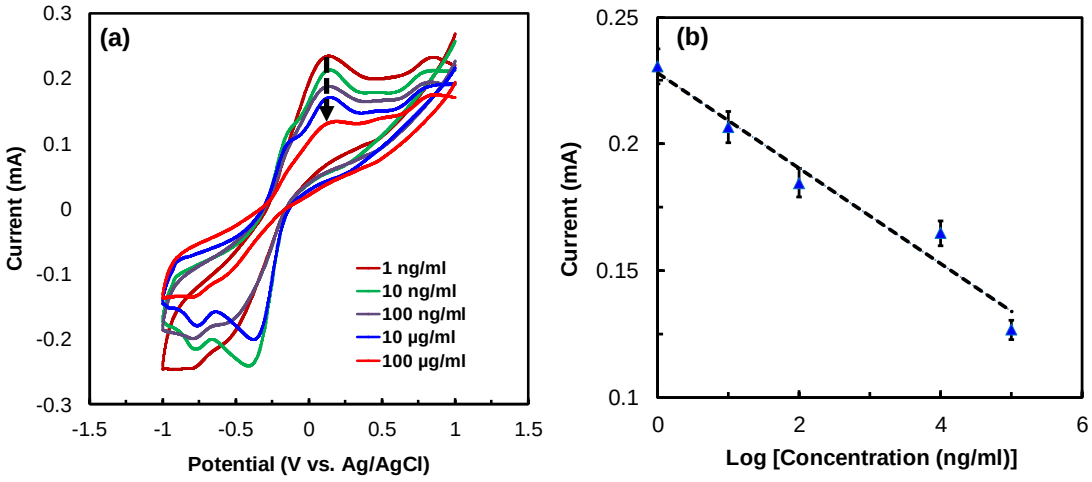

Figure 3-4: (a) CV studies of immunosesnors as function of EtG concentration varying from 1ng/ml to 100ug/ml for BSA/EtG-AB/ZnO-NFs/Au/PET electrode (b) Calibration curve of the fabricated BSA/EtG-AB/ZnO-NFs/Au/PET biosensor for EtG concentration of 1ng/ml, 10ng/ml,100ng/ml and 100ug/ml

Sensor types	Electrode material	Analyte type	LoD in different bio-fluids	Sensitivity	Ref.
Metal oxide based immunosensor	ZnO-NFs	EtG	1 ng/ml	0.032 mA/ log (μM)/cm^2	This work
Metal oxide based immunosensor	ZnO	EtG	0.001 ng/ml (sweat)		[4]
Electrochemical enzymatic sensor	Pt-Pt-Ag	Alcohol oxidase	20 mM (interstitial fluid)	0.062 nA/mM	[40]
Electrochemical enzymatic sensor	Prussian blue conductive carbon ink, Ag/AgCl	Alcohol oxidase	3 mM (sweat)	0.362 ± 0.009 μA/mM	[41]
Electrochemical fuel cell	Nickel	Ethanol	5 ppm (skin perspiration)	0.23 nA ppm^{-1} cm^{-2}	[42]

Table 3-1: Comparison of fabrication of ZnO-NSs based immunosensors with the state-of-art technologies.

3.3.2. EIS Measurements

EIS is employed to study the electron transfer characteristics and association constant for binding interactions at the electrode surface in between the receptor (R) and ligand (L) molecules. Figure 5a demonstrates the Nyquist plot of the EIS spectra for bare Au/PET, ZnO-NFs/Au/PET,EtG-AB/ZnO-NFs/Au/PE,BSA/EtG-AB/ZnO-NFs/Au/PET electrodes. These data were satisfactorily fitted with the equivalent 'Randles Circuit' shown in Figure 5b with the values and relative errors (%) given in Table 3-2. In this model,

R_s represents the solution/electrolyte resistance, R_{ct} is the electron transfer resistance, CPE is the constant phase element, and Z_w denotes the Warburg impedance. The diameter of the semicircle represents the charge transfer resistance (R_{ct}) on the electrode surface. The value of R_{ct} changes from 1.045 kΩ for bare Au/PET electrode to 2.213 kΩ for ZnO-NFs/Au/PET electrode, which further increases to 3.961 kΩ with the addition of antibody. Introducing the insulating material (BSA) on the electrode surface, the charge transfer resistance increases significantly. Therefore, the redox current decreases. Consequently, the R_{ct} value for BSA/EtG-AB/ZnO-NFs/Au/PET electrode raises to 5.587 kΩ. The electrons transfer from the electrolyte $[Fe(CN)_6]^{3-/4-}$ in phosphate-buffered saline **(** PBS) to the electrode is hindered with the addition of antibody, which further decreases after the addition of BSA. CV studies of The electron transfer rate (K_{et}) at the electrode interface can be estimated by using the EIS following the equation [43].

$$K_{\text{et}} = \frac{\mathbf{1}}{\mathbf{2}\,(\boldsymbol{R_{ct}})(\boldsymbol{CPE})} \qquad (1)$$

The binding constant K_{ac} is indicative of the stable binding between the nanoparticles and antibody that can be estimated by using the following equation [44].

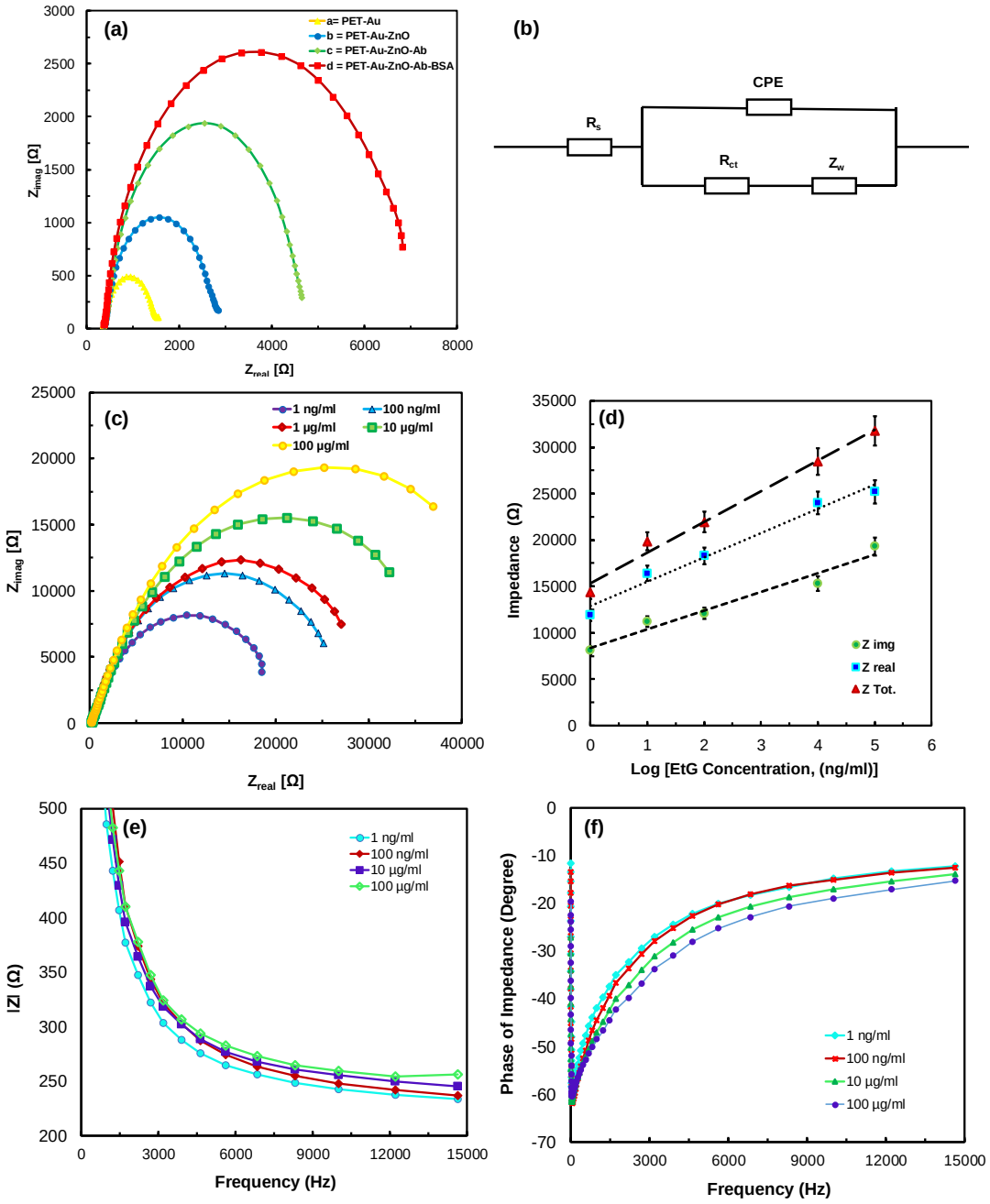

Figure 3-5: (a)Rise of R_{ct} from bare Au electrode to BSA/ EtG-AB /ZnO-NFs/Au/PET immunoelectrodes, (b) Randles equivalent circuit, (c) Charge in EIS of BSA/ EtG-AB/ZnO-NFs/Au/PET immunoelectrode with respect to EtG concentrations with the frequency range of 1 Hz-13000 Hz (d) Dose responses of total impedance output in histogram for calibrating sensor for EtG (inset: the linear regression curve for real impedance, imaginary impedance and total impedance for the EtG sensor) and (e) Bode plot impedence spectra and (f) phase spectra for understanding the behavior of the sensor with the change of concentrations

$$\boldsymbol{K_{ac}} = \frac{\Delta \boldsymbol{R_{ct}}}{\boldsymbol{R_{ct}(C_0)}} \quad (2)$$

where ΔR_{ct} is the difference in charge transfer resistance due to the introduction of antibody and R_{ct} (C_0) is charge transfer resistance without antibody. The results of the EIS at various steps of electrode fabrication are given in Table 3-2. In Figure 3-5c, the Nyquist plot represents different values of $R_{ct,}$ which have progressive increments with respect to the EtG concentration. Real and imaginary parts of the impedance, as well as the total impedance (Ztot) for different EtG concentrations, are plotted in Figure 3-5d. The impedances are taken for the maximum values of the R_{ct} with the frequency range of 1Hz-13 kHz and the initial voltage of 0.209 V. Linear regression analysis resulted from the coefficient of determinant $R_2 = 0.987$, which indicates significant linearity for the sensor. The relative changes of Z_{tot} are 86.81%, 90.45%, 91.32%, 93.33%, and 94.01%, respectively for the five mentioned concentrations. The higher rate of impedance changes for the concentration (1ng/ml) comparing with the high concentration (100 µg/ml) supports the higher sensitivity of the sensor for low concentrations of EtG.

In Figures 3-5e and 3-5f, Bode plots show the impedance and its phase, respectively, for different doses of EtG. It is observed that there is a progressive increase in impedance with respect to EtG concentration, whereas it's the opposite for the phase of the impedance. This phenomenon supports the reasoning of reduction of current with the increase of concentration described in section 3.1. The trend in Figure 3-5f helps to understand the binding property on the surface of the ZnO-NFs based electrode. The output signal lags 60° in phase, indicating the capacitive property of the sensor electrode. This capacitive property dominates the CPE and confirms that a double layer capacitance was formed at the electrode surface-solution interface following the Gouy-Chapman model.

Hence, the phase angle decreases with the increase of the concentration, and the electrode behaves capacitive in nature.

	R_s (Ω) – % error	R_{ct} (kΩ) – % error	CPE (μF) – % error	K_{et} (s^{-1})	K_{ac}
Au/PET	380.7 (1.4%)	1.045 (2.2%)	2.370 (3.5%)	201.88	
ZnO-NFs/Au/PET	419.9 (1.7%)	2.213 (2.1%)	1.687 (2.8%)	133.9	
EtG-AB/ZnO-NFs/Au/PET	429 (2.2%)	3.961 (2.9%)	1.329 (3.1%)	94.95	0.789
BSA/EtG-AB/ZnO-NFs/Au/PET	409.1(3.0%)	5.587 (4.0%)	1.538 (3.8%)	58.19	

Table 3-2: Theoretical fit of experimental results obtained in the stepwise fabrication process of BSA/EtG-AB/ZnO-NFs/Au/PET sensor from EIS measurements.

3.3.3. Repeatability and Reproducibility Measurements

For the repeatability measurements, the working electrode of the ZnO nanostructure-based EtG sensor was submerged into three different concentrations of EtG (1ng/ml, 100 ng/ml, and 100 μg/ml) five different times. A comparison of the signals for these concentrations is shown in Figure 3-6a. It was observed that the range of the data set for these three concentrations is 0.027 mA, 0.026 mA, and 0.043 mA, and the averages are 0.201 mA, 0.2456 mA, and 0.3214 mA, respectively. The maximum signal deviations from the averages are 0.018 mA, 0.0204 mA, and 0.0254 mA, respectively. Standard deviation (SD) values were determined from the corresponding data are 0.011 mA, 0.017 mA, and 0.0173 mA, respectively. Relative standard deviation (RSD) calculated from the SD values and averages are less than 8%. For the 100 μg/ml, 100 ng/ml and 1 ng/ml of concentrations, the RSD values are 5.393%, 7.085% and 5.383%, respectively. As the ranges and SD values

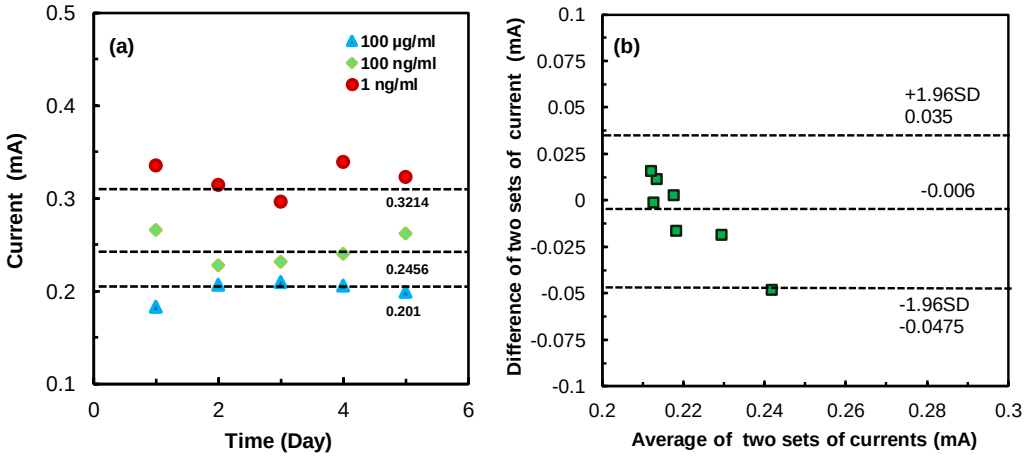

Figure 3-6: (a)Repeatability study for three different concentrations (b) Reproducibility study in between of two identical sensors for the concentration of 100 ng/ml

of the measurement for each concentration are in sub-mA, and the RSD values are below 8%, the signals do not significantly overlap during the repeatability measurements. In addition, the differences between the responses are 0.076 mA (1 ng and 100 ng) and 0.045 mA (100 ng and 100 µg), respectively. Hence, our sensor is sensitive to a lower concentration range rather than a higher one, which supports the argument above. Reproducibility of the sensor was also presented using the Bland-Altman plot in Figure 3-6b. The plot shows the average and difference between two measurements of current on the x and y-axes, respectively. In the reproducibility measurement, seven measurements of each of two different sensors were studied. The concentration of EtG was 10 µg/ml for all the measurements. The limits of agreement (LoA) are expressed as averages of the differences ±1.96 SD within 95% confidential interval. The upper and lower limits of LoA for the reproducibility were 0.035 and -0.0475, respectively. Only one outlier was found beyond the LoA, which supports the reproducibility of two different sensors for the specific concentration of EtG.

3.3.4. Shelf-life Studies

The shelf-life characteristics of the proposed immunosensor were investigated by periodic cyclic voltammetry measurements. This study was bifurcated in time frames to understand the sensor's short-term and long-term performances, and in both cases, the oxidation current was determined for 100 µg/ml of concentration. Short-term stability measurements were taken once a day for five consecutive days (shown in Figure 3-7a), starting immediately after the repeatability measurements described before. Contrarily, the long-term stability measurements were taken once every five days for 35 days (shown in Figure 3-7b). The long-term stability measurements started two months after the short-term shelf-life study. The sensor was stored in a sterile, humid, air-tight container at 4^{o}C between the measurements. For the short-term stability test, the SD and RSD values were low (mentioned in section 3.3), and the maximum oxidation current deviated only 8.9% from the average. It is observed that the current signal in the first measurement after two months of storage deteriorated ~ 58% compared to the average of the short-term test results. The redox peak current at the end of the 35 day-period reduced ~ 22% compared to the first data of the long-term stability test. This indicates that the fabricated biosensor can be employed over a month with a nominal degradation of its performance. The rate of deterioration of stability was an average of ~26% after every month. We attribute this deterioration to the following possible reasons: i) degradation of electrostatic bonding in between of antibody and electrode surface, ii) each freeze-thaw cycle causes the reagent to be less efficient, which leads to the degradation of the antibody.

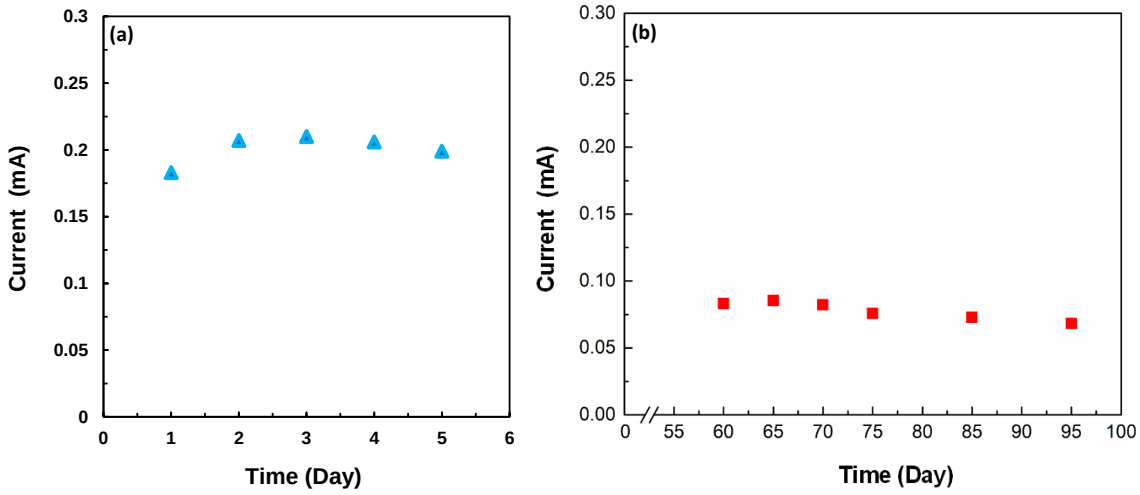

Figure 3-7: Shelf life of the ZnO-NFs based immunosensor, where the measurements were carried out for 100ug/ml of EtG (a) Short-time stability test during five consecutive days and (b) The performance of stability of one in a week during the period of 35 days after two months of short-time stability test

3.4 Conclusions

In this paper, we demonstrated highly sensitive EtG sensors based on sonochemically synthesized ZnO nanostructures. The sonochemical method allows the synthesis of nanostructures in ambient conditions (room temp, atmospheric pressure) and hence virtually on any substrates, including flexible ones. This method would also allow large-scale nanostructures synthesis (e.g., roll to roll). The high isoelectric point of ZnO (~9.5) allows the binding of antibody molecules without needing an additional linker layer and thereby simplifying the fabrication process and improving the long-term stability. Biosensing capabilities of the fabricated sensors were characterized by cyclic voltammetry and electrochemical impedance spectroscopy measurements. The sensitivity of the sensors was found to be 0.032 mA/log (μM)/cm^2 for the EtG concentration range of 1 ng/ml-100

µg/ml, which covers the physiological range while the limit of detection LoD was much lower than 1 ng/ml. Repeatability measurements showed low relative standard deviation (8%<), indicating negligible signal overlap. The shelf-life study demonstrated that the performance of the proposed sensor doesn't change significantly over a two-month period. The proposed method and device would help to realize wearable continuous alcohol sensing and monitoring platforms.

3.5 References

1. McPherson, S., Lucey, M. R., Moriarty, K. J., "Decompensated Alcohol Related Liver Disease: Acute Management," BMJ, vol. 352, pp.124, 2016.

2. Kendrick, S., Day, C., "Risk Factors for Alcohol-Related Liver Disease. In Alcohol abuse and liver disease," John Wiley & Sons, Ltd: Chichester, UK, pp 47–53. 2015.

3. Allie Johnson, "Drunken Driving: A $132 Billion Problem in America," 2013.

4. Panneer Selvam, A., Muthukumar, S.; Kamakoti, V., Prasad, S. A., "Wearable Biochemical Sensor for Monitoring Alcohol Consumption Lifestyle through Ethyl Glucuronide (EtG) Detection in Human Sweat," Sci. Rep., vol. 6 no.1,pp. 23111, 2016.

5. Goodman, R. A., Mercy, J. A., Loya, F., Rosenberg, M. L., Smith, J. C., Allen, N. H., Vargas, L., Kolts, R., "Alcohol Use and Interpersonal Violence: Alcohol Detected in Homicide Victims," Am. J. Public Health, vol.76 no.2, 144–149, 1986.

6. Drunk Driving | NHTSA https://www.nhtsa.gov/risky-driving/drunk-driving (accessed Feb 19, 2018.

7. Room, R., Babor, T., Rehm, J., "Alcohol and Public Health," Lancet, vol.365 no. 9458, pp. 519–530, 2005.

8. WHO | Global Status Report on Alcohol and Health WHO 2016.

9. Mason, M. F., Dubowski, K. M., "Alcohol, Traffic, and Chemical Testing in the United States: A Résumé and Some Remaining Problems," Clin. Chem., vol. 20, no. 2, pp. 126–140, 1974.

10. Dubowski, K. M., “Quality Assurance in Breath-Alcohol Analysis,” J. Anal. Toxicol., Vol.18, no. 6, pp.306–311, 1994.

11. Zuba, D., “Accuracy and Reliability of Breath Alcohol Testing by Handheld Electrochemical Analysers,” Forensic Sci., Int., vol. 178,pp. 29–e33, 2008.

12. Polissar, N. L., Suwanvijit, W., Gullberg, R. G., “The Accuracy of Handheld Pre-Arrest Breath Test Instruments as a Predictor of the Evidential Breath Alcohol Test Results,” J. Forensic Sci., vol. 60, no.2, pp. 482–487,2015.

13. Jatlow, P., O’Malley, S. S., “Clinical (Nonforensic) Application of Ethyl Glucuronide Measurement: Are We Ready?” Alcohol. Clin. Exp. Res. vol. 34, no. 6, pp. 968–975, 2010.

14. Jatlow, P. I., Agro, A., Wu, R., Nadim, H., Toll, B. A., Ralevski, E.; Nogueira, C.; Shi, J., Dziura, J. D., Petrakis, I. L., “Ethyl Glucuronide and Ethyl Sulfate Assays in Clinical Trials, Interpretation, and Limitations: Results of a Dose Ranging Alcohol Challenge Study and 2 Clinical Trials,” Alcohol. Clin. Exp. Res., 2014, 38 (7), 2056–2065.

15. Crunelle, C. L., Yegles, M., Nuijs, A. L. N. van, Covaci, A., De Doncker, M., Maudens, K. E., Sabbe, B., Dom, G., Lambert, W. E., Michielsen, P., “Hair Ethyl Glucuronide Levels as a Marker for Alcohol Use and Abuse: A Review of the Current State of the Art,” Drug Alcohol Depend., vol.134, pp.1–11, 2014.

16. Høiseth, G., Yttredal, B., Karinen, R., Gjerde, H., Christophersen, A., “Levels of Ethyl Glucuronide and Ethyl Sulfate in Oral Fluid, Blood, and Urine after Use of Mouthwash and Ingestion of Nonalcoholic Wine,” J. Anal. Toxicol. ,vol. 34 no.2, pp. 84–88, 2010.

17. Stewart, S. H., Koch, D. G., Burgess, D. M., Willner, I. R.; Reuben, A., “Sensitivity and Specificity of Urinary Ethyl Glucuronide and Ethyl Sulfate in Liver Disease Patients,” Alcohol. Clin. Exp. Res., vol. 37, no.1, 1pp. 50–155, 2013.

18. McDonell, M. G., Skalisky, J., Leickly, E., McPherson, S., Battalio, S., Nepom, J. R.,Srebnik, D., Roll, J., Ries, R. K., “Using Ethyl Glucuronide in Urine to Detect Light and Heavy Drinking in Alcohol Dependent Outpatients,” Drug Alcohol Depend., vol.157, pp.184–187, 2015.

19. Sinha, S., Sinha, A. K., De Luca, A., Ali, S. Z., Udrea, F.; Guha, P. K., Ray, S. K., Gardner, J. W., “Mask-Less Deposition of Au–SnO_2 Nanocomposites on CMOS MEMS Platform for Ethanol Detection,” Nanotechnology, vol. 27, no.12, pp.125502, 2016.

20. Jiang, G., Goledzinowski, M., Comeau, F. J. E., Zarrin, H., Lui, G., Le-nos, J., Veileux, A., Liu, G., Zhang, J., Hemmati, S., “Free-Standing Functionalized Graphene Oxide

Solid Electrolytes in Electrochemical Gas Sensors," Adv. Funct. Mater., vol. 26, no.11, pp.1729–1736, 2016.

21. Sanford, C. L.; Mantooth, B. A.; Jones, B. T., "Determination of Ethanol in Alcohol Samples Using a Modular Raman Spectrometer," J. Chem. Educ., vol.78, no. 9, pp.1221, 2001.

22. Shabaneh, A. A., Girei, S. H., Arasu, P. T., Rahman, W. B. W. A., Bakar, A. A. A., Sadek, A. Z., Lim, H. N., Huang, N. M., Yaacob, M. H., "Reflectance Response of 22.
23. Semwal, V., Shrivastav, A. M., Verma, R., Gupta, B. D., "Surface Plasmon Resonance Based Fiber Optic Ethanol Sensor Using Layers of Silver/silicon/hydrogel Entrapped with ADH/NAD," Sensors Actuators B Chem., vol. 230, pp. 485–492, 2016.

24. Williams, M. B.; Reese, H. D., "Colorimetric Determination of Ethyl Alcohol, Anal. Chem., vol. 22, no.12, pp.1556–1561, 1950.

25. Jalal, A. H., Umasankar, Y., Bhansali, S., "Development and Characterization of Fuel Cell Sensor for Potential Transdermal Ethanol Sensing," ECS Transactions, vol. 72, no. 31, pp. 25-31, 2016.

26. Swift, R. M., Martin, C. S., Swette, L., LaConti, A., Kackley, N., "Studies on a Wearable, Electronic, Transdermal Alcohol Sensor," Alcohol. Clin. Exp. Res., vol.16, no. 4, pp.721–725, 1992.

27. Umasankar, Y., Jalal, A. H., Gonzalez, P. J.; Chowdhury, M., Alfonso, A., Bhansali, S., "Wearable alcohol monitoring device with auto-calibration ability for high chemical specificity," 2016 IEEE 13th International Conference on Wearable and Implantable Body Sensor Networks (BSN), San Francisco, CA, pp. 353-358, 2016.

28. Vabbina, P. K., Karabiyik, M., Al-Amin, C., Pala, N., Das, S.; Choi, W., Saxena, T., Shur, M., "Controlled Synthesis of Single-Crystalline ZnO Nanoflakes on Arbitrary Substrates at Ambient Conditions," Part. Part. Syst. Charact., vol. 31, no.2, pp.190–194, 2014.

29. Vabbina, P. K., Nayyar, P., Nayak, A. P., Katzenmeyer, A. M., VJ, L., Pala, N., Islam, M. S., Talin, A. A., "Synthesis of Crystalline ZnO Nanostructures on Arbitrary Substrates at Ambient Conditions," International Society for Optics and Photonics, Vol. 8106, pp. 81060H, 2011.

30. Arya, S. K., Saha, S., Ramirez-Vick, J. E., Gupta, V., Bhansali, S., Singh, S. P., "Recent Advances in ZnO Nanostructures and Thin Films for Biosensor Applications: Review," Anal. Chim. Acta., Vol. 737, pp.1–21, 2012.

31. Nozaki, S., Sarangi, S. N., Uchida, K., Sahu, S. N., “Hydrothermal Growth of Zinc Oxide Nanorods and Glucose-Sensor Application,” Soft Nanosci. Lett., vol.3, no.4, pp. 23–26, 2013.

32. Psychoyios, V. N.; Nikoleli, G.-P., Tzamtzis, N., Nikolelis, D. P., Psaroudakis, N., Danielsson, B., Israr, M. Q., Willander, M., “Potentiometric Cholesterol Biosensor Based on ZnO Nanowalls and Stabilized Polymerized Lipid Film,” Electroanalysis, vol.25, no.2, pp. 367–372, 2013.

33. Xu, C., Yang, C., Gu, B., Fang, S., “Nanostructured ZnO for Biosensing Applications,” Chinese Sci. Bull., vol.58, no.21, pp. 2563–2566, 2013.

34. Zhou, J., Xu, N., Wang, Z. L., “Dissolving Behavior and Stability of ZnO Wires in Biofluids: A Study on Biodegradability and Biocompatibility of ZnO Nanostructures,” Adv. Mat., vol.18, no.18, pp. 2432-2435, 2006.

35. Li, Z.,Yang, R., Yu, M., Bai, F., Li, C., Wang, Z. L., “Cellular Level Biocompatibility and Biosafety of ZnO Nanowires,” J. Phys. Chem. C ., vol. 112, no. 51, pp. 20114–20117, 2008.

36. Israr, M. Q., Sadaf, J. R., Asif, M. H.; Nur, O., Willander, M., “Danielsson, B. Potentiometric Cholesterol Biosensor Based on ZnO Nanorods Chemically Grown on Ag Wire,” Thin Solid Films, vol. 519, no. 3, pp.1106–1109, 2010.

37. Vabbina, P. K., Kaushik, A., Pokhrel, N., Bhansali, S., Pala, N., “Electrochemical Cortisol Immunosensors Based on Sonochemically Synthesized Zinc Oxide 1D Nanorods and 2D Nanoflakes,” Biosens. Bioelectron. vol., 63, pp. 124–130, 2015.

38. Vabbina, P. K., Sinha, R., Ahmadivand, A., Karabiyik, M., Gerislioglu, B., Awadallah, O., Pala, N., “Sonochemical Synthesis of a Zinc Oxide Core–Shell Nanorod Radial P–n Homojunction Ultraviolet Photodetector,” ACS Appl. Mater. Interface, vol. 9, no.23, pp. 19791–19799, 2017.

39. Calzolari, A., Nardelli, M. B., “Dielectric Properties and Raman Spectra of ZnO from a First Principles Finite-Differences/finite-Fields Approach,” Sci. Rep., vol.3, no.1, pp. 2999, 2013.

40. Mohan, A. M. V., Windmiller, J. R., Mishra, R. K., Wang, J., “Continuous Minimally-Invasive Alcohol Monitoring Using Microneedle Sensor Arrays,” Biosens. Bioelectron., vol. 91, pp. 574–579, 2017.

41. Kim, J., Jeerapan, I., Imani, S., Cho, T. N., Bandodkar, A., Cinti, S., Mercier, P. P., Wang, J., “Noninvasive Alcohol Monitoring Using a Wearable Tattoo-Based Iontophoretic-Biosensing System,” ACS Sens., vol. 1, no. 8, pp. 1011–1019, 2016.

42. Jalal, A. H., Umasankar, Y., Gonzalez, P. J., Alfonso, A., Bhansali, S., “Multimodal Technique to Eliminate Humidity Interference for Specific Detection of Ethanol,” Biosens. Bioelectron., vol. 87, pp. 522–530, 2017.

43. Nkosi, D., Pillay, J., Ozoemena, K. I., Nouneh, K., Oyama, M., “Heterogeneous Electron Transfer Kinetics and Electrocatalytic Behaviour of Mixed Self-Assembled Ferrocenes and SWCNT Layers,” Phys. Chem. Chem. Phys., vol. 12, no. 3, pp. 604–613, 2010.

44. Arya, S. K., Kongsuphol, P., Wong, C. C., Polla, L. J., Park, M. K., “Label Free Biosensor for Sensitive Human Influenza Virus Hemagglutinin Specific Antibody Detection Using Coiled-Coil Peptide Modified Microelectrode Array Based Platform,” Sensors Actuators B Chem., vol. 194, pp. 127–133, 2020.

CHAPTER IV
ZnO NANOFLAKES BASED ENZYMATIC LACTATE BIOSENSORS

This chapter We report on a highly sensitive, selective, and flexible enzymatic sensor based on Zinc oxide nanoflakes (ZnO NFs) for noninvasive L-lactate sensing in sweat. A single-step sonochemical process was used to synthesize ZnO NFs on gold-coated flexible polyethylene terephthalate (PET) substrates. The lactate oxidase enzyme (LOx) immobilized on the as-synthesized ZnO-NFs-based sensing electrode provided a high level of selectivity for lactate sensing. The sensor was tested in the range of 10 pM – 20 mM, which covered the entire physiological range and demonstrated the sensitivity of 11.76 μA/decade/cm^2 and the limit of detection (LoD) of 1.26 nM. The presented sensor does not require a linker due to the high isoelectric point of ZnO-NFs yet demonstrated ~55 times better response compared to conventional gold electrodes with a linker. Our statistical analysis showed that the sensor also has high reproducibility.

4.1 Background of Wearable Lactate Biosensor Measurement Systems

Lactate is considered a key biomarker for oxidative tissue stress and an indicator of the healthy state of an individual when the required energy of the tissues cannot be encountered under regular aerobic states [1,4]. The pyruvic acid under anaerobic conditions is the source of lactic acid (lactate or 2-Hydroxypropanoic acid) which is commonly found in skeletal muscles, brain, red blood cells, and kidneys [5]. Lactate in human sweat has clinical importance and has been recommended as an early pointer of pressure ischemia [6]. Thus, for many health care applications, point-of-care (POC) monitoring of lactate

levels is ultimately important for its fast, accurate, and non-invasive manner [7]. The fluctuation of lactate levels from the normal may act as an indicator for the diagnosis of the severity of the patient's health status during surgery. Also, this fluctuation can be a potential tool for understanding the physiological condition of athletes or chronic diabetic or cardiac patients.

Biosensing is the process of sensing bio-compounds by monitoring the physical, biological, or chemical changes that they cause with their presence [8,9]. Two major types of biosensing techniques are commercially available: optical and electrochemical. In electrochemical bio-sensing, enzyme coupling (as biocatalyst) is an important archetype to amplify signals. Enzymes are easily available and are one of the most effective forms of natural catalysts. Enzymatic biosensors are simple, direct, fast, and provide biocompatibility, high selectivity, and sensitivity. The lactate oxidase (LOx) and lactate dehydrogenase (LDH) is the most commonly used enzymes for lactate assays [10].

Semiconducting metal-oxides and their nanomaterials are extensively used for biosensing applications to achieve selectivity, sensitivity, portability, miniaturization, simplicity, and low cost. Among them, ZnO exhibits several unique physical and chemical features such as chemical stability in physiological environments, high catalytic efficacy, biocompatibility, low toxicity, piezoelectric nature [11], and higher isoelectric point (IEP). Various morphologies of ZnO nanostructures (NSs), including nanowires [12], nanobelts [13], nanorods [14], quantum dots [15], nanoflower [16], and nanowalls [17], have been employed for immobilizing matrix within the design of different electrochemical enzymatic biosensors. Moreover, these nanostructures improve the detection mechanism

and sensing properties such as selectivity, sensitivity, and stability of several biomarkers, including glucose, galactose, and cholesterol [18,19]. ZnO nanoflakes (ZnO-NFs) offer several exclusive advantages compared to bulk materials. For example, polarized (0001) plane orientation enhances enzyme immobilization which improves sensing performance [20]. A high isoelectric point (9.5) of ZnO NFs [21], [22] enhances the immobilization of any biomolecules, which eliminates the necessity of an additional binding layer. This elimination of additional layers and immobilization of the enzyme offers a steady and shorter pathway for quick electron transportation, increasing the electron transfer rate. Moreover, modification of the ZnO–biomolecules interface through the plane orientation enriches the sensing ability of a ZnO NFs-based enzymatic sensor. Engineering of the morphology and size of NFs, effective surface area and adsorption capability, functionality [23] also improve electron transport.

We present a highly sensitive and selective enzymatic sensor based on ZnO nanoflakes synthesized on Au-coated stretchable polyethylene terephthalate (PET) substrates and decorated with LOx for lactic acid detection in sweat. The sonochemical synthesis method would allow fabrication and integration of the demonstrated sensors on various other flexible substrates, including fabrics and papers. Combined with their small form factor and biocompatibility, our ZnO-NF-based sensor platform is a strong candidate for wearable and PoC continuous lactic acid monitoring systems. Such a wearable integrated system would also include miniaturized potentiostat and wireless communication components such as Bluetooth transceivers [25-28].

4.2 Experimental

4.2.1 Chemicals and Apparatus

Materials The LOx enzyme (Aerococcus viridans species) was purchased from MYBioSource, USA Hexamethylenetetramine [HMT; $(CH_2)_6$ N_4], thiol-based cross-linker, Zinc Nitrate hexahydrate [ZNH; Zn $(NO_3)_2$ $6H_2O$], dithiobis-succinimidyl-propionate (DTSP), L-lactic acid, sodium borohydride ($NaBH_4$), were purchased from Sigma-Aldrich (USA). NaH_2PO_4 (Sodium phosphate monobasic) and Na_2HPO_4 (sodium phosphate dibasic) salts through-plane from Sigma Aldrich, which used to prepare phosphate buffer solution (PBS, pH 6.5) for electrochemical studies. Human sweat samples were purchased from Innovative Research. All the chemicals which have been used in the experiments were of analytical grade. In addition, CHI604D, CH Instruments, USA (an electrochemical analyzer) was employed for the Lactate detection measurements. Nomadic Raman microscope (BaySpec) with 532 nm laser was used to measure the peak shift before and after the immobilization to ensure the successful immobilization of LOx enzyme on the ZnO-NFs based electrodes. Scanning Electron Microscopy (SEM, JOEL 7000FSEM) was used to image the nanostructures of the ZnO surface. NanoIonics Multiview 2000TS Atomic Force Microscope (AFM) was used to measure the surface roughness, Selective Area Electron Diffraction (SAED), and High-Resolution Transmission Electron Microscopy (HRTEM) were used for imaging of ZnO nanoflake structures.

4.2.2 Fabrication and Surface Functionalization of ZnO-NFs Electrodes

An ultrasonic bath was used to wash the PET substrates for 15 min each with IPA (isopropanol) and DI (deionized) water for the fabrication of the gold (Au)-deposited PET substrates. Subsequently, they were dried up using nitrogen gas (N_2). By using the e-beam evaporation, gold (60 nm) was coated on PET substrates with a thin adhesive layer of Titanium (20 nm), as shown in Figure 4-1 (a). The substrates were cleaned with DI water and dried by N_2 gas for ZnO-NFs growth. The PET/Au/ZnO-NFs based lactate sensing sensor, as shown in Figure 1(b), and its flexible nature were presented in Figure 4-1(c) and 1(d).

For the NFs synthesis, a single-step sonochemical approach reported in [24] was employed. A solution mixture with 20 mM ZNH and 20 mM HMT was prepared by stirring with a magnetic stir bar at the speed of 350 rpm at room temperature and pressure for the duration of 5 min to ensure the progress of 2D ZnO- NFs. By using a commercial high-intensity ultrasound set up, the submerged substrate in the solution was then irradiated by for 15 min. of four cycles at the intensity of 30 Wcm^{-2} and the frequency of 20 kHz. The temperature was maintained by $\leq 50°$ C of the aqueous mixture of ZNH and HMT. Lastly, DI water and N_2 were used for cleaning the substrate after each cycle in a similar manner.

ZnO-NFs have good adherence to the substrate (PET). We had analyzed several ZnO-NFs based PET substrates by using SEM before and after the electrochemical tests and did not observe any delamination.

ZnO-NFs based flexible electrodes were surface functionalized by immobilizing with lactate oxidase via electrostatic physical adsorption owing to the variation in the IEP

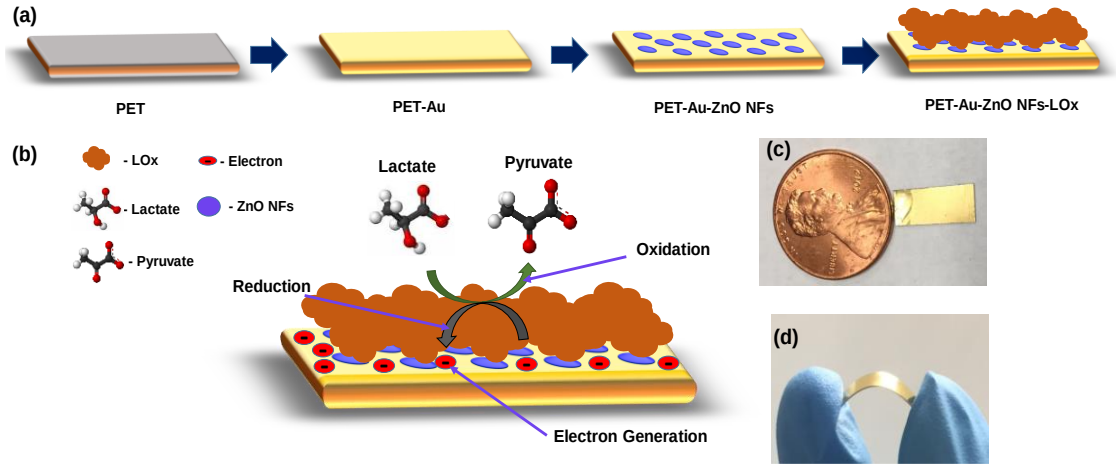

Figure 4-1: (a)Enzymatic lactate sensor: Fabricating and immobilizing process (b) Working mechanism and redox reaction of enzymatic lactate sensor (c)PET/Au/ZnO-NFs based electrode and (c) flexibility of PET/Au/ZnO-NFs electrode

of the enzyme (4.2) and ZnO (9.5). The difference in IEP eliminates the necessity of an intermediary thin film as a linker. 0.1 M PBS (pH 6.5) having a concentration of 27 mg/mL of the enzyme was used to prepare a LOx solution. The PET/Au/ZnO-NFs based electrodes had a working area of 0.5cm × 0.5cm. 10 µL of LOx was used on the working area of the electrodes for the immobilization of lactate oxidase. The electrodes were carefully washed with PBS and DI water to eliminate any unbound enzyme immediately after the immobilization. The fabricated sensors were then preserved at 4^{o}C in a refrigerator.

4.2.3 Material Characterization of ZnO-NFs Based Electrodes

The SEM was used to image the nanostructures of the ZnO surface during several phases of electrode fabrication. Uniform and well-oriented synthesis of ZnO-NFs on the gold-deposited PET substrates were found, as presented in Figures 4-2(a) and 4-2(b). The

average lateral dimensions of ZnO NFs were 0.5cm × 0.5cm and thickness of 20nm. Figure 4-2(c) represents that the surface of the electrode became smoother and uniform after LOx immobilization. The morphological modification indicates that the LOx has been properly introduced over the ZnO-NFs matrix. The selective area electron diffraction (SAED) and high-resolution transmission electron microscopy (HRTEM) studies in Figures 4-2(d) and 2(f) were performed using an electron microscope with a 300KeV electron beam. The selective area electron diffraction (SAED) analysis in Figure 4-2(d) was carried out using commercial software (Single Crystal). The SAED measurements depict that the 2D ZnO nanoflakes exhibit hexagonal wurtzite structure with a=3.25Å and c=5.21 Å, oriented along (0001) plane and the lateral growth direction perpendicular to the (0110) plane. The HRTEM images are taken at the major edge of the flakes showed that the fringes are almost parallel to the edge with a lattice spacing of 2.74Å. To measure the surface roughness, an atomic force microscope (AFM) was used, as shown in Figure 4-2(e). A Cr tip having with a diameter of 20 nm was used for this purpose which functioned at the resonance frequency of 34.95 kHz. After the immobilization of the enzyme, LOx/ZnO-NFs/PET/Au electrode exhibited average surface roughness of 0.321 µm while the roughness of the surface of the PET/Au /ZnO-NFs electrode was higher with an average surface roughness of 1µm. The decrement in roughness value was owing to the introduction of the LOx enzyme, which occupies the porous electrode surface. The peak of the Raman spectra was found at ~ 600 cm^{-1} for PET/Au/ZnO-NFs (shown in Figure 4-2(g)) electrode using Raman Spectroscopy which can be attributed to the second-order longitudinal optical phonon vibration [29]. LOx/ZnO-NFs/PET/Au electrode (Figure 4-2(h)) was also analyzed with Raman

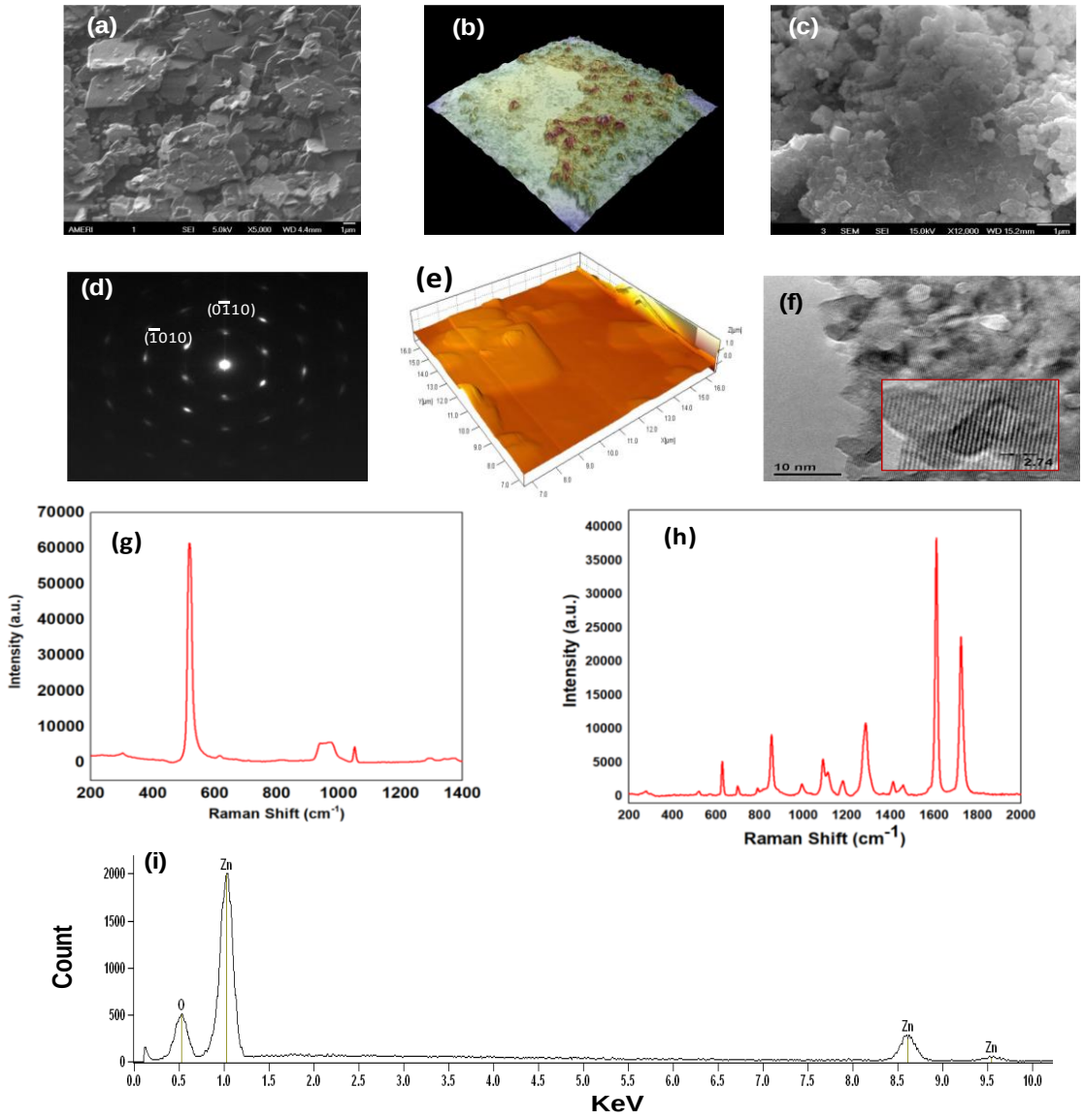

Figure 4-2: (a) SEM image of PET/Au/ZnO-NFs (b) FSEM image (3D) of PET/Au/ZnO-NFs (b) FSEM image (3D) of PET/Au/ZnO-NFs (c) SEM image of PET/Au/ZnO-NFs/LOx (d) SAED pattern of ZnO-NFs (e) AFM image of PET/Au/ZnO-NFs (f) HRTEM at the edge of a flake (g) Raman spectra on PET/Au/ZnO-NFs electrode and (h) Raman spectra of PET/Au/ZnO-NFs/LOx electrodes (i) EDS data ensures the grown of nano flakes are pure ZnO

Spectroscopy which demonstrated additional peaks compared to that characteristic of wurtzite ZnO-NFs. Moreover, the shifting of this peak to ~1600 cm^{-1} is evidence of

successful immobilization of LOx enzyme on ZnO-NFs based electrode. The composition of the element of the nanoflakes is confirmed by EDS (energy-dispersive X-ray spectroscopy) data demonstrated in Figure 4-2-(i), which showed that the nanoflakes are purely ZnO with no observed contaminations.

4.2.4 Working Principle of ZnO-NFs Based Lactate Sensor

Electrochemical sensing techniques based on catalytic electron transfer mechanism were used in the presented lactate sensor. The electron transfer is associated with the catalytic conversion of the substrate to the product. LOx, the redox enzyme, acts as an electrocatalyst, enabling the flow of the electrons between the substrate molecule and the electrode containing no intermediary layer, as shown in Figure 4-1 (a, right). Because of the redox reaction in the presence of L-lactic acid in biofluids, the output response of the sensor changes. Due to the oxidation of LA in the existence of introduced LOx, unbalanced pyruvic acid is formed in the aqueous solution. This acid is instinctively transformed into pyruvate and H_2O_2, as given in Figure 4-1 (b) and the redox pair equations (1), (2), and (3) [30] [31]:

$$\text{L-lactic acid} + O_2 \rightarrow \text{Pyruvic acid} + H_2O_2 \quad (1)$$

$$H_2O_2 \rightarrow O_2 + H^+ + e^- \quad (2)$$

$$\frac{1}{2}O_2 + 2H^+ + 2e^- \rightarrow H_2O \quad (3)$$

Thus, enzymatic biosensors usually offer selectivity since their range of operating potential is closer to the redox potential of the enzyme itself, which prevents interfering reactions.

A three-electrode system was used in the sensing experiments. The PET/Au/ZnO-NFs/LOx biosensor was used as the working electrode, Ag/AgCl, 0.1M KCl was used as a

reference electrode, and Pt served as an auxiliary electrode. 3mL PBS (pH 6.5) was employed for all measurements. In such a setup, since the PBS (0.1M) is saturated with oxygen, the lactic acid (LA) is oxidized in the presence of LOx at the electrolyte/ZnO-NFs-based electrode interface, and the pyruvic acid and H_2O_2 is produced as the byproducts. Later, H_2O_2 disintegrates into O_2 and H^+ ions and generates electrons. These electrons are rapidly transferred through the electrode, forming a current that is measured as the sensor response. Contrarily, the reduction occurs in the auxiliary electrode in the presence of O_2 and H^+ ions, and H_2O is produced.

4.3 Results and Discussions

4.3.1 Calibration of the Enzymatic Lactate Sensor Based on ZnO-NFs

The operation Cyclic Voltammetry (CV) technique was employed to examine the electrochemical phenomenon of electrodes and to determine the sensitivity of the fabricated LOx/ZnO- NFs/Au/PET electrodes over a range of LA concentration. PEM Six different concentrations of LA within the range of 10 pM – 20 mM was introduced in the presence of 10 μL of LOx on the PET/Au/ZnO-NFs based working electrode. The CV measurements were taken in the potential range of -0.1V – 1.2V at a scan rate of $50mVs^{-1}$ (For example, both the oxidation and reduction peaks were observed for the 10mM of LA in Figure 4-3 (a), inset). During the experiments, the sensor's output signals (oxidation peaks) varied significantly with the variation of LA concentration. With the increase of the LA concentration, a gradual increment of oxidation peaks was observed, as shown in Figure 4-3 (a).

In the presence of immobilized lactate oxidase, LA converted into pyruvic acid as a mid-product and later formed pyruvate and H_2O_2 as byproducts following the equation (1). For the effectiveness of a biosensor, factors such as electron transfer rate and enzyme binding play major roles. The ZnO-NFs exhibit a positive surface charge due to high IEP (~9.5). For all the experiments, a pH value of 6.5 was used, which offers binding sites for LOx with an IEP of 4.2, which exhibits negative charge under the experimental conditions.

Six different concentrations (10 pM, 1 nM, 1 μM, 1 mM, 10 mM, and 20 mM) were considered for the current vs. concentration curve as shown in Figure 4-3 (b), where the output current for each concentration was measured ten times. The fabricated electrochemical lactate sensor presented a linear response (in logarithmic scale) within the range of 10 pM to 20 mM of L-lactic acid concentrations, as shown in Figure 4-3 (b). The sensitivity of the enzymatic lactate biosensor was determined to 11.76 μA/decade/cm^2. The trend of the curve is significantly linear, and the coefficient of determination (R^2) was found 0.93. The limit of detection [32] of the sensor was determined by ~1.26 nM. Also, the sensor showed linearity within the physiological range having with $R^2 = 0.97$ (Figure 4-3 (b), inset).

DTSP linker layer was introduced on PET/Au/LOx electrodes having a similar size to the fabricated PET/Au/ZnO electrodes to show the benefit of such kinds of electrodes. A comparison study of the responses of the conventional thin-film gold electrode with the additional linker layer and the ZnO- NFs electrode without binding layer for L-Lactate sensing was shown in Figure 4-3(c). Due to the advantage of the high isoelectric point of

ZnO, this ZnO-NFs-based electrode exhibited ~55 times better response owing to the removal of the intermediary linker layer.

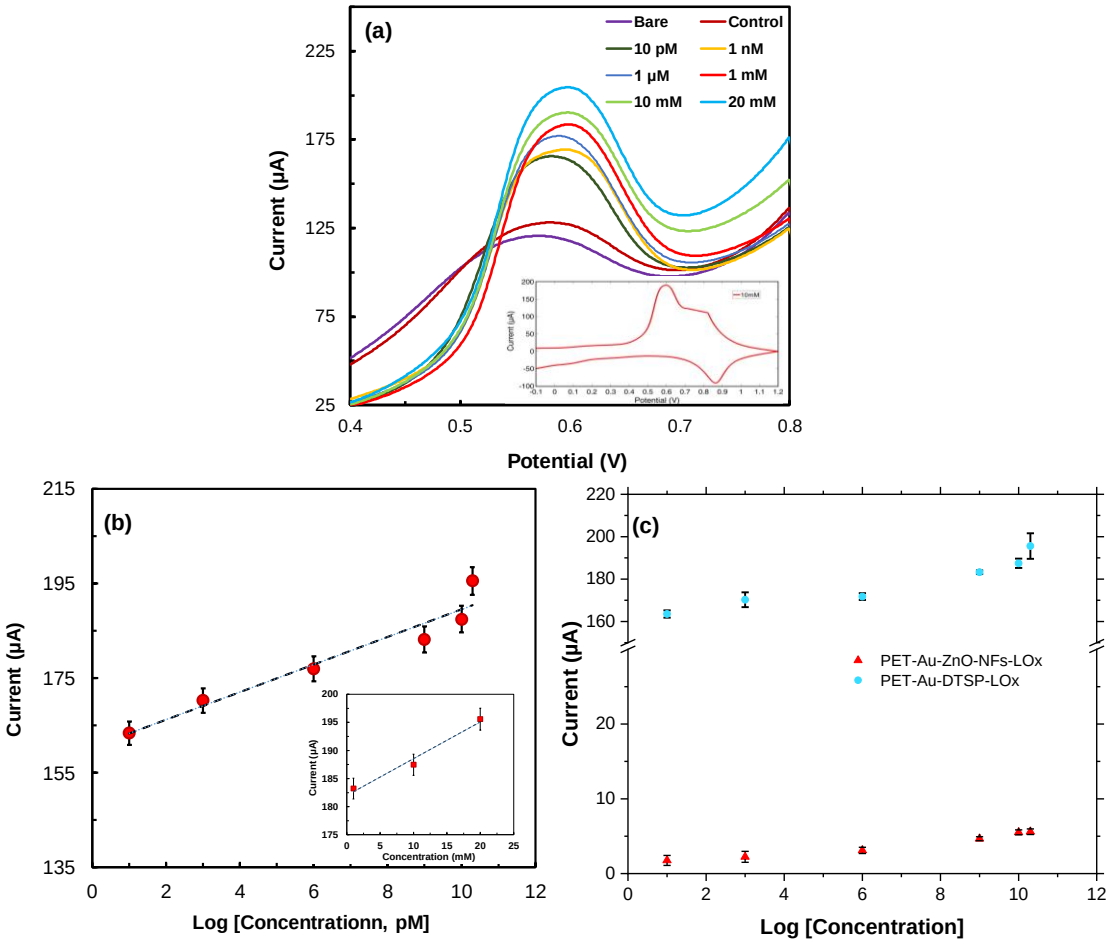

Figure 4-3: CV studies of LOx immobilized ZnO NFs biosensor for LA concentration varying from 10 pM to 20 mM (b) Linear curve fitting (c) Responses of PET/Au/ZnO-NFs/LOx electrode (solid blue circles) and PET/Au/DTSP/LOx electrode (solid red squares) for L-lactic acid detection

4.3.2 Electrochemical Impedance Spectroscopy (EIS) Measurements

For the analysis of complex electrical properties of a system, EIS was considered as a robust and sensitive tool to surface phenomena. Impedance spectra can be analyzed

with an equivalent electrical circuit to extract the values of its components, which model the interfacial phenomena. Figure 4-4 (a) represents the Nyquist plot of the EIS spectra for ZnO-NFs/Au /PET/Lox electrodes with different concentration (1 nM, 1 µM, 1 mM, 10 mM, and 20 mM) of lactic acid. We performed the EIS measurements in the 1000 Hz - 100KHz frequency range by applying an AC voltage of 0.239 V Using a CHI instrument (CHI604D) impedance analyzer. The Z View software is used to fit EIS data and equivalent parameters. The equivalent circuit, as shown in Figure 4-4 (inset), was satisfactorily fitted for the EIS data, and the values are given in Table 4-1. In the model, R_s signified the cell resistance, R_1 indicated the resistance at the interface between the ZnO-NFs/Au /PET/LOx electrode and the electrolyte where ions are generated, Constant Phase Element (CPE1) represented impedance of bio-active area of the electrode, CPE2 represented the impedance of the surface of the electrode without functional groups. In Figure 4-4, the Nyquist plot denoted diverse values of R_1, which showed progressive decrement with respect to the LA

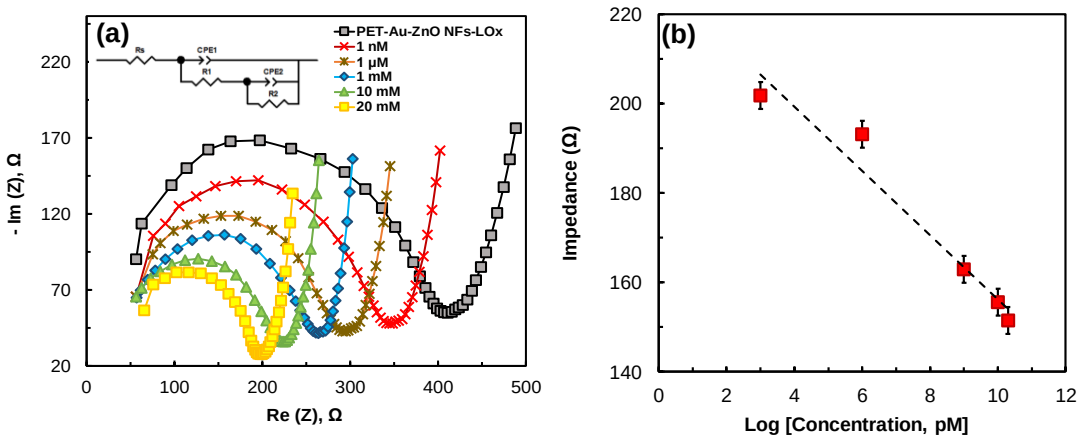

Figure 4-4: Nyquist plots of EIS response of PET-Au-ZnO NFs-LOx when the immobilization of series concentrations of five samples: 1 nM to 20 mM concentrations. The inset shows the equivalent circuit model and (b) Dose responses of total impedance output for calibrating sensor for different concentration (1 nM-20 mM) of lactic acid

concentration. Figure 4-4 (a) depicted that there was a significant reduction in impedance with LA concentration. This occurrence supports the reasoning of the cumulative current with the increasing LA concentration in Figure 3. The cumulative impedances for the five different concentrations of lactic acid (1nM – 20 mM) were determined from the real and imaginary impedances and plotted in Figure 4-4 (b). For each concentration, the impedance was determined five times. The impedances were extracted from the maximum values of the R*1* with the frequency range of 1000 Hz -100 kHz and the initial voltage of 0.239 V. The calibration plot resulted in a substantially linear relationship with the coefficient of determinant, $R^2 = 0.95$.

4.3.3 Measurement of Repeatability and Reproducibility

The working electrode of the fabricated lactate sensor was immersed in three different concentrations of lactate (1 nM, 1mM, and 20 mM) solution ten different times.

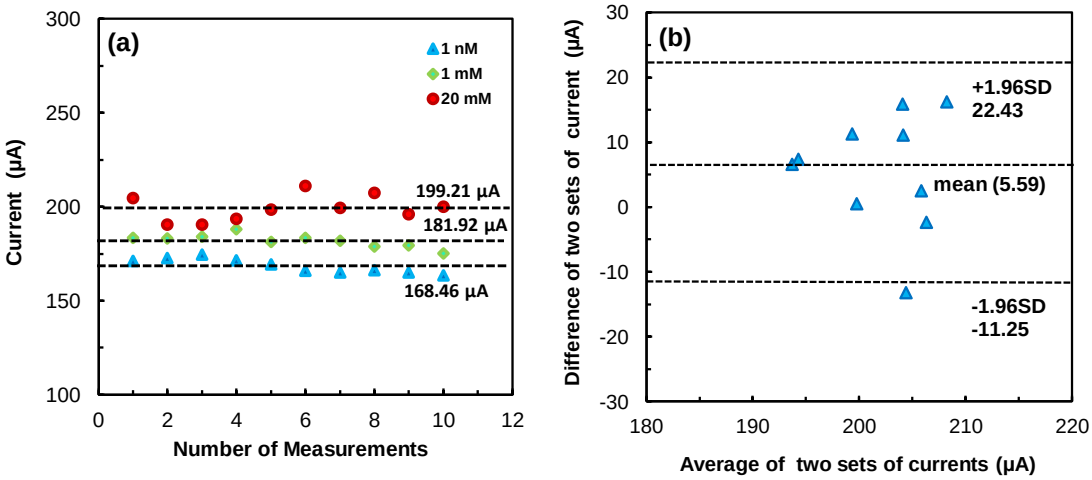

Figure 4-5: Repeatability study of a single ZnO NFs based enzymatic lactate sensor for three different concentrations: 1 nM, 1 mM, and 20 mM identical sensors used for reproducibility study for the concentrations of 20 mM

A nominal deviation was evident from the current data of these concentrations. For each concentration, the standard deviation (SD) of these data was below 7 μA, whereas the relative standard deviation (RSD) of these measurements was below 4%. Also, the average differences of the current (ΔA) in between the signals were 13.46 μA (1 nM and 1 mM) and 17.29 μA (1 mM and 20 mM), respectively. However, it was evident that the currents values were separated from each other with minimum overlaps.

The experimental Bland-Altman plot [33] was used to analyze the reproducibility of the sensor, as shown in Figure 4-5(b). Here, this plot demonstrated a relationship between the average and difference of two sets of amperometric data for the reproducibility test. In this study, each data set contained ten measurements of each of two different sensors. The entire study was executed following a specific concentration of lactate (20 mM) for all the measurements of both data sets. A student t-test was also executed to corroborate the reproducibility results from the above two different data sets (10 measurements each) of two identical lactate sensors. The results showed that the p (T<=t) value for the data sets was 0.08 (> 0.05). Based on the p-values, it is evident that the data sets supported the null hypothesis. Hence, we inferred that the results from both sensors' data were reproducible.

4.3.4 Measurement of Lactic Acid in Biological Samples

To assess the performance of our sensor for real-life cases, we measured the lactate concentration in human sweat samples. Six different human sweat samples (S1, S2, S3, S4, S5, and S6) were obtained from de-identified subjects. Lactate levels in the samples were

determined using standard lactic acid assay protocols prior to our analysis, as listed in Table II. The samples were diluted with 0.01 M PBS solution before the measurements. We then measured the lactate levels in the samples through electrochemical analysis using PET-Au-ZnO-NFs-LOx electrode and their corresponding linear calibration curves obtained from the standard assay concentrations. The results were compared to the values obtained

Sample	By Standard Assay (mM)	ByOur Biosensor (mM)	Recovery (%)	RDS (%)
S1	25	27.25	89	6.97
S2	10	7.13	71.3	14.91
S3	2	1.41	70.5	70.98
S4	45	48.36	92.53	10.16
S5	35	37.43	93.06	10.2
S6	55	50.71	92.2	1.88

Table 4-1: Determination of lactate in human sweat using the ZnO-NFs/Au /PET/Lox electrode.

previously by standard protocols and are also listed in Table 4-1. It can be seen from Table II that our biosensor provided recovery rates between 70.5 % - 93.06 % and the RSD values between 1.38% - 14.91%. These results showed that ZnO NFs-based enzymatic biosensor could provide reliable lactate detection (average of ~85% recovery) in human sweat samples.

4.4 Conclusion

A linker-free electrochemical biosensor consisting of ZnO NFs with immobilized lactate oxidase has been successfully demonstrated for monitoring L-lactate in sweat. A

wide range of linearity (with R^2 of 0.97) covering the physiological range has been observed with a sensitivity of 11.76 μA/decade/cm^2 and a limit of detection of 1.26 nM. The enzymatic sensor also showed good repeatability for three sample concentrations. The SD and RSD values of the measurements for each concentration were < 7 μA and < 4%, respectively. The reproducibility data for two identical sensors were found within the LoA of the Bland-Altman plot with a statistically significant p-value of 0.08 that derived from the student t-test. The sensor was also tested with real human sweat samples for future implementation on wearables. The average recovery was found ~85% with < 10% of RSD, which supports the fact that the proposed sensors are reliable for real-life applications. The proposed method and device would help to realize wearable and PoC platforms for continuous lactate monitoring.

4.5 References

1. Wan, J. J., Z. Qin, P. Wang, Y. Sun and X. Liu, "Muscle fatigue: general understanding and treatment," Experim. & Molecular Med., vol.49, 2017.

2. Papadimitriou, K., Alegría, Á., Bron, P. A., de Angelis, M., Gobbetti, M., Kleerebezem, M., Lemos, J. A., Linares, D. M., Ross, P., Turroni, C. S. F., van Sinderen, D., Varmanen, P., Ventura, M., Zúñiga, M., Tsakalidou, E., Kok, J., "Stress physiology of lactic acid bacteria," Microbiology and Molecular Biology Rev., vol. 80, 2016.

3. Pundir, C. S., Narwal, V., and Batra, B., *Biosens. and Bioelec.*, vol. 86, pp. 777,2016.

4. DeBacke, D., Ceteu, J., Zhang, H.B., Norrenberg., and Vincent, J.L., "Lactate production by the lungs in acute lung injury," Am J. Respir Crit. Care Med, vol. 156, pp. 1099, 1997.

5. Alam, F., RoyChoudhury, S., Jalal, A.H., Umasankar, Y., Forouzanfar, S, Akter, N., Bhansal, S. and Pala, N., "Lactate biosensing: the emerging point-of-care and personal health monitoring," Biosensors and Bioelectronics, vol. 117, pp. 818-829, 2018.

6. Mehrotra, P., “Biosensors and their applications – A review,” J. Oral Biol Craniofac Res.,vol. 6, pp. 153–159, 2016.

7. Bhalla, N., Jolly, P., Formisano, N., and Estrela, P., “Introduction to biosensors” Essays in Biochem., vol. 60, pp. 1-8, 2016.

8. Salazar, P., Martín, M., O’neill, R., Roche, R., González-Mora, J.L., “Biosensors based on prussian blue modified carbon fibers electrodes for monitoring lactate in the extracellular space of brain tissue,” Int. J. Electrochem. Sci., vol. 7, pp. 5910–5926, 2012.

9. Alam, F., Aghaei, S.M., Jalal, A.H., and Pala, N., "Flexible piezoelectric nanogenerator based on sonochemically synthesized ZnO nanoflakes for self-powered devices and wearable energy harvesting”, MRS Advances, vol. 4, pp. 1355-1360,2018.

10. Zang, J., Li, C. M.,Cui, X., Wang, J., Sun, X., Dong, H., and Cun, C.Q., “Tailoring Zinc Oxide Nanowires for High Performance Amperometric Glucose Sensor”, Electroanalysis, vol. 19, no. 9, pp. 1008–1014, 2007.

11. Wang, J. X., Sun, X.W., Xie, S.S., Yang, Y., Chen, H.Y., Lo G.Q.,and Kwong, D.L.,” Preferential Growth of SnO_2 Triangular Nanoparticles on ZnO Nanobelts”, J. Phys. Chem. C, vol. 111, pp. 7671-7675,2007.

12. Liu, X.,Hu, Q., Wu, Q., Zhang, W., Fang, Z., and Xie, Q., “ Aligned ZnO nanorods:A useful film to fabricate Amperometric glucose biosensor”, Colloids and Surfaces B: Biointerfaces, vol.74, pp. 154-158, 2009.

13. Microneedles Integrated with ZnO Quantum-Dot-Capped Mesoporous Bioactive Glasses for Glucose-Mediated Insulin Delivery”, ACS Biomater.Sci. Eng., vol. 4, pp. 2473-2483,2018.

14. Sharma, V., Mohammad, A., Mishra, V., Chaudhary, A., Kapoor K., and Mobin, S. M.,“Fabrication of innovative ZnO nanoflowers showing drastic biological activity”, New J. Chem., vol. 40, pp. 2145-2155, 2016.

15. Psychoyios, V. N., et al., “Potentiometric cholesterol biosensor based on ZnO nanowalls and stabilized polymerized lipid film,” Electroanalysis, vol. 25, no. 2, pp. 367–372, 2013.

16. Nozaki, S., Sarangi, S. N., Uchida, K., and Sahu, S. N., “Hydrothermal Growth of Zinc Oxide Nanorods and Glucose-Sensor Application,” Soft Nanosci. Lett., vol. 3, no. 4, pp. 23–26, 2013.

17. Psychoyios, V. N., G.-P. Nikoleli, N. Tzamtzis, D. P. Nikolelis, N. Psaroudakis, B. Danielsson, M. Q. Israr, and M. Willander, "Potentiometric Cholesterol Biosensor Based on ZnO Nanowalls and Stabilized Polymerized Lipid Film," Electroanalysis, vol. 25, no. 2 pp. 367–372, 2013.

18. Vabbina, P. K. , Kaushik, A., Pokhrel, N., and Bhansali, S., " Electrochemical cortisol immunosensors based on sonochemically synthesized zinc oxide 1D nanorods and 2D nanoflakes," Biosens. Bioelec. vol. 63, pp. 124-130,2015.

19. Zhou, J.,Xu, N., and Wang, Z. L.,"Dissolving Behavior and Stability of ZnO Wires in Biofluids: A Study on Biodegradability and Biocompatibility of ZnO Nanostructures," Adv. Mat., vol. 18, no. 18, pp. 2432–2435, 2006.

20. Li, Z., Yang, R., Yu, M., Bai, F., Li, C., and Wang, Z. L., "Cellular Level Biocompatibility and Biosafety of ZnO Nanowires," J. Phys. Chem. C., vol. 112, no. 51pp. 20114–20117, 2008.

21. Vabbina, P. K., Sinha, R., Ahmadivand, A., Karabiyik, M., Gerislioglu, B., Awadallah, O., and Pala, N., "Sonochemical Synthesis of a Zinc oxide Core-Shell Nanorod Radial p-n Homojunction Ultraviolet Photodetector," ACS Appl. Mater. Interfaces., vol. 9, no. 23, 19791–19799, 2017.

22. Vabbina, P. K., Karabiyik, M., Al-Amin, C., N. Pala, "Controlled Synthesis of Single-Crystalline ZnO Nanofl akes on Arbitrary Substrates at Ambient Conditions," Part & Part. Syst. Charact., vol. 31, pp. 190-194, 2014.

23. Panneer Selvam, A., Muthukumar, S., Kamakoti, V., and Prasad, S., "A wearable biochemical sensor for monitoring alcohol consumption lifestyle through Ethyl glucuronide (EtG) detection in human sweat," Sci. Rep., vol. 6, no. 1, pp. 23111,2016.

24. Kim, J., Imani, S., de Araujo, W. R., Warchall, J., Valdés-Ramírez, G., Paixão, T. R.L.C., Mercier, P. P., and Joseph Wang, "Wearable salivary uric acid mouthguard biosensor with integrated wireless electronics," Biosens. Bioelec. vol. 74, pp. 1061-1068,2015.

25. Kim, J., Jeerapan, I., Imani, S., Cho, T. N., Bandodkar, A., Cinti, S., Mercier, P. P., and Wang, J., "Noninvasive Alcohol Monitoring Using a Wearable Tattoo-Based Iontophoretic-Biosensing System," ACS Sens., vol. 1, pp. 1011–1019, 2016.

26. Umasankar, Y., Jalal, A. H., Gonzalez, P. J., Chowdhury, M., Alfonso, A., and Bhansali, S., "Wearable alcohol monitoring device with auto-calibration ability for high chemical specificity," in 2016 IEEE 13th International Conference on Wearable and Implantable Body Sensor Networks (BSN), San Francisco, CA, 2016, pp. 353-358.

27. Calzolari, A., Nardelli, M. B., “Dielectric properties and Raman spectra of ZnO from a first principles finite-differences/finite-fields approach,” Sci. Rep., vol. 3, no. 1, pp. 2999, 2013.

28. Zhang, Y., Kang, Z., Yan, X., and Liao, Q., “ZnO nanostructure in enzyme biosensors,” Sci. China Mat. vol. 58, pp. 60-76,2015.

29. Nesakumar, N., Thandavan, K., Sethuraman, S., Krishnan U. M., and Rayappan, J.B.B., “An electrochemical biosensor with nanointerface for lactate detection based on lactate dehydrogenase immobilized on zinc oxide nanorods”, J. Colloid and Interface Sci., vol. 414, pp. 90-96,2014.

30. Armbruster D. A., and Pry, T., “Limit of Blank, Limit of Detection and Limit of Quantitation”, Clin. Biochem Rev., vol. 29, pp. 49—52, 2008.

31. Giavarina, D., “Understanding Bland Altman analysis”, Biochemia Medica, vol. 25, pp. 141–151, 2015.

CHAPTER V
THIN-FILM NANOSTRUCTURE-BASED ENZYMATIC ALCOHOL SENSOR

Fast and accurate detection and monitoring of alcohol consumption have significant importance for safety and clinical applications. The excessive consumption of alcohol causes many health issues, such as colon, rectum, mouth, and throat cancers, liver cirrhosis, stroke, cardiovascular disease, and several psychiatric comorbidities. Alcohol addiction treatments also require close monitoring of consumption. The correlation of alcohol concentration levels in sweat with the blood alcohol content (BAC) encourages developing a wearable sensing platform for alcohol detection noninvasively, continuously, and in real-time. Moreover, sweat is considered one of the most useful body fluids for biosensing applications since it contains several biomarkers with crucial medical information and is easy to collect. ZnO has exclusive chemical and physical characteristics to enhance chemical stability in physiological environments. Moreover, it has higher catalytic activity, biocompatibility, and a higher isoelectric point (IEP) of 9.5. Such a high IEP of ZnO nanoflakes (NFs) improves any biomolecules' immobilization. Hence, there is no necessity for an additional binding layer between the enzyme and the sensing electrode. A single-step sonochemical approach was developed to synthesize a thin layer of ZnO-NFs virtually on any substrate. This technique is fast, catalyst-free, less expensive, and ecologically benign, which enables a well-oriented growth on polyethylene terephthalate (PET) over an extensive range. In this study, an electrochemical biosensor was fabricated by immobilization of alcohol oxidase (AOX) on ZnO nanoflakes with a thickness of 20nm,

synthesized on Au-coated PET. The results demonstrated a fast response within 5s. The sensor was tested in the range of 1 mg – 400 mg, which covers the entire physiological range, and the sensitivity of the sensor was determined by 3.47 *n*A/mg/dL/cm^2.

5.1 Background

Alcohol addiction is one of the major leading global risks for mortality. Such addiction causes nearly 2.5 million fatalities each year globally and is the primary cause of several disorders, diseases, and accidents. Alcohol Use Disorder (AUD) is a prevalent case among Americans, and only one-seventh of 18 million AUD case patients received treatment. The AUD patients face several complicacy during the post-treatment, and the relapse rate of such patients varies between 20 to 80 percent [1]. Hence, it is a demand to improve such conditions. A noninvasive, continuous, and real-time monitoring system can ensure to fulfill such necessity and immediately diagnose the amount of alcohol consumption of AUD patients. Such information is more reliable than any self-reported data.

After alcohol consumption, the liver predominantly metabolizes it, and it distributes it to different biofluids through blood, such as urine [2], saliva [3], blood [4], breath, interstitial fluids, and sweat [5]. Different alcohol monitoring technologies have been invented, relying on detecting alcohol from these biofluids to prevent AUD. The most reliable technology for determining blood alcohol content (BAC) level is blood sampling methods. However, they are invasive and time-consuming. Monitoring from urine is noninvasive but limited to its discontinuous and long testing duration. Saliva and breath

are promising for noninvasive and real-time alcohol detection; however, such technologies have a high false-positive rate due to interference of other compounds existing in the mouth. Therefore, Enzyme-based electrochemical biosensors are promising for noninvasive alcohol detection from sweat. In the 1970s, Guilbault [6] and Christian [7] demonstrated that the enzyme – alcohol oxidase (AOX) could selectively detect alcohol in the presence of other interferants. AOX does not need any extrinsic cofactor, e.g., NAD+ along with ADH, and hereafter is not issuing to deteriorate these biosensors' stability and selectivity. Such biosensors are noninvasive, wearable, and compatible with continuous and real-time monitoring of AUD patients. The reaction mechanism of alcohol detection in the existence of catalyst AOX relies on the oxidation reaction of ethanol as follows:

$$\text{Ethanol} + O_2 \xrightarrow{\text{AOX}} H_2O_2 + \text{Acetaldehyde} \qquad (1)$$

Metal oxide-based nanostructures with a high isoelectric point (IEP) have recently become extremely significant as nanomaterials, which provide an effective and required surface for the immobilization of low-IEP biomolecules desired polarized plane orientation, better conformation, and high biological activity contributing to the development of enhanced biosensing platforms [8]. Among all the various metal oxide-based nanomaterials, Zinc oxide (ZnO) has been found as an excellent candidate material because it possesses all the necessary characteristics for wearable biosensing applications. ZnO, a semiconducting material with high catalytic efficiency, biocompatibility, chemical stability in physiological environments, low toxicity, and a high isoelectric point (IEP) 9.5, has been proposed for biosensing applications. ZnO nanostructures (NSs) with different morphologies such as nanorods, nanowalls, nanobelts, and quantum dots have been used

as immobilizing matrices in the fabrication process of biosensors for the detection of physiologically relevant biomarkers. Many techniques have been developed to synthesize various ZnO NSs considering their promising properties and potential applications. Compared to bulk materials, the 2D ZnO NFs provide unique sensing advantages with polarized (0001) plane orientation and high surface charge density. The high isoelectric point allows immobilization of most biomolecules without any additional binding layer. This provides a direct, stable pathway for rapid electron transport when an analyte is immobilized on NFs and improves the electron transfer rate greater than 1D ZnO nanorods. This high isoelectric point results in a change of resistance. In this work, we utilize ZnO NFs, synthesized on Au-deposited flexible polyethylene terephthalate (PET) substrate, as electrode sensing elements in developing a flexible, label-free, highly sensitive biosensor suitable for sweat based detection of alcohol. This attractive ZnO-based biosensing platform is expected to find applications in a new generation of miniaturized, smart biosensing healthcare devices for point of care detection.

5.2 Materials

5.2.1 Chemicals and Components

The enzyme-AOX from Pichia pastoris (10–40 units/mg protein) was obtained from Sigma-Aldrich, USA. Zinc Nitrate hexahydrate [ZNH; Zn $(NO_3)_2$ $6H_2O$] and Hexamethylenetetramine [HMT; $(CH_2)_6$ N_4], absolute ethyl alcohol (≥99.5%), were procured from Sigma-Aldrich. The phosphate buffer solution (PBS, pH 6.5) used for electrochemical studies was prepared from sodium phosphate monobasic (NaH_2PO_4) and

sodium phosphate dibasic (Na_2HPO_4) salts (Sigma Aldrich). All other chemicals were of analytical grade and were used without further purification. Different characterization tools, such as scanning electron microscopy (SEM, JOEL 7000FSEM) and Nomadic Raman microscope by BaySpec (532 nm laser), were used. In addition, an electrochemical analyzer (CHI604D, CH Instruments, USA) was employed for the measurement of alcohol.

5.2.2 Fabrication Mechanism

PET has gained popularity as a substrate for wearables because of its intrinsic elasticity, thermal stability, hydrophobicity, excellent dielectric properties, low coefficient of thermal expansion, structural resiliency against repeated bending forces, and compatibility with roll-to-roll fabrication processes for low cost and scalable manufacturing. The fabrication of gold-coated PET substrates was as follows: firstly, the PET substrates were cleaned with isopropanol and DI water in an ultrasonic bath for 15 min each and dried by nitrogen gas. After that, a thin film of 20nm of titanium (Ti) as an adhesive layer, followed by a layer of 60 nm thickness of gold, was initially deposited on PET substrates by e- beam evaporation, as shown in Figure 5-1.

5.2.3 Synthesis Technique

2D ZnO-NFs were synthesized on flexible Au-coated polyethylene terephthalate (PET) substrate using a simple one-step sonochemical approach. We choose this method as it is fast, inexpensive, catalyst-free, CMOS compatible, and environmentally benign; the reaction rate is 100 times faster than hydrothermal methods and allows for a well-oriented

growth over a wider range of substrates. The process of growing ZnO NFs was as follows: first of all, the gold-coated PET substrates were washed with deionized water and dried by N_2 gas. A solution of 20mM ZNH and 20mM HMT was prepared at room temperature by stirring with a magnetic stir bar at 350 rpm for 5 min to ensure a mixed solution was used as the only solution for the growth of 2D ZnO-NFs. The solution with the immersed substrate was then irradiated using a commercially available high-intensity ultrasound setup (750 W ultrasonic processor, Sonics and Systems) for 15min cycles at an amplitude of 70% of the maximum amplitude of the ultrasonic probe for 20 min providing the solution with an intensity of $30Wcm^{-2}$ and frequency of 20 kHz. The temperature of the aqueous solutions did not exceed 50 °C. The substrate was rinsed with DI water and then dried with N_2 after each cycle.

ZnO NFs based biosensor was developed by immobilizing with alcohol oxidase via electrostatic interaction due to the difference in isoelectric point (IEP) of ZnO (9.5) and enzyme (4.5) using physical adsorption. This difference in IEP between ZnO and enzyme eliminates the use of the intermediate linker layer. Alcohol oxidase solution was prepared in 0.1 M PBS (pH 6), having a concentration of 10-40 un/mg (protein) of the enzyme. For the immobilization of alcohol oxidase, 5uL of AOX solution from the stock solution was dropped above the working area of 0.5×0.5 cm^2 of PET/Au/ZnO NFs based working electrode. The sensor was then thoroughly rinsed with PBS and DI water to remove any unbound enzyme. The fabricated PET/Au/ZnO NFs/AOXsensors were then preserved in the refrigerator at 4^0C in idle operating conditions.

5.3 Results and Discussion

5.3.1 Characterization of the Electrodes

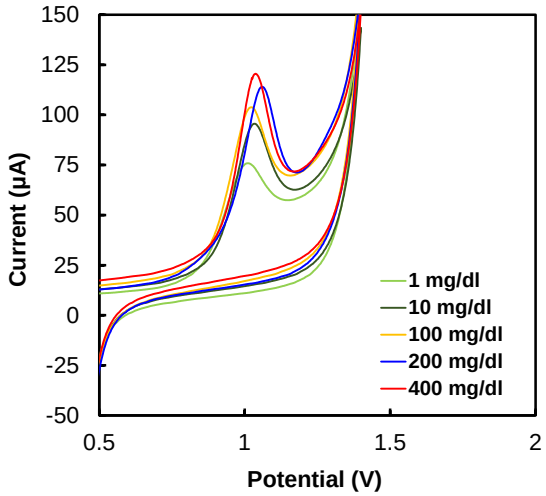

Figure 5-1: Cyclic Voltammetry studies with ethanol concentration varying from 1mg/dL to 400md/dL for ZnO NFs/Au/PET/AOX electrode

The morphological study of the surface of ZnO NFs was carried out using scanning electron microscopy. It was found that well-aligned, and uniform ZnO NFs were grown on the gold-coated PET substrates, as shown in Figures 5-2(a). ZnO NF is 20 nm thick and has an average lateral dimension of 5×5 μm^2. The visual representation in Figure 5-2(b) demonstrates the greater uniformity and smoothness while the AOX enzyme was introduced. Such morphological changes infer that the better immobilization over ZnO nanoparticles matrix. The Raman Spectroscopy result, shown in Figure 5-2(c), was found at 1050 cm^{-1} for PET/Au/ZnO NFs that agree to the second-order longitudinal optical phonon vibration.

5.3.2 Calibration of AOX/ZnO-NFs/Au/PET Alcohol Sensor

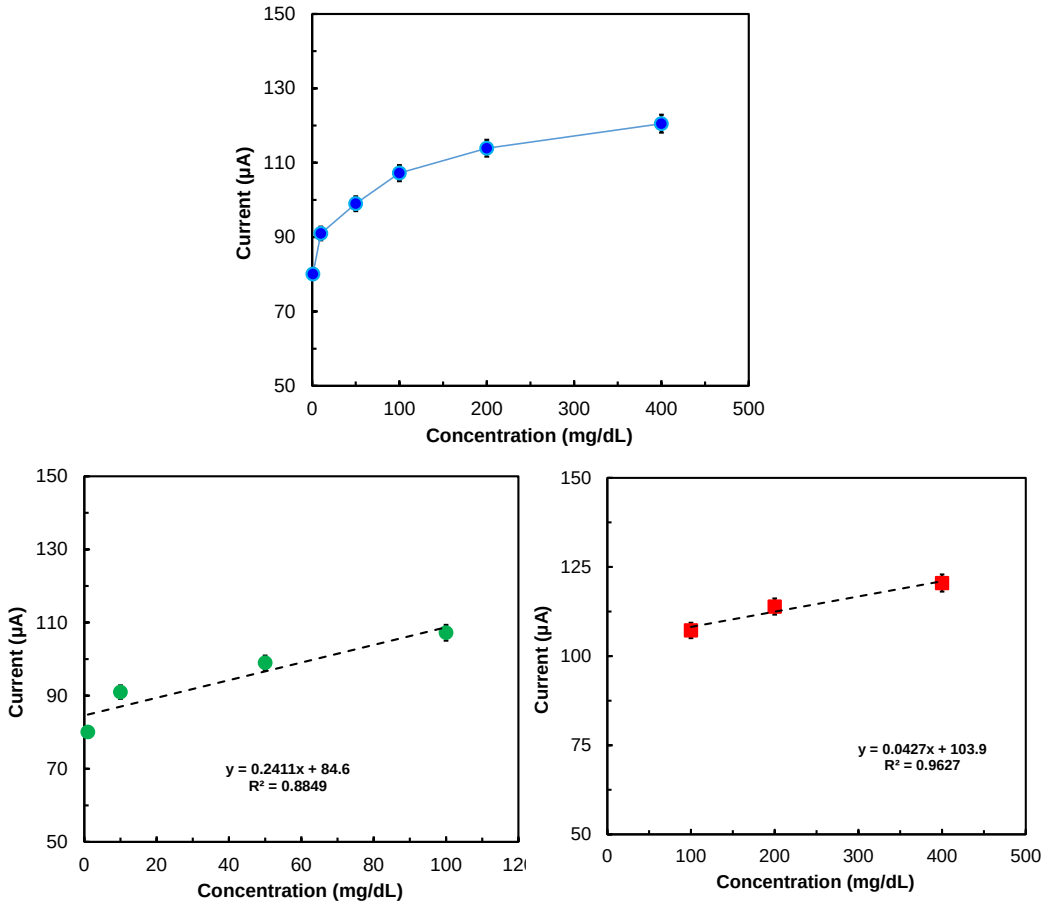

Figure 5-2: (a) Linear calibration fit (b) Calibration curve within the range from 1mgldL to 100mg/dL (segment 1) (c) Calibration curve within the range from 100mg/dL to 400mg/dL (segment 2)

A traditional three-electrode system in 3mL PBS (pH 6), a constituent of the fabricated AOX/ZnO-NFs/Au/PET bioelectrode as working electrode (anode), Pt as an auxiliary electrode (cathode), and Ag/AgCl, 0.1M KCl as a reference electrode was employed for all cyclic voltammetry (CV) measurements. The CV measurements were executed in the potential range of -1V to 1 V across the anode at a scan rate of 50mVs^{-1} for the ethanol concentrations of 1mg/dL – 400mg/dL, as shown in Figure 5-3. During the investigations, this sensor's output signal varied concerning the ethanol concentration in the test solutions.

In the presence of immobilized AOX, ethanol is oxidized into acetaldehyde and H_2O_2 as following the equation (1). For a fabricated effective biosensor, factors such as enzyme binding and electron transfer rate play a major role. 2D ZnO-NFs with high IEP (~9.5) has a positive surface charge. All the experiments were performed at a pH 6 that offers binding sites for AOX with an IEP of 4.2. Therefore, it is negatively charged under experimental conditions. The current vs. concentration curve was plotted in Figure 4-4(a) – 5-4(c) for six different concentrations, and data for each concentration were recorded five times. The demonstrated alcohol biosensor showed linear response within the range in between 1 mg/dL to 400 mg/dL of ethanol concentrations, as shown in Figure 5-4(a). The sensitivity of the proposed biosensor was obtained at 3.47 *n*A/mg/dL/cm^2. The curve trend is significantly linear, and the coefficient of determination was found around 80%. This alcohol sensor's minimum detected value was obtained 1 mg/dL, which covers the physiological range. Figure 5-4 (b and c) revealed two different calibration segments: 1≤ Conc≤100 mg/dL Figure 5-4 (b), and 100≤ Conc≤400 mg/dL Figure 5-4 (c). The rate of increment of the response for segment 1 is higher than segment 2. This phenomenon suggested that the sensor developed in this study would be most sensitive at low ethanol concentrations. The coefficient of determinations of segment 1 and segment 2 is 88.49% and 96.27%, respectively. So, from here, we can conclude that segment 2 is more linear than segment 1.

5.4 Conclusion

In this work, we have successfully demonstrated electrochemical biosensors for ethanol using ZnO NFs with immobilized alcohol oxidase without any linker layer. The

biosensors showed significant stability, linearity, high sensitivity in the physiological concentration ranges, and a very low detection limit. The LOD of the demonstrated sensor was found to be 1mg/dL, and the sensitivity was calculated as 3.47 *n*A/mg/dL/cm^2. The proposed sensing approach and device would help realize wearable continuous alcohol monitoring sensing platforms in a selective, noninvasive, real-time, and continuous manner.

5.5 References

1. Dougherty, D.M., Hill-Kapturczak, N., Liang, Y., Karns, T.E., Cates, S.E., Lake, S.L., Mullen, J.J., Roache, D., "Use of continuous transdermal alcohol monitoring during a contingency managementprocedure to reduce excessive alcohol use,". Drug Alcohol Depend., vol.142, pp. 301–306, 2014.

2. Jones, A.W., "Continuous minimally-invasive alcohol monitoring using microneedle sensor arrays," Toxicol. Rev., vol. 25, pp. 15–36, 2006.

3. Swift, R., "Transdermal alcohol measurement for estimation of blood alcohol concentration," Alcohol Clin. Exp. Res., vol. 24, pp. 422–423, 2000.

4. Payne -James, J. Keys, D.W., Jerreat, P.G., "Salivary alcohol measurement: Use in clinical forensic medical practice," J. Clin. Forensic Med., vol. 2, pp. 41–44, 1995.

5. Alam, F., Jalal A.H., Forouzanfar S., Karabiyik M., Rabiei Baboukani A., Pala N., "Flexible and Linker-Free Enzymatic Sensors Based on Zinc Oxide Nanoflakes for Noninvasive L-Lactate Sensing in Sweat," IEEE Sens., vol. 20, no. 10, pp. 5102- 5109, 2020.

6. Nanjo, M., Guilbault GG., "Amperometric determination of alcohols, aldehydes and carboxylic-acids with an immobilized alcohol oxidase enzyme electrode," Anal Chim Acta., vol. 75, pp. 169–180, 1975.

7. Thomas, L.C., Christian G.D., "Voltammetric measurement of reduced nicotinamide-adenine nucleotides and application to amperometric measurement of enzyme reactions," Anal Chim Acta., vol. 78, pp. 271–276, 1975.

8. Alam, F., Jalal A.H., Pala N., “Selective detection of alcohol through Ethyl-Glucuronide (EtG) immunosensor based on 2D Zinc Oxide nanostructures,” IEEE Sens., vol. 19, no. 11, pp. 3984 - 3992, 2019.

CHAPTER VI
THIN-FILM NANOSTRUCTURE-BASED ENZYMATIC GLUCOSE SENSOR

Diabetes is one of the major causes of fatality throughout the world today. The deficiency of insulin and hyperglycemia is caused by the metabolic disorder of diabetic patients [1]. This metabolic disorder promotes high risks of kidney failure, heart attack, chronic liver diseases, and blindness [2]. Thus, constricted day-to-day monitoring of glucose concentration is a demand for the diagnosis and treatment of diabetes. Also, fast, accurate, and continuous monitoring of glucose concentration is of great importance. As a successful consumer product of wearable biosensors, it is greatly important to demonstrate reliability, multiplexed functionality, and ease-to-use noninvasive monitoring of glucose from the body fluids [3]. Sweat is considered as one of the most widely used body fluids significant medical information, and easy to analyze [4]. However, the introduction of nanomaterials allows many new signal-transduction technologies to result in improved sensitivity of these biosensors. ZnO thin film-based biosensors [5] are promising to determine the glucose levels in sweat with better sensitivity, reliability continuously and in a non-invasive manner. ZnO itself has exclusive chemical and physical characteristics to enhance chemical stability in physiological environments.

In this part of the dissertation, an electrochemical glucose biosensor was fabricated by immobilization of glucose oxidase on ZnO nanoflakes with a thickness of 20nm, synthesized on Au-coated stretchable PET. The results demonstrated a fast response within 5s. The sensor was tested in the range of 10 pM – 20 mM, which covers the entire physiological range and is capable of detecting as low as 1 μM of the glucose concentration.

The sensitivity of the sensor was determined by 4.53 μA/decade/cm^2. Moreover, the sensor performed repeatable characteristics having with average standard deviation (S.D.) of 0.14 μA. Moreover, in our experiment, the fabrication process is simple, and the nano biosensor provides good performance in stability, selectivity, sensitivity, and reproducibility.

6.1 Materials

6.1.1 Chemicals and Components

The enzyme-GOx was obtained from Sigma-Aldrich, USA. Zinc Nitrate hexahydrate [ZNH; Zn $(NO_3)_2$ $6H_2O$] and Hexamethylenetetramine [HMT; $(CH_2)_6$ N_4], absolute ethyl alcohol (≥99.5%), were procured from Sigma-Aldrich. The phosphate buffer solution (PBS, pH 6.5) used for electrochemical studies was prepared from sodium phosphate monobasic (NaH_2PO_4) and sodium phosphate dibasic (Na_2HPO_4) salts (Sigma Aldrich). All other chemicals were of analytical grade and were used without further purification. Different characterization tools, such as scanning electron microscopy (SEM, JOEL 7000FSEM) and Nomadic Raman microscope by BaySpec (532 nm laser), were used. In addition, an electrochemical analyzer (CHI604D, CH Instruments, USA) was employed for the measurement of alcohol.

6.1.2 Fabrication Mechanism

PET has gained popularity as a substrate for wearables because of its intrinsic elasticity, thermal stability, hydrophobicity, excellent dielectric properties, low coefficient of thermal expansion, structural resiliency against repeated bending forces, and

compatibility with roll-to-roll fabrication processes for low cost and scalable manufacturing.

The fabrication of gold-coated PET substrates was as follows: firstly, the PET substrates were cleaned with isopropanol and DI water in an ultrasonic bath for 15 min each and dried by nitrogen gas. After that, a thin film of 20nm of titanium (Ti) as an adhesive layer, followed by a layer of 60 nm thickness of gold, was initially deposited on PET substrates by e- beam evaporation, as shown in Figure 1.

6.1.3 Synthesis Technique

2D ZnO-NFs were synthesized on flexible Au-coated polyethylene terephthalate (PET) substrate using a simple one-step sonochemical approach. We choose this method as it is fast, inexpensive, catalyst-free, CMOS compatible, and environmentally benign; the reaction rate is 100 times faster than hydrothermal methods and allows for a well-oriented growth over a wider range of substrates. The process of growing ZnO NFs was as follows: first of all, the gold-coated PET substrates were washed with deionized water and dried by N_2 gas. A solution of 20mM ZNH and 20mM HMT was prepared at room temperature by stirring with a magnetic stir bar at 350 rpm for 5 min to ensure a mixed solution was used as the only solution for the growth of 2D ZnO-NFs. The solution with the immersed substrate was then irradiated using a commercially available high-intensity ultrasound setup (750 W ultrasonic processor, Sonics and Systems) for 15min cycles at an amplitude of 70% of the maximum amplitude of the ultrasonic probe for 20 min providing the solution with an intensity of $30 Wcm^{-2}$ and frequency of 20 kHz. The temperature of the aqueous

solutions did not exceed 50 °C. The substrate was rinsed with DI water and then dried with N_2 after each cycle.

ZnO NFs based biosensor was developed by immobilizing with alcohol oxidase via electrostatic interaction due to the difference in isoelectric point (IEP) of ZnO (9.5) and enzyme (4.5) using physical adsorption. This difference in IEP between ZnO and enzyme eliminates the use of the intermediate linker layer. Glucose oxidase solution was prepared in 0.1 M PBS (pH 6), having a concentration of 10-40 un/mg (protein) of the enzyme. For the immobilization of glucose oxidase, 5uL of GOX solution from the stock solution was dropped above the working area of 0.5 × 0.5 cm^2 of PET/Au/ZnO NFs based working electrode. The sensor was then thoroughly rinsed with PBS and DI water to remove any unbound enzyme. The fabricated PET/Au/ZnO NFs/AOX sensors were then preserved in the refrigerator at 4^0C in idle operating conditions.

6.2 Results and Discussion

6.2.1 Characterization of the Electrodes

The selective area electron diffraction (SAED) and high-resolution transmission electron microscopy (HRTEM) studies in Figures 6-1(a) and 6-1(b) were performed using an electron microscope with a 300KeV electron beam. The selective area electron diffraction (SAED) analysis in Figure 6-1(a) was carried out using commercial software (Single Crystal). The SAED measurements depict that the 2D ZnO nanoflakes exhibit hexagonal wurtzite structure with a=3.25Å and c=5.21 Å, oriented along (0001) plane and the lateral growth direction perpendicular to the (0110) plane. The HRTEM images are

taken at the major edge of the flakes showed that the fringes are almost parallel to the edge with a lattice spacing of 2.74Å.

The Morphological study of the surface of ZnO NFs was carried out using scanning electron microscopy. It was found that well-aligned, and uniform ZnO NFs were grown on the gold-coated PET substrates, as shown in Figures 6-1(c). ZnO NF is 20 nm thick and has an average lateral dimension of 5×5 μm^2. The visual representation in Figure 6-1(d) demonstrates the greater uniformity and smoothness while the GOX enzyme was introduced. Such morphological changes infer that the better immobilization over ZnO nanoparticles matrix.

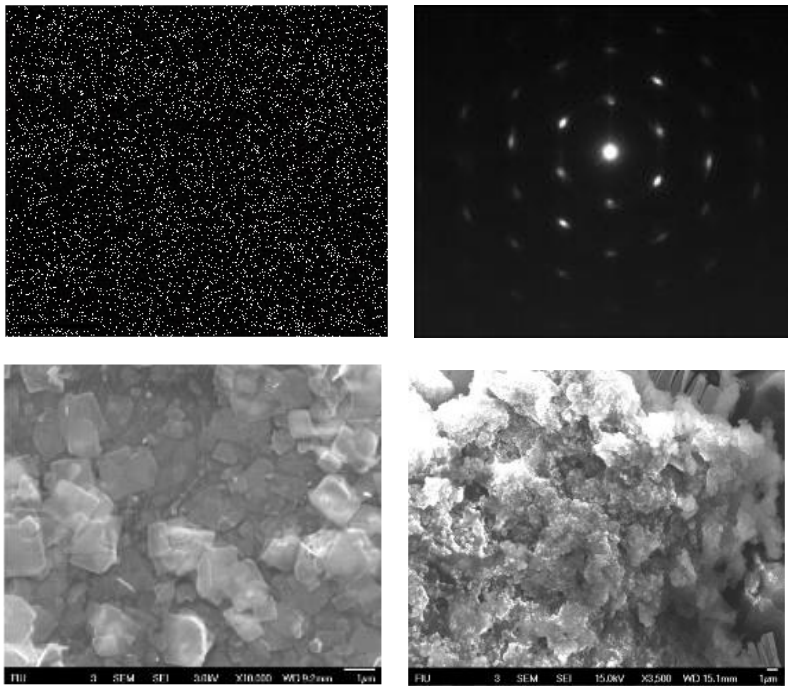

Figure 6-1: (a) SAED and (b)HTEM of the center and edge of the flakes (c) SEM of PET/Au/ZnO-NFs and (d)PET/Au/ZnO-NFs/GOX

6.2.2 Calibration of GOX/ZnO-NFs/Au/PET Glucose Sensor

A traditional three-electrode system in 3mL PBS (pH 6), a constituent of the fabricated GOX/ZnO-NFs/Au/PET bioelectrode as working electrode (anode), Pt as an auxiliary electrode (cathode), and Ag/AgCl, 0.1M KCl as a reference electrode was employed for all cyclic voltammetry (CV) measurements. The CV measurements were executed in the potential range of -1V to 1.2 V across the anode at a scan rate of 50mVs^{-1} for the ethanol concentrations of 1mM – 20 mM, as shown in Figure 6-2(a). During the investigations, this sensor's output signal varied concerning the glucose concentration in the test solutions. For a fabricated effective biosensor, factors such as enzyme binding and electron transfer rate play a major role. 2D ZnO-NFs with high IEP (~9.5) has a positive surface charge. All the experiments were performed at a pH 6.5 that offers binding sites for GOX with an IEP of 4.2. Therefore, it is negatively charged under experimental conditions. The current vs. concentration curve was plotted in Figure 6-2 (b) for four different concentrations, and data

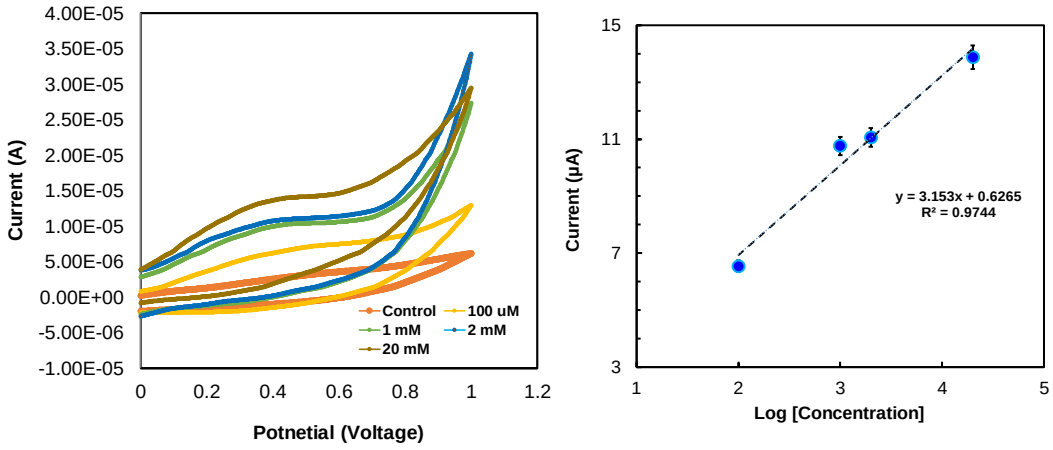

Figure 6-2: (a) Cyclic Voltammetry studies with glucose concentration varying from 1mM to 20mM for ZnO NFs/Au/PET/GOX electrode (b) Linear calibration curve within the range from 1mM to 20mM

for each concentration were recorded five times. The demonstrated glucose biosensor showed linear response within the range in between 1 mM to 20 mM of glucose concentrations, as shown in Figure 6-2(b). The sensitivity of the proposed biosensor was obtained at 12.6 μA/decade/cm^2. The curve trend is significantly linear, and the coefficient of determination was found around 97.44. This glucose sensor's minimum detected value was obtained 1 mM, which covers the physiological range. This phenomenon suggested that the sensor developed in this study would be most sensitive at low glucose concentrations.

6.3 Conclusion

We have successfully demonstrated electrochemical biosensors for glucose using ZnO NFs with immobilized glucose oxidase without any linker layer. The biosensors showed significant stability, linearity, high sensitivity in the physiological concentration ranges, and a very low detection limit. The LOD of the demonstrated sensor was found to be 1uM, and the sensitivity was calculated as 12.6 *u*A/decade/cm^2. The proposed sensing approach and device would help realize wearable continuous glucose monitoring sensing platforms in a selective, non-invasive, real-time, and continuous manner.

6.4 References

1. Genuth, S., Alberti,K.G., Bennett, P., Buse, J., DeFronzo, R., Kahn, R., Kitzmiller, J., Knowler, W.C., Lebovitz, H., Lernmark, A., Nathan, D., Palmer, J., Rizza, R., Saudek, C., Shaw, J., Steffes, M., Stern, M., Tuomilehto, J., Zimmet, P., "Expert Committee on the Diagnosis and Classification of Diabetes Mellitus. Followup report on the diagnosis of diabetes mellitus," Diabetes Care, vol. 26, pp.-3160– 3167, 2003.

2. Landon, M.B., Spong, C.Y., Thom, E., Carpenter, M.W., Ramin, S.M., Casey, B., Wapner, R.J., Varner, M.W., Rouse, D.J., Thorp, J.M., Jr., Sciscione, A., Catalano, P., Harper, M., Saade, G., Lain, K.Y., Sorokin, Y., Peaceman, A.M., Tolosa, J.E, Anderson. G.B., "A multicenter, randomized trial of treatment for mild gestational diabetes," N Engl J. Med., vol. 361, pp. 1339–1348, 2001.

3. Badugu, R., Lakowicz, J.R., Geddes, C.R., "Ophthalmic glucose monitoring using disposable contact lenses—A review," J. Fluoresc., vol.14, pp. 617–633, 2004.

4. Baker, L.B., Lang, J.A., Kenney, W.L., "Change in body mass accurately and reliably predicts change in body water after endurance exercise," Eur J Appl Physiol., vol. 105, pp. 959–967, 2009.

5. Alam F., Jalal A.H., Forouzanfar S., Karabiyik M., Rabiei Baboukani A., Pala N., "Flexible and Linker-Free Enzymatic Sensors Based on Zinc Oxide Nanoflakes for Noninvasive L-Lactate Sensing in Sweat," IEEE Sens., vol. 20, no. 10, pp. 5102-5109, 2020.

CHAPTER VII
MINIATURIZED, WIRELESS MULTI-CHANNEL POTENTIOSTAT

A three-electrode system has been integrated with a miniaturized potentiostat to monitor different analytes. Such a potentiostat circuit has been designed to have the feature of four-channel multiplexing to operate different electrochemical cells simultaneously. The device is Bluetooth-connected to a user-controlled mobile app through which the system is regulated. The personalized data from the analysis are shown in the mobile APP. The system is comprised of four units: digital to analog converter (DAC), multiplexing unit, control unit, and current to voltage converter (CVC). The circuit is run by Arduino NANO 33 BLE. Firstly, the Arduino's digital PWM signal is converted into an analog signal through the DAC unit to run the scanning. The realized scanning range of the potentiostat is from -1V to 2V. This output of the DAC unit is then fed into the multiplexing unit to distribute it to all four control units one at a time. Later, each control unit of the respective cells performs scanning through the three-electrode system connected to the control unit. The real-time scanning data collected from the cell is sent to the CVC unit and converted into a voltage to be readable by the Arduino. The acquired data is sent wirelessly to a user-friendly mobile app by the Arduino through its built-in Bluetooth system. the whole system is fully user-controlled through the app, including selecting the cells to scan and scan rate.

7.1 Experimental

7.1.1 Components and Apparatus

Arduino NANO 33 BLE is used in the device, which has an nRF52840 microcontroller integrated into it. The resolution of the ADC of the Arduino is 12 bit, and it has a built-in Bluetooth module. LM324 operational amplifiers were used for the amplifying operation in our circuit. For the four-channel multiplexing operation, CD74HC4052E multiplexer/demultiplexer IC was used that has a 4:1 configuration. Apart from this, we used LT3032EDD5PBF and LT3015EDD-3.3PBF voltage converters to get a constant voltage supply of (±5V) and (-3.3V) volts for the power supply section, respectively.

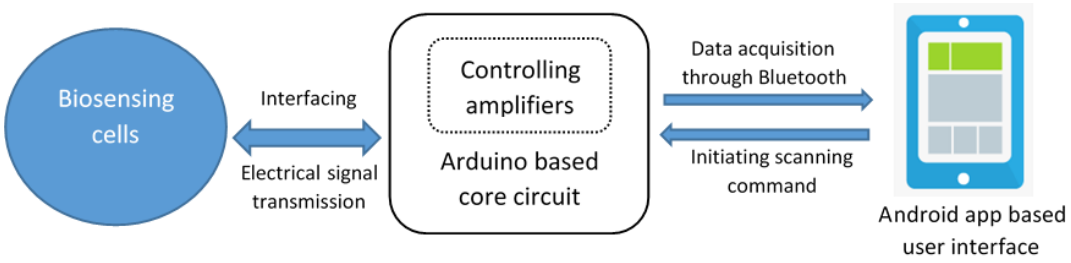

Figure 7-1: Block diagram of the wireless sensing platform.

7.1.2 Interfacing Between s\Sensing Units and i\Integrated Potentiostat

The potentiostat was comprised of four units as follows: i) digital to analog converter (DAC), ii) summing amplifier unit, iii) multiplexing/demultiplexing unit, control unit, and iv) current to voltage converter (CVC). The circuit was run by Arduino NANO 33 BLE. The DAC unit was connected to one of the analog pulse width modulator (PWM) output pins of the Arduino. Next, the summing amplifier section was linked between the

DAC unit and the multiplexing/demultiplexing unit. The Arduino controlled the multiplexing/demultiplexing unit, and it was connected to two of the Arduino digital output pins for channel selection. This unit was also attached to the controlling amplifier unit, where four controlling amplifiers were situated for each of the corresponding biosensing cells. The four sensing cells were interfaced with their corresponding controlling amplifiers of the controlling amplifier unit through the reference (RE) and the working (WE) electrodes. The counter electrodes (CE) were connected to the current to voltage converter (CVC) unit, which is a transimpedance amplifier via the multiplexing/demultiplexing section. Lastly, the CVC unit's output was interfaced with one of the Arduino analog input pins. This whole potentiostat device was connected to the user's mobile device through the integrated Bluetooth module of the Arduino. Detailed interfacing of the different sections of the circuit is shown in Figures 7-2.

7.1.3 Working Principle of the Potentiostat

We used a double-layer printed circuit board (PCB) to implement the designed circuit. Most of the electronic components with CD74HC4052E multiplexer/demultiplexer IC, voltage converters (LT3032EDD5PBF & LT3015EDD-3.3PBF) and, one of the LM324 operational IC was placed on the bottom layer of the PCB, and the rest of the components, including Arduino NANO 33 BLE were placed on the top layer of the Determination of isoflurane from human sweat.

7.1.4 Digital to Analog Converter (DAC) Unit

Firstly, the digital PWM signal from the Arduino is sent to the DAC unit to be converted into an analog signal. However, a potential ramp has to be applied for the cyclic voltammetry experiment. So, the DAC unit converts the stepped signal from the Arduino into an actual analog signal. The PWM signal from the Arduino has an 8-bit resolution. As the operating voltage of the Arduino is 3.3V, so the 0 to 3.3V is discretized into 256 voltage levels.

7.1.5 Summing Amplifier Unit

The PWM signal of the Arduino only has the positive portion (3.3V), but for the cyclic voltammetry operation, the scanning range should be from negative to positive range. The DAC unit's output is fed into this section to adjust the 0 to 3.3V ramp into the required -1 V to 2 V potential ramp. The realized scanning range of the potentiostat is from -1V to 2V. The output of the summing amplifier is controlled by (1).

$$V_o = -R_4 ((V_{in}/R_6) + (-3.3/R_1)) \quad (1)$$

The input-output table of the summing amplifier is shown in Table 6-1.

Input(V/PWM level)	**Output(V)**
0/0	2
1.65/127	0
3.3/255	-1

Table 7-1: Input/output voltage of the summing amplifier with PWM levels.

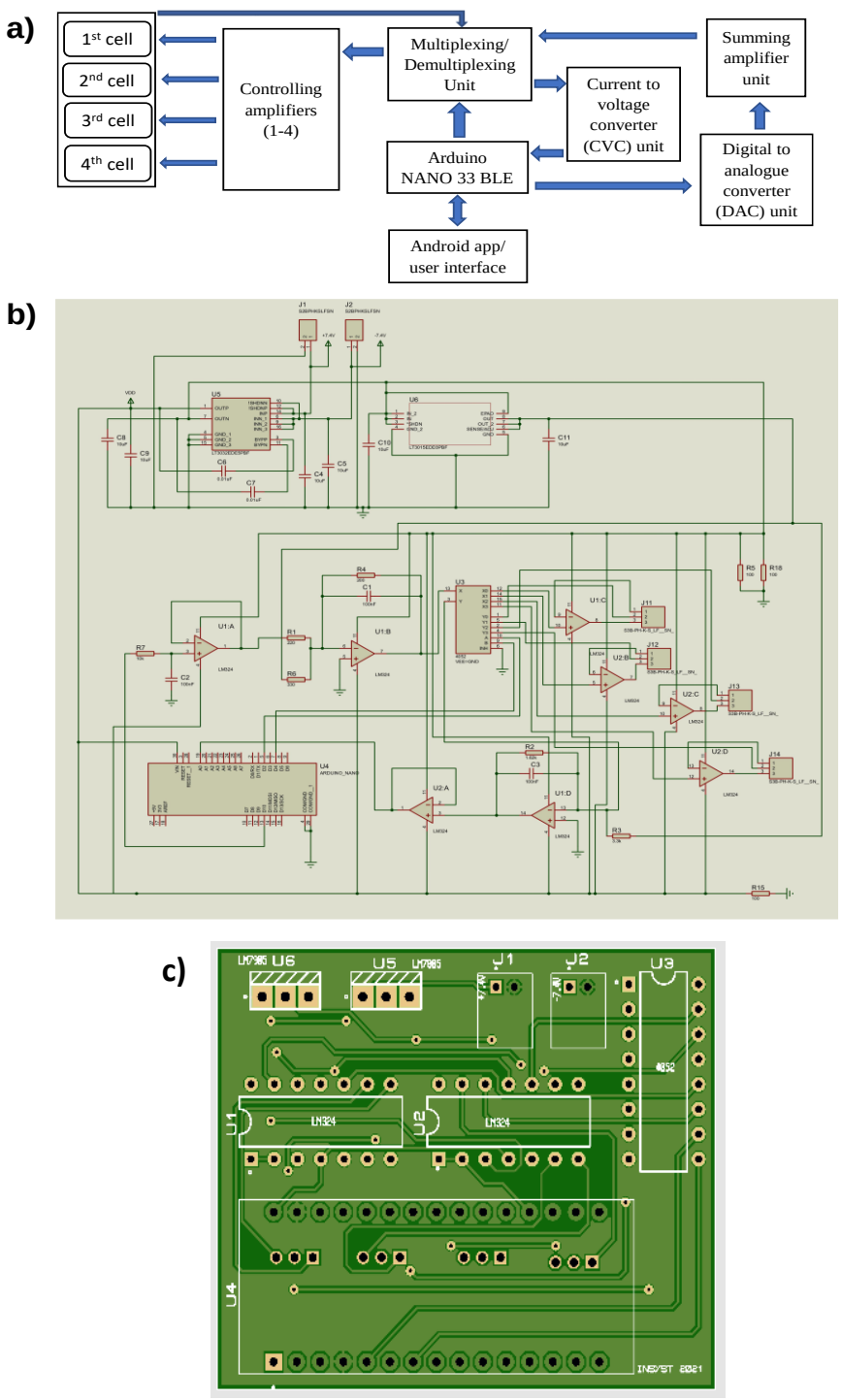

Figure 7-2: a)Detailed block diagram of the circuit of the sensing platform, and b) the circuit layout in Proteus (c) Ordered PCB schematic.

7.1.6 Multiplexing/demultiplexing Unit

This output of the summing amplifier unit is then fed into the multiplexing unit to distribute it to all four control units one at a time. The Arduino controlled the CD74HC4052E 4:1 multiplexer to select the required channel. The same IC was used for demultiplexing when the data was collected through the cells' contour electrodes.

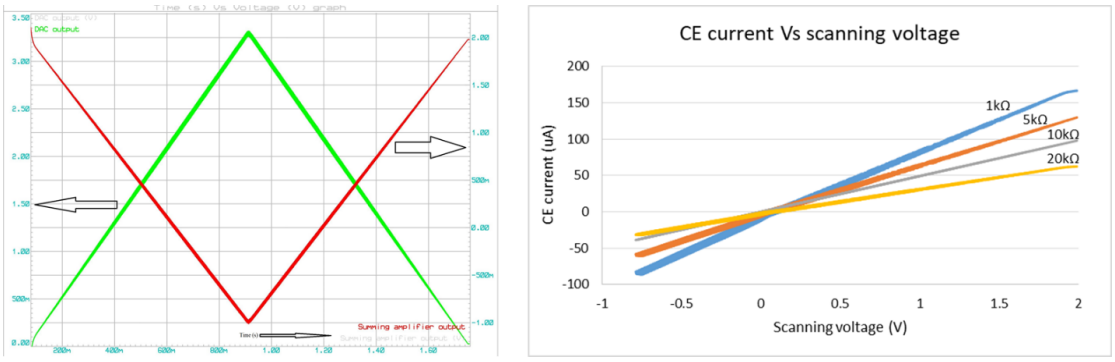

Figure 7-3: (a) DAC and summing amplifier output voltage Vs current; and b) Counter electrode current Vs scanning voltage curve for different resistance values

7.1.7 Controlling Amplifier Unit

These Four different controlling amplifiers were placed into this unit for the four corresponding sensing cells. This unit is the most vital section of the potentiostat and for the three-electrode system. The scanning voltage (-1V to 2V) is then applied between the working electrode and the reference electrode by using this amplifier. The controlling amplifier mainly keeps the voltage difference constant between these two electrodes.

7.1.8 Electrochemical Signal Generation

The chemical reactions between analyte and enzyme took place on the WE of the sensor. Therefore, electrons are generated and collected by the counter electrode [10].

Electrochemical sensing techniques based on catalytic electron transfer mechanisms were used in this experiment. The electron transfer is associated with the catalytic conversion of the substrate to the product. The biorecognition elements act as an electrocatalyst, enabling the flow of electrons between the substrate molecule and the electrode containing no intermediary layer [11]. Because of the oxidation-reduction reaction in the presence of biological elements in biofluids, the output response of the sensor changes.

7.1.9 Current to Voltage Converter (CVC) Unit

The counter electrode collects current from the cell, and this CVC unit converts that current into a recognizable voltage signal. This unit was built by a trans-impedance amplifier. This converted voltage signal is then sent to the Arduino through its analog input pin with a 12-bit resolution to read the voltage signal. The transimpedance amplifier was modeled so that the converted highest voltage will always be 3.3V or less than that because the Arduino NANO 33 BLE cannot take input voltage higher than 3.3V. The current limit of this amplifier was set to be ±1000 μA. The current of the transimpedance amplifier is controlled by the feedback resistor following Eqn. (2):

$$V_{CVC:out} = I_{(CE\ current)} \times R_{2\ (feedback\ resistor)} \quad (2)$$

The collected sensed data is then sent to the Arduino, where it was transformed again to current. Consequently, these current values with their respective scanning voltages are then wirelessly sent to the user's mobile device for data monitoring using the Arduino built-in Bluetooth module.

7.1.10 Arduino NANO 33 BLE

This device was selected for its extra small packaging size and built-in Bluetooth module, which saved us a lot of space in the PCB design. It has an open-source IDE and simple programming language with a built-in library function for easy integration of the device with the android application for data transfer. Also, its low voltage operation of 3.3V made it suitable for our application. Other than that, features like 1MB flash memory, 256KB SRAM, and 12-bit ADC for reading analog data from the CVC have made its use convenient for the device.

7.2 Results and Discussion

PWM signal from the Arduino is converted to a 0 to 3.3V analog potential ramp by DAC, as shown in Fig. 5. As the required scanning range for our biosensing is from -1V to 2V, the DAC output is then adjusted to the required voltage range by the summing amplifier is shown in Fig. 3a. When the DAC output goes from 0 to 3.3V, the summing amplifier output runs from 2V to -1V. The opposite happens for the next cycle. The output current from the counter electrode was plotted against the scanning voltage in Fig. 6-3b. It can be seen that the curve is linear fits with the voltage for different resistance values (1kΩ, 5kΩ, 10kΩ, and 20kΩ). Also, the level of CE current is changing in accordance with the change of resistance. The circuit design and the simulation were performed using Proteus 8 [2].

The LM324 operational amplifier needs a positive and negative power supply with respect to the ground. For this circuit, a ±5V power supply was needed for the LM324. Also, to power up the Arduino through its V_{in} pin +5V was required. To get this constant ±5V power supply rail, we used the LT3032EDD5PBF converter, which provided a ±5V

supply, converted from the ±7.4V supplied from lithium-ion batteries. Another voltage converter LT3015EDD-3.3PBF was used to get a constant -3.3V supply for the summing amplifier and the transimpedance amplifier. These voltage converters were chosen for their smaller size and multiple voltage output features, which helped us significantly reduce the device's size. In total, four 3.7V lithium-ion batteries were used to power up the device. A simple, user-friendly android application was built to control the sensing platform, data monitoring, and post-processing. The simple, user-friendly interface was sectioned into an input tab and four different tabs assigned to four sensor cells. The device can be connected and disconnected according to the user's preference. Different scanning rates and cells can be selected from the application. After the completion of the scanning, the data is sent to the app for post-processing and monitoring. The I/V curves and the corresponding data of the individual cells are shown in their respective tabs. The respective current and voltage values are saved in the application in .csv format, which can be used for later analysis.

7.3 Conclusions

This work has successfully modeled and simulated the wireless potentiostat which is capable of collecting and processing small electrical signals from the three-electrode system-based electrochemical cells. The device has the feature of sensing four different analytes in the same platform. Also, the potentiostat is connected to the mobile user device through Bluetooth for data monitoring which can be extended further for IoT applications in the future. Most importantly, the device is miniaturized enough instead of possessing multi-channeling and Bluetooth functions. These characteristics of the proposed potentiostat are suitable to implement in wearable multi-analyte sensing platforms.

7.4 References

1. Meloni, N., “Building a microcontroller based potentiostat: A inexpensive and versatile platform for teaching electrochemistry and instrumentation,” J. Chem. Educ., vol. 93, no. 7, pp. 1320–1322, 2016.

2. Jalal, A. H., Umasankar, Y., Gonzalez, P. J., A. Alfonso, and S. Bhansali, “Multimodal technique to eliminate humidity interference for specific detection of ethanol,” Biosens. Bioelectron., vol. 87, pp. 522–530, 2017.

3. Vergani, M., *et al.*, “Multichannel bipotentiostat integrated with a microfluidic platform for electrochemical real-time monitoring of cell cultures,” IEEE Trans. Biomed. Circuits Syst., vol. 6, no. 5, pp. 498–507, 2012.

4. Ning, Z. H., Huang, J. Q., S. X. Guo, and L. H. Wang, “A Portable Potentiostat for Three-Electrode Electrochemical Sensor,” J. Phys. Conf. Ser., vol. 1550, no. 4, 2020.

5. Dryden, M. D. M., and Wheeler, A. R., “DStat: A versatile, open-source potentiostat for electroanalysis and integration,” PLoS One, vol. 10, no. 10, Oct. 2015.

6. Rowe, A. A., *et al.*, “CheapStat: An Open-Source, ‘Do-It-Yourself’ Potentiostat for Analytical and Educational Applications,” PLoS One, vol. 6, no. 9, p. e23783, Sep. 2011.

7. “Arduino Nano 33 BLE with headers |Arduino Official Store.” https://store.arduino.cc/usa/nano-33-ble-with-headers (accessed Mar. 21, 2021).

8. Ainla, A., *et al.*, “Open-Source Potentiostat for Wireless Electrochemical Detection with Smartphones,” Anal. Chem., vol. 90, no. 10, pp. 6240–6246, May 2018.

9. W. Gao *et al.*, “Fully integrated wearable sensor arrays for multiplexed in situ perspiration analysis,” Nature, vol. 529, no. 7587, pp. 509–514, Jan. 2016.

10. Alam, F., Jalal, A.H., Forouzanfar, S., Karabiyik, M., Baboukani, A. R.,N. Pala, “Flexible and Linker-Free Enzymatic Sensors Based on Zinc Oxide Nanoflakes for Noninvasive L-Lactate Sensing in Sweat,” IEEE Sens. 20 (10), vol. 20, no. 10, pp. 5102–5109, 2020.

11. F. Alam, Jalal, A.H., Pala, N., “Selective detection of alcohol through Ethyl-Glucuronide (EtG) immunosensor based on 2D Zinc Oxide nanostructures,” IEEE Sens.19 (11), vol. 19, no. 11, pp. 3984–3992, 2019.

12. “PCB Design and Circuit Simulator Software - Proteus.” https://www.labcenter.com/ (accessed).

CHAPTER VIII
CONCLUSIONS

8.1 Summary and conclusions

In summary, we explore wearable biosensors that continuously monitor alcohol, lactate, and various biomarkers affecting a patient's health have significant implications for hundreds of millions of people worldwide. Such biosensors have shown outstanding results in detecting biomarkers that aid in diagnosing and supervising patients suffering from several diseases, thus saving countless lives. This is due to the high demand for miniature diagnostic devices and expanding the application scope for wearable biosensors in the medical field.

We report the multiple phases of developing two-dimensional (2D) Zinc Oxide Nanoflakes (ZnO NFs) based nano biosensors for point-of-care and wearable health quality monitoring applications. I aim to develop a self-powered, highly sensitive, wearable enzymatic and immune sensors array for continuous and selective sensing of ethanol, lactate, and glucose in human sweat. The designed nano biosensors can be mass-produced and be easily embedded in available technologies. To achieve this goal, I have planned my project in a bottom-up manner. For the first phase of my research, I synthesized ZnO-NFs on gold-deposited flexible polyethylene terephthalate substrate as electrode sensing elements in developing a flexible, label-free, highly sensitive biosensor suitable for sweat based detection of ethanol through ethyl glucuronide (EtG). This sensor's sensitivity was found to be 0.032 mA/decade/cm^2 for the EtG concentration range of 1 ng/ml – 100 µg/ml, which covers the physiological range. The proposed method and device would help to

realize wearable continuous alcohol sensing and monitoring platforms and obviate the need for lengthy and costly procedures.

I developed a linker-free electrochemical biosensor consisting of ZnO NFs with immobilized lactate oxidase, which has also been successfully demonstrated to monitor L-lactate from sweat. A wide range of linearity covering the physiological range has been observed with the sensitivity of 11.76 μA/decade/cm^2. The sensor was tested with real human sweat samples for future implementation on wearables. The proposed method and device would help to realize point-of-care wearable platforms for continuous lactate monitoring. My consequent studies focus on system integration by designing wearable multiple sensor arrays in the same platform and integrating with a Bluetooth device for continuous and simultaneous monitoring of ethanol, lactate, and glucose.

8.2 Recommendations for future research

For the further improvement of enzyme based sensors, this work needs to improve in the following domains. They are:

1. Nanostructure based sensing active layers need be integrated for flexible skin attachable sweat analysis system.
2. Integrating enzymes with electrospinning deposited conductive polymers could provide effective sensing platform for sweat analysis.

VITA

FAHMIDA ALAM

2016 – 2021	Doctor of Philosophy Department : Electrical and Computer Engineering (ECE) University : Florida International University (FIU), Miami, FL
2006 – 2010	B.S. in Engineering Department : Electrical and Electronic Engineering (EEE) University : Chittagong University of Engineering and Technology (CUET)

JOURNAL AND CONFERENCE PAPERS

1. Fahmida Alam, Ahmed Hasnain Jalal, Shahrzad Forouzanfar, Mustafa Karabiyik, Amin Rabiei Baboukani, and Nezih Pala; Flexible and Linker-Free Enzymatic Sensors Based on Zinc Oxide Nanoflakes for Noninvasive L-Lactate Sensing in Sweat, IEEE Sensors Journal, vol. 20 (10), pp. 5102- 5109, May 15, 2020.
2. Fahmida Alam, Ahmed Hasnain Jalal and Nezih Pala; Selective Detection of Alcohol Through Ethyl-Glucuronide (EtG) Immunosensor Based on 2D Zinc Oxide Nanostructures, IEEE Sensors Journal, vol. 19 (11), pp. 3984 - 3992, June 1, 2019.
3. Fahmida Alam, Sadegh Mehdi Aghaei, Ahmed Hasnain Jalal and Nezih Pala; Sonochemically Synthesized ZnO Nanostructured Piezoelectric Layers for SelfPowered Sensor Applications, MRS Advances, vol. 4 (23, Biomaterials and Soft Materials), pp. 1355-1360, February 11, 2019.
4. Fahmida Alam, Sohini RoyChoudhury, Ahmed Hasnain Jalal, Yogeswaran Umasankar, Shahrzad Forouzanfar, Naznin Akter, Shekhar Bhansali1, and Nezih Pala; Lactate Biosensing: The Emerging Point-of-Care and Personal Health Monitoring, J. Biosensors and Bioelectronics, vol. 117, pp. 818-829, October 15, 2018.
5. Fahmida Alam, Ahmed Hasnain Jalal, Raju Sinha, Yogeswaran Umasankar, Shekhar Bhansali, and Nezih Pala; Sonochemically Synthesized ZnO Nanostructure-based LLactate Enzymatic Sensors on Flexible Substrates, MRS Advances, vol. 3 (5), pp. 277282, January 16, 2018.
6. Fahmida Alam, Ahmed Hasnain Jalal, Shahrzad Forouzanfar, and Nezih Pala; Thin film nanostructure-based enzymatic alcohol sensor for wearable sensing and monitoring applications, SPIE Defense + Commercial Sensing, Orlando, Florida, April 11 – 15, 2021.
7. Fahmida Alam, Muhammad Mahmudul Hasan, Ahmed Hasnain Jalal, Masudur Rahman Siddiquee, and Nezih Pala; Miniaturized, wireless multi-channel potentiostat platform for wearable sensing and monitoring applications, SPIE Defense + Commercial Sensing, Orlando, Florida, April 11 – 15, 2021.
8. Fahmida Alam, Ahmed Hasnain Jalal, Shahrzad Forouzanfar, Chunlei Wang and Nezih Pala; ZnO Nanoflakes based Enzymatic Sensor for the determination of Lactic Acid in Sweat, 2019 IEEE SENSORS, Montreal, QC, Canada, pp. 1-3, October 2730,2019.

9. Fahmida Alam, Ahmed Hasnain Jalal, Raju Sinha, Yogeswaran Umasankar, Shekhar Bhansali, and Nezih Pala; ZnO Nanoflakes-based Mediator Free Flexible Biosensors for the Selective Detection of Ethyl Glucuronide (EtG) and Lactate, SPIE Defense + Commercial Sensing, vol. 10639, pp. 106392O-1 – 106392O-6, Orlando, Florida, April 15 – 19, 2018.
10. Fahmida Alam, Raju Sinha, Ahmed Hasnain Jalal, Pandiaraj Manickam, Phani Kiran Vabbina, Shekhar Bhansali, and Nezih Pala; Sonochemically Synthesized Zinc Oxide Nanoflakes Based Electrochemical Immunosensor for Ethyl Glucuronide (EtG) Detection, ECS Transactions, vol. 80 (10), pp. 1287-1294, National Harbor, Maryland, October 1-6, 2017.
11. Shahrzad Forouzanfar, Fahmida Alam, Nezih Pala, and Chunlei Wang; Highly Sensitive Label-Free Electrochemical Aptasensors Based on Photoresist Derived Carbon for Cancer Biomarker Detection, J. Biosensors and Bioelectronics, pp. 112598, September 18, 2020.
12. Shahrzad Forouzanfar, Fahmida Alam, Iman Khakpour, Amin Rabiei Baboukani, Nezih Pala, and Chunlei Wang; Highly Sensitive Lactic Acid Biosensors Based on Photoresist Derived Carbon, IEEE Sensors Journal, vol. 20 (16), pp. 8965- 8972, August 15, 2020.
13. Ahmed Hasnain Jalal, Amit Kumar Sikder, Fahmida Alam, Sharraf Samin, Sharmin S. Rahman, Md Morshed A. Khan, and Masudur R. Siddiquee. Early Diagnosis with Alternative Approaches: Innovation in Lung Cancer Care, Focused Issue on A New Era in Lung Cancer Care: From Early Diagnosis to Personalized Treatment, Shanghai Chest, pp. 1-14, May 6, 2020.
14. Shahrzad Forouzanfar, Fahmida Alam, Nezih Pala, and Chunlei Wang; A Review of Electrochemical Aptasensors for Label-Free Cancer Diagnosis, J. Electrochem. Soc., vol 167 (6), pp. 067511, March 27, 2020.
15. Md. Nurul A. Tarek, Fahmida Alam, Ahmed Hasnain Jalal, and Mohammad A. Ahad; Multi-frequency Assessment of the Electrical Impedance Myography Parameters on 3d Malignant Breast, MRS Advances, vol. 4 (23, Biomaterials and Soft Materials), pp. 1285-1291, Boston, Massachusetts, December 26, 2018.
16. Ahmed Hasnain Jalal, Fahmida Alam, Sohini RoyChoudhury1, Yogeswaran Umasankar, Nezih Pala, and Shekhar Bhansali; Prospects and Challenges of Volatile Organic Compound Sensors in Human Healthcare, ACS Sensors, Vol. 3(7), pp. 12461263, June 8, 2018.
17. Imtiaz Parvez, Maryamossadat Aghili, Arif I. Sarwat, Shahinur Rahman and Fahmida Alam; Online Power Quality Disturbance Detection by Support Vector Machine in Smart Meter, J. of Mod. Power Systems and Clean Energy, Vol. 7(31), pp. 1-12, December 26, 2018.
18. Naznin Akter, JJ Becerril-Gonzalez, Mustafa Karabiyik, Fahmida Alam, Nezih Pala, G Oskam, O Arés-Muzio; FDTD modeling of sputtered Mo–Al2 O 3 nanocomposites, Solar Energy Mat. And Solar Cells, Vol. 255, pp. 111027, June 15, 2021.
19. Shahrzad Forouzanfar, Iman Khakpour, Fahmida Alam, Nezih Pala, Chunlei Wang; Novel application of electrochemical bipolar exfoliated graphene for highly sensitive disposable label-free cancer biomarker aptasensors, Nanoscale Adv., Vol. 3, pp. 5848-5958, August 12, 2021.